

---

# Fast Tree Variants of Gromov-Wasserstein

---

Tam Le<sup>\*1</sup> Nhat Ho<sup>\*2</sup> Makoto Yamada<sup>31</sup>

## Abstract

Gromov-Wasserstein (GW) is a powerful tool to compare probability measures whose supports are in different metric spaces. GW suffers however from a computational drawback since it requires to solve a complex non-convex quadratic program. We consider in this work a specific family of ground metrics, namely *tree metrics* for a space of supports of each probability measure in GW. By leveraging a tree structure, we propose to use *flows* from a root to each support to represent a probability measure whose supports are in a tree metric space. We consequently propose a novel tree variant of GW, namely flow-based tree GW (*FlowTGW*), by matching the flows of the probability measures. We then show that *FlowTGW* shares a similar structure as a univariate optimal transport distance. Therefore, *FlowTGW* is fast for computation and can scale up for large-scale applications. In order to further explore tree structures, we propose another tree variant of GW, namely depth-based tree GW (*DepthTGW*), by aligning the flows of the probability measures hierarchically along each depth level of the tree structures. Theoretically, we prove that both *FlowTGW* and *DepthTGW* are pseudo-distances. Moreover, we also derive tree-sliced variants, computed by averaging the corresponding tree variants of GW using random tree metrics, built adaptively in spaces of supports. Finally, we test our proposed discrepancies against other baselines on some benchmark tasks.

## 1. Introduction

Optimal transport (OT) theory provides a powerful set of tools to compare probability measures. OT has recently gained traction in machine learning community (Cuturi, 2013; Perrot et al., 2016; Genevay et al., 2016; Muzellec & Cuturi, 2018; Mena & Niles-Weed, 2019; Luise et al., 2019;

Alaya et al., 2019; Paty & Cuturi, 2019; Togninalli et al., 2019), and played an increasingly important role in several research areas such as computer graphics (Solomon et al., 2015; Bonneel et al., 2016; Lavenant et al., 2018; Solomon & Vaxman, 2019), domain adaptation (Courty et al., 2016; 2017; Bhushan Damodaran et al., 2018; Redko et al., 2019), and deep generative models (Arjovsky et al., 2017; Gulrajani et al., 2017; Genevay et al., 2018; Kolouri et al., 2019; Wu et al., 2019; Nadjahi et al., 2019) to name a few.

When probability measures are discrete and their supports belong to the same space, OT distance can be recasted as a linear program, which can be solved by standard interior-point method algorithms. However, these algorithms are not efficient when the number of supports is large. In order to account for the scalability of OT distance, Cuturi (2013) proposed to regularize OT by the entropy of transport plans, which result in entropic regularized OT. Several efficient algorithms have been proposed to solve the entropic problem recently (Altschuler et al., 2017; Dvurechensky et al., 2018; Lin et al., 2019; Altschuler et al., 2019).

When probability measures are discrete and their supports lie in different spaces, classical OT distance is no longer valid to measure their discrepancy. In the seminal work, Mémoli (2011) introduced Gromov-Wasserstein (GW) distance to compare probability measures whose supports are in different metric spaces. GW is defined based on the discrepancy between distance matrices of supports (i.e., pair-wise distances of supports) corresponding to the probability measures. GW has been used in several applications, including quantum chemistry (Peyré et al., 2016), computer graphics (Solomon et al., 2016), cross-lingual embeddings (Alvarez-Melis & Jaakkola, 2018; Grave et al., 2019), graph partitioning and matching (Xu et al., 2019a;b), and deep generative models (Bunne et al., 2019). However, since GW is a complex non-convex quadratic program and NP-hard for arbitrary inputs (Peyré & Cuturi, 2019) (§10.6.3), its computation is very costly, which hinders applications, especially in large-scale settings where the number of supports is large.

Reposing on the entropic regularization idea from OT, Peyré et al. (2016) proposed an entropic GW discrepancy. The entropic GW can be efficiently solved by Sinkhorn algorithm under certain cases of regularization parameter and a specific family of loss functions. Nevertheless, entropic GW

<sup>\*</sup>Equal contribution <sup>1</sup>RIKEN AIP <sup>2</sup>University of California, Berkeley <sup>3</sup>Kyoto University. Correspondence to: Tam Le <tam.le@riken.jp>.

requires the regularization to be sufficiently large for a fast computation, which leads to a poor approximation of GW. Following the direction of leveraging entropic regularization, Xu et al. (2019a;b) proposed algorithmic approaches to further speed up GW for graph data. Another approach for scaling up the computation of GW is sliced GW (Vayer et al., 2019), which relies on a one-dimensional projection of supports of the probability measures. Consequently, similar to sliced-Wasserstein, sliced GW albeit fast limits its capacity to capture high-dimensional structure in a distribution of supports (Liutkus et al., 2019; Le et al., 2019). Additionally, sliced GW can be only either applied for discrete measures with same number of supports and uniform weights, or required an artifact zero padding for measures having different number of supports (Vayer et al., 2019).

In this work, we consider a particular family of ground metrics, namely *tree metrics* for a space of supports of each probability measure in GW. Although it is well-known that one can leverage tree metrics to speed up a computation of arbitrary metrics (Bartal, 1996; 1998; Charikar et al., 1998; Indyk, 2001; Fakcharoenphol et al., 2004), our goal is rather to sample tree metrics for spaces of supports, and use them as ground metrics, similar to tree-(sliced)-Wasserstein (TSW) (Le et al., 2019). However, different to TSW, one may not apply this idea straightforwardly by only using tree metrics as ground metrics to scale up GW. Therefore, by exploiting a tree structure, we propose to leverage *flows* from a root to each support to represent a probability measure whose supports are in tree metric space, instead of pair-wise distances of supports as in traditional GW. Consequently, we propose a novel tree variant of GW, namely flow-based tree GW (*FlowTGW*), by matching the flows of the probability measures whose supports are in different tree metric spaces. *FlowTGW* is fast for computation and can scale up for large-scale applications due to sharing a similar structure as a univariate OT. In order to further explore tree structures, we propose to align the flows hierarchically along each depth level of the tree structures, namely depth-based tree GW (*DepthTGW*). Theoretically, we prove that both *FlowTGW* and *DepthTGW* are pseudo-metrics. Furthermore, we derive tree-sliced variants, computed by averaging the corresponding tree variants of GW using random tree metrics, sampled by a fast adaptive method, e.g., clustering-based tree metric sampling (Le et al., 2019) (§4).

The paper is organized as follows: we briefly review tree metrics and define tree GW for probability measures whose supports are in different tree metric spaces in §2. We propose two novel tree variants of GW: *FlowTGW* and *DepthTGW* in §3 and §4 respectively. In §5, we derive tree-sliced variants of GW for practical applications, and then evaluate our proposed discrepancies against other baselines on some benchmark tasks in §6 before concluding in §7.

**Notations.** We denote  $[n] = \{1, 2, \dots, n\}$ ,  $\forall n \in \mathbb{N}_+$ . Given  $x \in \mathbb{R}^d$ , let  $\|x\|_1$  be the  $\ell_1$ -norm of  $x$ , and  $\delta_x$  be the Dirac function at  $x$ . For a discrete probability measure  $\mu$ , denote  $|\mu|$  for the number of supports of  $\mu$ .

## 2. Tree Gromov-Wasserstein

In this section, we give a brief review about tree metric space, and define tree GW between probability measures whose supports are in different tree metric spaces.

### 2.1. Tree metric space

Given a tree  $\mathcal{T}$ , let  $d_{\mathcal{T}}$  be a tree metric on  $\mathcal{T}$ . The tree metric  $d_{\mathcal{T}}$  between two nodes in tree  $\mathcal{T}$  is equal to a length of the (unique) path between them (Semple & Steel, 2003) (§7, p.145–182). Given node  $x \in \mathcal{T}$ , let  $\Gamma(x)$  be the set of nodes in the subtree of  $\mathcal{T}$  rooted at  $x$ , i.e.,  $\Gamma(x) = \{z \in \mathcal{T} \mid x \in \mathcal{P}(r, z)\}$  where  $\mathcal{P}(r, z)$  is the (unique) path between root  $r$  and node  $z$  in  $\mathcal{T}$ ,  $\mathcal{S}(x)$  be the set of child nodes of  $x$ , and  $|\mathcal{S}(\cdot)|$  is the cardinality of set  $\mathcal{S}(\cdot)$ . Given an edge  $e$ , we write  $u_e$  and  $v_e$  for the nodes that are respectively at a shallower (closer to  $r$ ) and deeper (further away from  $r$ ) level of edge  $e$ , and  $w_e$  be the non-negative length of that edge. We illustrate those notions in Figure 1.

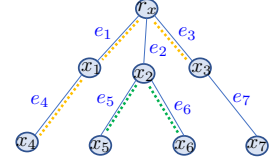


Figure 1. An illustration for a tree metric space.  $r_x$  is at depth level 1, while  $x_4, x_5, x_6, x_7$  are at depth level 3.  $\mathcal{P}(x_3, x_4)$  contains  $e_3, e_1, e_4$  (the orange dot path),  $\Gamma(x_2) = \{x_2, x_5, x_6\}$  (the green dot subtree), and  $\mathcal{S}(r_x) = \{x_1, x_2, x_3\}$ . For edge  $e_5$ ,  $v_{e_5} = x_5$  and  $u_{e_5} = x_2$ .

Throughout the paper, we are given two probability measures  $\mu = \sum_{i \in [k]} a_i \delta_{x_i}$  and  $\nu = \sum_{j \in [k']} b_j \delta_{z_j}$  whose supports  $x_i \mid_{i \in [k]}$  and  $z_j \mid_{j \in [k']}$  are in different tree metric spaces  $(\mathcal{T}_X, d_{\mathcal{T}_X})$  and  $(\mathcal{T}_Z, d_{\mathcal{T}_Z})$  respectively;  $a_i, b_j \in \mathbb{R}_+, \forall i \in [k], j \in [k']$ , and  $\sum_{i \in [k]} a_i = \sum_{j \in [k']} b_j = 1$ . Our goal is to define discrepancies between these probability measures.

### 2.2. Tree Gromov-Wasserstein

Let tree GW be GW distance between probability measures whose supports are in different tree metric spaces. Therefore, tree GW between  $\mu$  and  $\nu$  takes the following form:

$$\mathcal{GW}^2(\mu, \nu) := \min_{T \in \Pi(\mu, \nu)} \sum_{i, j, i', j'} |d_{\mathcal{T}_X}(x_i, x_{i'}) - d_{\mathcal{T}_Z}(z_j, z_{j'})|^2 T_{ij} T_{i'j'}, \quad (1)$$

where  $\Pi(\mu, \nu) := \left\{ T \in \mathbb{R}_+^{k \times k'} \mid \sum_{j \in [k']} T_{ij} = a_i, \sum_{i \in [k]} T_{ij} = b_j, \forall i \in [k], j \in [k'] \right\}$  is a set of the transport plans between  $\mu$  and  $\nu$ ;  $d_{\mathcal{T}_X}(x_i, x_{i'}) \mid_{i, i'}$  and

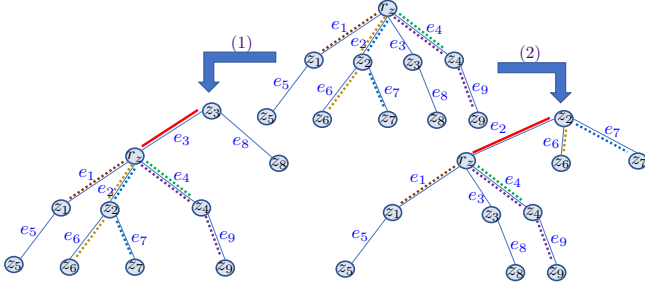


Figure 2. An illustration for an efficient computation for *FlowTGW*. Given a measure  $\nu = b_1\delta_{z_1} + b_2\delta_{z_6} + b_3\delta_{z_7} + b_4\delta_{z_4} + b_5\delta_{z_9}$ , when the new root  $\bar{r}_z = z_3$  ( $z_3$  is in the subtree rooted at  $z_3$ , and not containing any supports of  $\nu$ ), the order of  $d_T(r_z, z_i) |_{z_i \in \nu}$  is the same as that of  $d_T(z_3, z_i) |_{z_i \in \nu}$ , and  $d_T(z_3, z_i) = d_T(r_z, z_i) + d_T(r_z, z_3), \forall z_i \in \nu$  (a.k.a. Case 1, illustrated in the left bottom tree). Additionally, when the new root  $\bar{r}_z = z_2$  ( $z_2$  is in the subtree rooted at  $z_2$ , and containing supports  $\Omega_\nu = \{z_6, z_7\}$  in  $\nu$ ), the order of  $d_T(r_z, z_i) |_{z_i \in \nu, z_i \notin \Omega_\nu}$  is the same as that of  $d_T(z_3, z_i) |_{z_i \in \nu, z_i \notin \Omega_\nu}$ , and  $d_T(z_2, z_i) = d_T(r_z, z_i) + d_T(r_z, z_3), \forall z_i \in \nu, z_i \notin \Omega_\nu$  (a.k.a Case 2, illustrated in the right bottom tree).

$d_{T_Z}(z_j, z_{j'}) |_{j, j'}$  are pair-wise distances of supports, i.e., distance matrices of supports, represented for  $\mu$  and  $\nu$  respectively.

However, one may not scale up GW by straightforwardly using tree metrics as ground metrics for supports of probability measures as in Equation (1) like TSW (Le et al., 2019). Therefore, we propose to leverage tree structure to form a novel representation for a probability measure based on *flows* from a root to each support to scale up GW. Consequently, we propose two novel variants of tree GW: *FlowTGW* and *DepthTGW*, detailed in §3 and §4 respectively. Especially, one can further scale up their computation by directly sampling *aligned-root tree metrics* in applications without priori knowledge about tree metrics for probability measures.

### 3. Flow-based tree GW discrepancy

In this section, we study a variant of tree GW, named flow-based tree GW (*FlowTGW*) discrepancy.

#### 3.1. Definition of flow-based tree GW

Different from the tree GW, *FlowTGW* takes into account tree structures to represent probability measures whose supports are in tree metric spaces.

**Definition 1.** The flow-based tree Gromov-Wasserstein discrepancy between two probability measures  $\mu$  and  $\nu$  is defined as follows:

$$\mathcal{GW}_{T_f}^2(\mu, \nu) := \min_{r_x, r_z, T \in \Pi(\mu, \nu)} \sum_{i, j} |d_{T_X}(r_x, x_i) - d_{T_Z}(r_z, z_j)|^2 T_{ij}. \quad (2)$$

As indicated in Definition 1, each probability measure in *FlowTGW* is represented by tree metric, i.e., the unique path (or *flow*) length, from a root to each support while a weight of each support can be regarded as a mass of a corresponding *flow*. Additionally, the minimization with roots  $r_x$  and  $r_z$  in Equation (2) is to ensure an optimal alignment for a pair of roots  $r_x$  and  $r_z$  in trees  $\mathcal{T}_X$  and  $\mathcal{T}_Z$  respectively. Similar to tree GW, we also determine an optimal transport plan  $T^*$  between  $\mu$  and  $\nu$  when computing *FlowTGW*  $\mathcal{GW}_{T_f}(\mu, \nu)$ .

**Theorem 1.** *FlowTGW* is a pseudo-distance.

See the supplementary for the proof of Theorem 1.

#### 3.2. Efficient computation for flow-based tree GW

A naive implementation for  $\mathcal{GW}_{T_f}$  has a complexity  $O(N^3 \log N)$  where  $N$  is the number of nodes in tree, if one exhaustively searches the optimal pair of roots for  $\mathcal{T}_X$  and  $\mathcal{T}_Z$ <sup>1</sup>. In this section, we present an efficient computation approach which reduces this complexity into nearly  $O(N^2)$ .

Consider *FlowTGW*  $\mathcal{GW}_{T_f}$  between two probability measures  $\mu, \nu$  in two different tree metric space  $\mathcal{T}_X, \mathcal{T}_Z$  rooted at  $r_x, r_z$  respectively. When one changes into the new root  $\bar{r}_z$  for tree  $\mathcal{T}_Z$ , as illustrated in Figure 2, there are two cases that can happen:

**Case 1:** The new root  $\bar{r}_z$  is one of the nodes in the subtree rooted at a node in  $\mathcal{S}(r_z)$ , which does not contain any supports in  $\nu$ , illustrated in the left-bottom of Figure 2. Then, for all supports  $z_i \in \nu$ , we have

$$d_{T_Z}(\bar{r}_z, z_i) = d_{T_Z}(r_z, z_i) + d_{T_Z}(\bar{r}_z, r_z). \quad (3)$$

Consequently, the order of the length of the path from root to each support does not change.

**Case 2:** The new root  $\bar{r}_z$  is one of the nodes in the subtree rooted at a node in  $\mathcal{S}(r_z)$ , containing some of the supports in  $\nu$ , named as  $\Omega_\nu$ , illustrated in the right-bottom of Figure 2. Then, for all supports  $z_j$  in  $\nu$ , except  $z_i \in \Omega_\nu$ , we have the same formulation as Equation (3), i.e.,  $d_{T_Z}(\bar{r}_z, z_j) = d_{T_Z}(r_z, z_j) + d_{T_Z}(\bar{r}_z, r_z)$ . Consequently, the order of the length of the path from the root to each support (except  $z_i \in \Omega_\nu$ ) is preserved. For supports in  $\Omega_\nu$  (illustrated in the supplementary), there are three following sub-cases:

- **Case 2a:** For supports  $z_i \in \Omega_\nu$  which  $\bar{r}_z \in \mathcal{P}(r_z, z_i)$ , we have  $d_{T_Z}(\bar{r}_z, z_i) = d_{T_Z}(r_z, z_i) - d_{T_Z}(r_z, \bar{r}_z)$ . Therefore, the path-length order of those supports are preserved.
- **Case 2b:** For supports  $z_i \in \Omega_\nu$  which  $z_i \in \mathcal{P}(r_z, \bar{r}_z)$ , we have  $d_{T_Z}(\bar{r}_z, z_i) = d_{T_Z}(r_z, \bar{r}_z) - d_{T_Z}(r_z, z_i)$ . Therefore, the path-length order of those supports are reversed.
- **Case 2c:** For supports  $z_i \in \Omega_\nu$  which  $\bar{r}_z \notin \mathcal{P}(r_z, z_i)$  and  $z_i \notin \mathcal{P}(r_z, \bar{r}_z)$ , one needs to find the corresponding closest common ancestor  $\zeta_i$  of  $\bar{r}_z$  and  $z_i$ , i.e.,  $\zeta_i$  is on both paths  $\mathcal{P}(r_z, \bar{r}_z)$  and  $\mathcal{P}(r_z, z_i)$ , so we have  $d_{T_Z}(\bar{r}_z, z_i) =$

<sup>1</sup>More details about the complexity of (aligned-root) *FlowTGW* are given in §3.3, and in the supplementary.

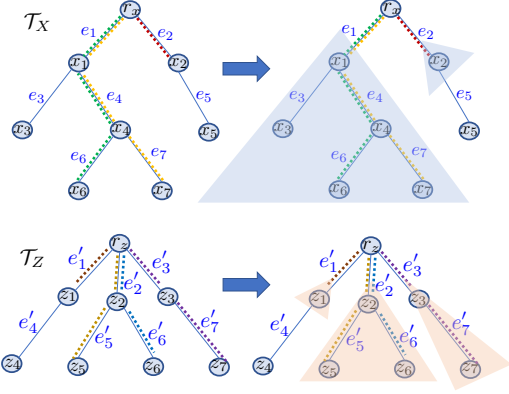


Figure 3. An illustration for the aligned-root  $\widehat{\mathcal{GW}}_{T_d}$  between  $\mu = a_1\delta_{x_6} + a_2\delta_{x_7} + a_3\delta_{x_2}$  on  $\mathcal{T}_X$  and  $\nu = b_1\delta_{z_1} + b_2\delta_{z_5} + b_3\delta_{z_6} + b_4\delta_{z_7}$  on  $\mathcal{T}_Z$ . In  $\widehat{\mathcal{GW}}_{T_d}$ , we consider the optimal alignment at each depth level. At depth level 1, root  $r_x$  is trivially aligned for root  $r_z$ . Since both  $r_x$  and  $r_z$  have their child nodes, the optimal alignment between  $r_x$  and  $r_z$  is recursive into depth level 2. For  $\mu$  in  $\mathcal{T}_X$ , root  $r_x$  has 2 subtrees rooted at  $x_1$  and  $x_2$ , considered as “leaves”. Therefore, for the 2-depth-level tree  $\mathcal{T}_{r_x}^2$ ,  $V(\mathcal{T}_{r_x}^2)$  contains 3 nodes:  $r_x$ ,  $x_1$ , and  $x_2$ , and  $\mu_{\mathcal{T}_{r_x}^2} = (a_1 + a_2)\delta_{x_1} + a_3\delta_{x_2}$ . Similarly, for  $\nu$  in  $\mathcal{T}_Z$ ,  $\nu_{\mathcal{T}_{r_z}^2} = b_1\delta_{z_1} + (b_2 + b_3)\delta_{z_2} + b_4\delta_{z_3}$ . The recursive procedure is repeated until the deepest level of the lower tree where there exists only simple cases (i.e., at least one of an aligned pair of nodes does not have any child nodes, or sum of weights of child nodes in corresponding 2-depth-level tree is 0).

$d_{\mathcal{T}_Z}(r_z, \bar{r}_z) + d_{\mathcal{T}_Z}(r_z, z_i) - 2d_{\mathcal{T}_Z}(r_z, \zeta_i)$ . Note that the path-length order of supports having the same  $\zeta_i$  is preserved.

Therefore, one only needs to merge these ordered arrays with the complexity nearly  $O(N)$  (except the degenerated case where each array has only 1 node).

From the above observation, one may not need to sort for the tree metrics between the new root  $\bar{r}_z$  and each support in  $\nu$  by leveraging the sorted order of the tree metrics between the root  $r_z$  and each support. Moreover, those computational steps can be done separately for each tree. Therefore, the complexity of  $\mathcal{GW}_{T_f}$  reduces from  $O(N^3 \log N)$  into nearly  $O(N^2)$ . More details can be seen in the supplementary.

### 3.3. Aligned-root flow-based tree GW

In this section, we consider a special case of  $\text{FlowTGW}$   $\mathcal{GW}_{T_f}$  where roots have been already aligned. Therefore, we can leave out minimization step with roots in Definition 1, and name this discrepancy as aligned-root  $\text{FlowTGW}$ .

**Definition 2.** Assume that root  $r_x$  in  $\mathcal{T}_X$  is aligned with root  $r_z$  in  $\mathcal{T}_Z$ . Then, the aligned-root flow-based tree GW discrepancy between  $\mu$  and  $\nu$  is defined as follow:

$$\widehat{\mathcal{GW}}_{T_f}^2(\mu, \nu; r_x, r_z) := \min_{T \in \Pi(\mu, \nu)} \sum_{i,j} |d_{\mathcal{T}_X}(r_x, x_i) - d_{\mathcal{T}_Z}(r_z, z_j)|^2 T_{ij}. \quad (4)$$

The  $\widehat{\mathcal{GW}}_{T_f}$  in Equation (4) is equivalent to the univariate Wasserstein distance between  $\tilde{\mu} := \sum_i a_i \delta_{d_{\mathcal{T}_X}(r_x, x_i)}$  and  $\tilde{\nu} := \sum_j b_j \delta_{d_{\mathcal{T}_Z}(r_z, z_j)}$ , i.e.,  $\widehat{\mathcal{GW}}_{T_f}^2(\mu, \nu; r_x, r_z) = W_2^2(\tilde{\mu}, \tilde{\nu})$  where we denote  $W_2$  as the 2<sup>nd</sup>-Wasserstein distance (Villani, 2003). Moreover, the univariate Wasserstein is equal to the integral of the absolute difference between the generalized quantile functions of these two univariate probability distributions (Santambrogio, 2015) (§2). Therefore, one only needs to sort  $d_{\mathcal{T}_X}(r_x, x_i) |_{i}$ , and  $d_{\mathcal{T}_Z}(r_z, z_j) |_{j}$  for the computation of  $\widehat{\mathcal{GW}}_{T_f}$ , i.e., linearithmic complexity. Due to sharing the same structure as a univariate Wasserstein distance,  $\widehat{\mathcal{GW}}_{T_f}$  inherits the same properties as those of the univariate Wasserstein distance. More precisely,  $\widehat{\mathcal{GW}}_{T_f}(\mu, \nu; r_x, r_z) = 0$  is equivalent to  $\tilde{\mu} \equiv \tilde{\nu}$ ;  $\widehat{\mathcal{GW}}_{T_f}$  is symmetric and satisfies triangle inequality. See the supplementary for an illustration of aligned-root  $\text{FlowTGW}$ .

Note that in practical applications where we usually do not have priori knowledge about tree metrics for spaces of supports of probability measures, we need to sample tree metrics for each support data space. Moreover, we can *directly sample aligned-root tree metrics*, e.g., by choosing means of support data distributions as roots when using the clustering-based tree metric sampling (Le et al., 2019) (§4). Consequently, we can use aligned-root  $\text{FlowTGW}$  formulation to reduce the complexity of  $\text{FlowTGW}$ .

**Aligned-root  $\text{FlowTGW}$  barycenter.** The aligned-root  $\text{FlowTGW}$  can be handily used for a barycenter problem, especially in large-scale applications. Given  $m$  probability measures  $\mu_i |_{i \in [m]}$  whose supports are in different tree metric spaces  $(\mathcal{T}_{X_i}, d_{\mathcal{T}_{X_i}}) |_{i \in [m]}$  with aligned-roots  $r_{x_i} |_{i \in [m]}$  respectively, and corresponding weights  $p_i |_{i \in [m]}$ , the aligned-root  $\text{FlowTGW}$  barycenter problem aims to find a flow-based tree structure representation  $\Delta_{\bar{\mu}} := \{d_{\mathcal{T}_X}(r_x, x_i), a_i\}_{i \in [k]}$  of an optimal probability measure  $\bar{\mu}$  whose number of supports is less than or equal to  $k$  in tree metric space  $(\mathcal{T}_X, d_{\mathcal{T}_X})$  that takes the form:

$$\Delta_{\bar{\mu}} \in \arg \min_{\Delta_{\bar{\mu}}} \left( \sum_{i=1}^m p_i \widehat{\mathcal{GW}}_{T_f}^2(\mu, \mu_i; r_x, r_{x_i}) \right), \quad (5)$$

where the roots  $r_{x_i}$  in  $\mathcal{T}_{X_i} |_{i \in [m]}$  are aligned with root  $r_x$  in  $\mathcal{T}_X$ . The barycenter problem in Equation (5) is equivalent to the free-support univariate Wasserstein barycenter which is efficiently solved, e.g., by using Algorithm 2 in (Cuturi & Doucet, 2014).

## 4. Depth-based tree GW discrepancy

$\text{FlowTGW}$  only focuses on flows from a root to each support, but ignores information about the depth level of supports in tree structures. In this section, we take into account the depth level of supports, and propose depth-based



tree GW (*DepthTGW*) discrepancy  $\mathcal{GW}_{T_d}$ . In particular, *DepthTGW* considers the alignment problem for flows hierarchically for each depth level along the tree structures.

We first introduce some necessary definitions to define  $\mathcal{GW}_{T_d}$ . Recall that given a node  $x$  in tree  $\mathcal{T}$ ,  $\mathcal{S}(x)$  is a set of child nodes of  $x$ .

**Definition 3.** Given a node  $x$  in tree  $\mathcal{T}$ , a 2-depth-level tree  $\mathcal{T}(x, \mathcal{S}(x))$ , or shortened as  $\mathcal{T}_x^2$ , is defined in  $\mathcal{T}$  rooted at  $x$ , i.e., root  $x$  is at depth level 1, and  $|\mathcal{S}(x)|$  subtrees rooted at  $\bar{x} \mid_{\bar{x} \in \mathcal{S}(x)}$ , considered as “leaves” at depth level 2 in  $\mathcal{T}_x^2$ .

Following Definition 3 for the 2-depth-level tree  $\mathcal{T}_x^2$ , let  $V(\mathcal{T}_x^2)$  be the set of vertices of  $\mathcal{T}_x^2$ , then  $V(\mathcal{T}_x^2)$  contains  $x$  and all  $\bar{x} \in \mathcal{S}(x)$ . Moreover, given  $\mu$  in  $\mathcal{T}$ , we have a corresponding  $\mu_{\mathcal{T}_x^2}$  in  $\mathcal{T}_x^2$ , defined as follow:  $\mu_{\mathcal{T}_x^2} = \sum_i \bar{a}_i \delta_{\bar{x}_i}$  where  $\bar{x}_i \in V(\mathcal{T}_x^2)$ , and  $\bar{a}_i = \mu(\Gamma(\bar{x}_i)) / \mu(\Gamma(x))$  if  $\bar{x}_i \neq x$ , otherwise  $\bar{a}_i = 1 - \left[ \sum_{\bar{x}_j \in \mathcal{S}(x)} \mu(\Gamma(\bar{x}_j)) \right] / \mu(\Gamma(x))$ .

In order to define *DepthTGW*, we start with its special case when roots are aligned.

**Definition 4.** Assume that root  $r_x$  in  $\mathcal{T}_X$  is aligned with root  $r_z$  in  $\mathcal{T}_Z$ . Then, the aligned-root depth-based tree GW discrepancy between two probability measures  $\mu$  and  $\nu$  is defined as follows:

$$\widehat{\mathcal{GW}}_{T_d}(\mu, \nu; r_x, r_z) := \sum_h \sum_{(x,z) \in \mathcal{M}_{h-1}} T_{h-1}^*(x, z) \widehat{\mathcal{GW}}_{T_f}(\mu_{\mathcal{T}_x^2}, \nu_{\mathcal{T}_z^2}; x, z), \quad (6)$$

where  $h$  is the considered depth level, starting from 2 to the deepest level of the lower tree between  $\mathcal{T}_X$  and  $\mathcal{T}_Z$ ;  $\mathcal{M}_h$  is a set of optimal aligned pairs at the depth level  $h$  where  $\mathcal{M}_1 = \{(r_x, r_z)\}$ ;  $T_h^*(x, z)$  is the optimal matching mass for the pair  $(x, z)$  at the depth level  $h$  where  $T_1^*(r_x, r_z) = 1$ .

Intuitively, at each depth level, we consider the alignment for the corresponding 2-depth-level trees. Note that the 2-depth-level tree structures are at the same depth level  $h$  for both  $\mathcal{T}_X$  and  $\mathcal{T}_Z$ , and one can consider  $\widehat{\mathcal{GW}}_{T_f}$  for the alignment. Moreover, at depth level 1,  $\widehat{\mathcal{GW}}_{T_d}$  trivially matches  $r_x$  to  $r_z$  with optimal matching mass 1. Thus, the matching procedure is recursive along all depth levels in trees. The simple case of the recursive procedure is that at least one node of the considered pair  $(x, z)$  does not have child nodes, or sum of weights of child nodes in the corresponding 2-depth-level tree is equal to 0.

When we would like an optimal alignment between the roots of trees  $\mathcal{T}_X$  and  $\mathcal{T}_Z$ , we have:

$$\mathcal{GW}_{T_d}(\mu, \nu) := \min_{r_x, r_z} \widehat{\mathcal{GW}}_{T_d}(\mu, \nu; r_x, r_z). \quad (7)$$

The above discrepancy is referred to as *DepthTGW*. Similar to *FlowTGW*, we have a following theorem:

**Theorem 2.** *DepthTGW* is a pseudo-distance.

See the supplementary material for the proof of Theorem 2.

## 5. Tree-sliced variants of GW by sampling tree metrics

Similar to tree-sliced-Wasserstein distance (Le et al., 2019) (or sliced-Wasserstein (Rabin et al., 2011), sliced-GW (Vayer et al., 2019)), computing (aligned-root) *FlowTGW/DepthTGW* requires to choose or sample tree metrics for each space of supports. We use fast adaptive methods, e.g., clustering-based tree metric sampling (Le et al., 2019), to sample tree metrics for a space of supports, and further average the corresponding (aligned-root) *FlowTGW/DepthTGW* using those random tree metrics.

**Definition 5.** Given two probability measures  $\mu, \nu$  supported on a set in which tree metric spaces  $\{(\mathcal{T}_{X_i}, d_{\mathcal{T}_{X_i}}) \mid i \in [n]\}$  and  $\{(\mathcal{T}_{Z_i}, d_{\mathcal{T}_{Z_i}}) \mid i \in [n]\}$  can be defined respectively, the (aligned-root) flow/depth-based tree-sliced GW is defined as an average of corresponding (aligned-root) flow/depth-based tree GW for  $\mu, \nu$  on tree metric spaces  $(\mathcal{T}_{X_i}, d_{\mathcal{T}_{X_i}})$ , and  $(\mathcal{T}_{Z_i}, d_{\mathcal{T}_{Z_i}})$  respectively.

As discussed in (Le et al., 2019), the average over several random tree metrics can help to reduce quantization effects, or clustering sensitivity problems in which data points may be partitioned or clustered to adjacent but different hypercubes or clusters respectively in tree metric sampling. Moreover, note that the complexity of tree metric sampling is negligible compared to that of GW computation. Indeed, the complexity of the clustering-based tree metric sampling is  $O(H_{\mathcal{T}} m \log \kappa)$  when one fixes the same number of clusters  $\kappa$  for the farthest-point clustering (Gonzalez, 1985) and sets  $H_{\mathcal{T}}$  for the predefined deepest level of tree  $\mathcal{T}$ , and  $m$  is the number of input data points.

**Remark 1.** For specific applications with priori knowledge about tree metrics for probability measures, one can apply *FlowTGW*, or consider *DepthTGW* in case the known tree structure for each probability measure is important for the applications. Moreover, if roots of those known tree metrics are already aligned, one can use the corresponding aligned-root formulations to reduce the complexity. For general applications without priori knowledge about tree metrics for probability measures, one can directly sample aligned-root tree metrics, e.g., by choosing a mean of support data as its root for the clustering-based tree metric sampling (Le et al., 2019), and use the aligned-root formulations for an efficient computation of the proposed tree variants of GW.

## 6. Experiments

We evaluate our proposed *FlowTGW* and *DepthTGW* discrepancies for quantum chemistry and document classification with *randomly linear transform* word embed-

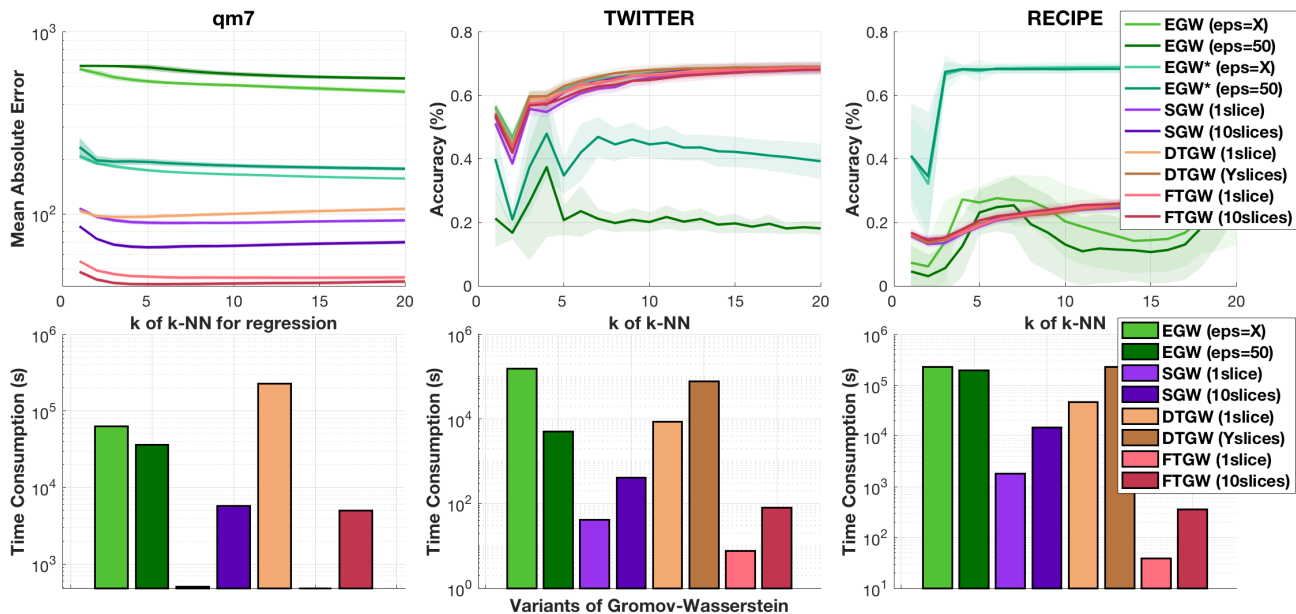


Figure 4. Results of MAE and time consumption for  $k$ -NN regression in  $qm7$  dataset, and results of averaged accuracy and time consumption for  $k$ -NN in TWITTER and RECIPE datasets. For EGW/EGW\* ( $\text{eps}=X$ ) where  $\text{eps}$  is the value of entropic regularization, we use  $X = 5$  for  $qm7$  and TWITTER, and  $X = 10$  for RECIPE (too slow with  $X = 5$  for RECIPE). For DTGW, we use  $Y = 10$  for TWITTER,  $Y = 5$  for RECIPE, and only 1 slice in  $qm7$  due to its slowness. For clustering-based tree metric sampling, we used its suggested parameters ( $\kappa = 4$ ,  $H_T = 6$ ).

dings. In addition, we also carry out the large-scale *FlowTGW* barycenter problem within  $k$ -means clustering for point clouds of handwritten digits in MNIST dataset rotated arbitrarily in the plane as in (Peyré et al., 2016).

**Setup.** We consider three following baselines: (i) entropic GW (EGW) (Peyré et al., 2016), (ii) a variant of entropic GW (EGW\*) which we only use the entropic regularization to optimize transport plan, but exclude it when computing GW discrepancy, and (iii) sliced GW (SGW) (Vayer et al., 2019). In all of our experiments, we do not have priori knowledge about tree metrics for probability measures. Therefore, we sample aligned-root tree metrics from support data points by applying the clustering-based tree metric approach (Le et al., 2019) where means of support data points are chosen as tree roots. Consequently, we can use the aligned-root formulations for both *FlowTGW* (FTGW) and *DepthTGW* (DTGW) to reduce their complexity. For sliced GW, since it can be only applied for discrete measures with same number of supports and uniform weights (Vayer et al., 2019) (§3), we follow Vayer et al. (2019) to add zero padding when discrete measures have different numbers of supports. We further use the binomial expansion trick to reduce its complexity (Vayer et al., 2019). For entropic GW and its variant, we use the log-stabilized Sinkhorn (Schmitzer, 2019) when optimizing transport plan<sup>2</sup>. In general, when entropic regularization becomes smaller, the

quality of entropic GW and its variant is better, but their computation is considerably slower. In our experiments, the computation for entropic GW is either usually blown up, or too slow for evaluation when entropic regularization is less than or equal 1. We run experiments with Intel Xeon CPU E7-8891v3 (2.80GHz), and 256GB RAM. Reported time consumption for all methods has already included their corresponding preprocessing, e.g., tree metric sampling for *FlowTGW* and *DepthTGW*, or one-dimensional projection for sliced GW.

## 6.1. Applications

**Quantum chemistry.** We carry out a regression problem on molecules for  $qm7$  dataset as in (Peyré et al., 2016). The task is to predict atomization energies for molecules based on similar labeled molecules instead of estimating them through expensive numerical simulations (Rupp et al., 2012; Peyré et al., 2016). For simplicity, we only used the relative locations in  $\mathbb{R}^3$  of atoms in molecules, *without information about atomic nuclear charges* as the experiments in (Rupp et al., 2012; Peyré et al., 2016). There are 7165 molecules in  $qm7$  dataset. Each molecule has no more than 23 atoms. We randomly split 80%/20% for training and test sets, and repeat 20 times. Following Peyré et al. (2016), we use a  $k$ -nearest neighbor ( $k$ -NN) regression approach.

**Document classification with non-registered word embeddings.** We next evaluate our proposed *FlowTGW* and *DepthTGW* for document classification with non-registered

<sup>2</sup>Available at <https://github.com/gpeyre/2016-ICML-gromov-wasserstein>

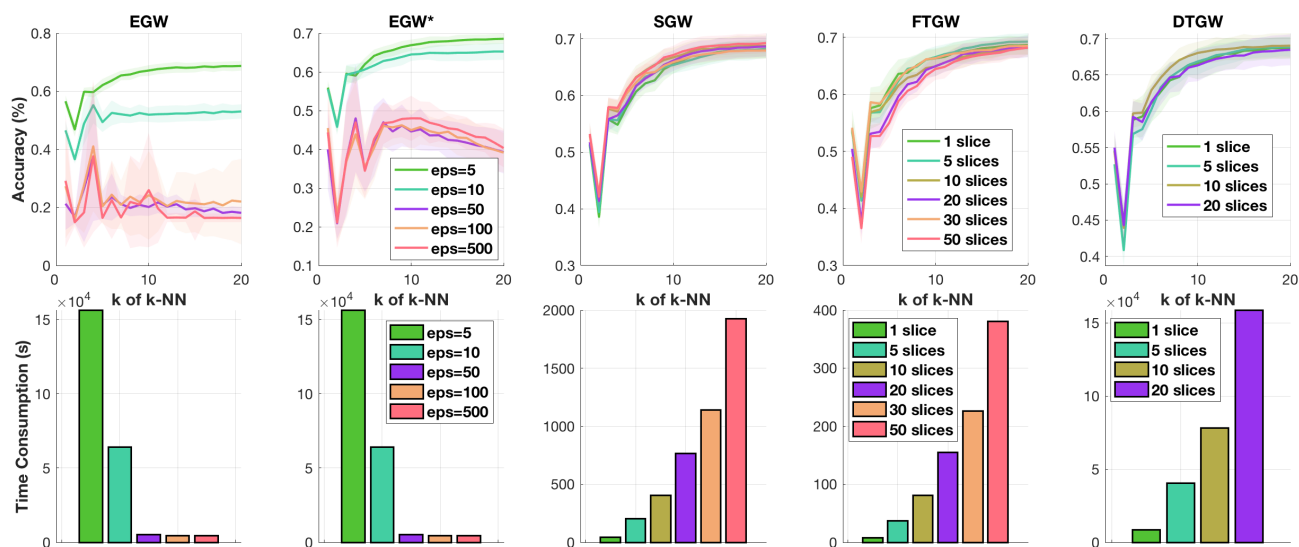


Figure 5. Results of averaged accuracy and time consumption for variants of GW with different parameters (e.g., entropic regularization in EGW/EGW\*, and the number of slices in SGW/FTGW/DTGW) in  $k$ -NN in TWITTER dataset. For clustering-based tree metric sampling, we used its suggested parameters ( $\kappa = 4$ ,  $H_T = 6$ ).

word embeddings in TWITTER and RECIPE datasets. For each document in these datasets, we use a *randomly linear transform* for *word2vec* word embedding (Mikolov et al., 2013), pre-trained on Google News<sup>3</sup>, containing about 3 million words/phrases. *word2vec* maps each word/phrase into a 300-dimensional vector. Following (Kusner et al., 2015; Le et al., 2019), we remove SMART stop words (Salton & Buckley, 1988), and also drop words in documents if they are not in the pre-trained *word2vec*. After preprocessing, there are 3108 documents in 3 classes where each document length is not more than 29 in TWITTER dataset, and 4370 documents in 15 classes where each document length is not more than 628 in RECIPE dataset. We randomly split 80%/20% for training and test sets, and repeat 20 times.

### Performance results, time consumption and discussions.

The results of averaged mean absolute value (MAE) for different  $k$  in  $k$ -NN regression, and time consumption of quantum chemistry in *qm7* dataset are illustrated in the first column of Figure 4, while the results of averaged accuracy for different  $k$  in  $k$ -NN, and time consumption of document classification with non-registered word embeddings in TWITTER and RECIPE datasets are shown in the second and third columns of Figure 4 respectively. The computational time of *FlowTGW* is at least comparative to that of sliced GW, and much faster than that of entropic GW. Especially, in RECIPE dataset, it took less than 6 minutes for *FlowTGW* (10 slices), while more than 4 hours for sliced GW (10 slices), and more than 2 days for entropic GW (even with entropic regularization  $\text{eps}=50$ ). Moreover, the performances of *FlowTGW* compare favorably with other baselines, except the variant of entropic GW in RECIPE dataset.

For *DepthTGW*, its performances are comparative with other baselines. However, *DepthTGW* is slow in practice due to solving a large number of sub-problems, i.e., aligned-root *FlowTGW* between corresponding 2-depth-level trees. We observe that the variant of entropic GW improves the performances of entropic GW. Therefore, the entropic term in entropic GW computation may harm its performances in applications, e.g., in *qm7* and RECIPE datasets. For entropic GW and its variants, their performances are improved when their entropic regularization is smaller, but their computational time is considerably increased. For example, in TWITTER dataset, the performances of entropic GW and its variants are comparative with other variants of GW, but their entropic regularization should be small enough (i.e.,  $\text{eps}=5$ ) which makes their computation about 1, 4, 5 order(s) slower than those of *DepthTGW*, sliced GW, *FlowTGW* respectively (for 1 slice). For sliced GW, when the lengths of documents are large, e.g., in RECIPE dataset, its computational time is slow down since it requires to use extra artificial zeros padding and uniform weights for probability measures with different number of supports (i.e., documents with different lengths), while note that other variants of GW work with an original number of supports (i.e., unique words in documents), and general weights (i.e., frequencies of unique words) for supports in probability measures.

Additionally, we show the trade-off between performances and time consumption for those variants of GW when their parameters, e.g., the entropic regularization in entropic GW and its variant, the number of slices in sliced GW, *FlowTGW* and *DepthTGW*, are changed for TWITTER dataset in Figure 5. Moreover, we also illustrate performances and time consumption of *FlowTGW* (10 slices) with different parameters of the clustering-based tree metric sam-

<sup>3</sup><https://code.google.com/p/word2vec>

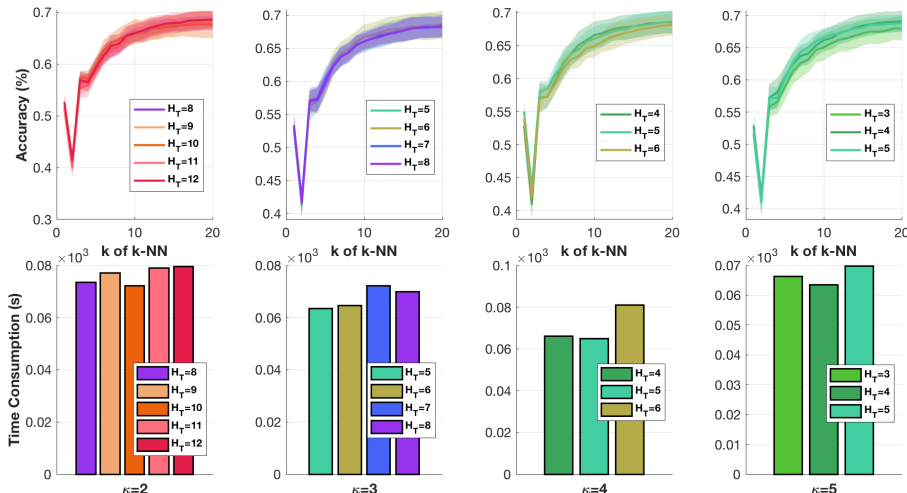


Figure 6. Results of averaged accuracy and time consumption for *FlowTGW* (10 slices) with different parameters (e.g., the predefined deepest level  $H_{\mathcal{T}}$ , the number of clusters  $\kappa$ ) in the clustering-based tree metric sampling in TWITTER dataset.

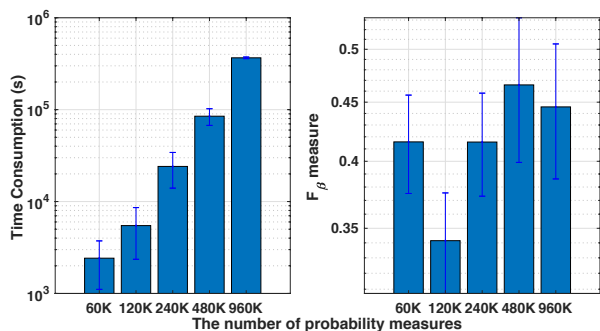


Figure 7. Results of time consumption and  $F_{\beta}$  measure for  $k$ -means clustering with *FlowTGW* for randomly rotated point clouds of handwritten digits in MNIST dataset.

pling (e.g., the predefined deepest level  $H_{\mathcal{T}}$ , the number of clusters  $\kappa$  for the farthest-point clustering) in TWITTER dataset in Figure 6. Similar to tree metric sampling for tree-(sliced)-Wasserstein (Le et al., 2019), we also observe that the clustering-based tree metric sampling for *FlowTGW* and *DepthTGW* is fast and its time consumption is negligible compared to that of either *FlowTGW* or *DepthTGW*. For examples, for each tree metric sampling with the suggested parameters ( $H_{\mathcal{T}} = 6, \kappa = 4$ ), it only took about 0.4 seconds for *qm7* dataset, 1.5 seconds for TWITTER dataset, and 11.0 seconds for RECIPE dataset. Many further experimental results can be seen in the supplementary.

## 6.2. Large-scale *FlowTGW* barycenter within $k$ -means clustering

We applied *FlowTGW* barycenter (§3.3), using Algorithm 2 in (Cuturi & Doucet, 2014) where we set  $k = 100$  for the maximum number of supports in barycenters, into a larger machine learning pipeline such as  $k$ -means clustering on MNIST dataset where point clouds of handwritten digits are rotated arbitrarily in the plane as in (Peyré et al., 2016).

For each handwritten digit, we randomly extracted 6000 point clouds. We evaluated  $k$ -means with *FlowTGW* for 60000, 120000, 240000, 480000, and 960000 handwritten-digit point clouds where each handwritten digit is randomly rotated 1, 2, 4, 8, and 16 times respectively. Furthermore, we grouped the handwritten digit 6 and digit 9 together due to applying random rotation. We used  $k$ -means++ initialization technique (Arthur & Vassilvitskii, 2007), set 20 for the maximum iterations of  $k$ -means, and repeated 10 times with different random seeds for  $k$ -means++ initialization. In Figure 7, we show the averaged time consumption and  $F_{\beta}$  measure (Manning et al., 2008) where  $\beta$  is chosen as in (Le & Cuturi, 2015) for the results of  $k$ -means clustering with *FlowTGW*. Note that, in these settings, the barycenter problem from entropic GW and its entropic variant has extremely slow running time.

## 7. Conclusion

We proposed in this paper two novel tree variants of GW, i.e., *FlowTGW* and *DepthTGW*, between probability measures whose supports are in different metric spaces by considering a particular family of ground metrics, namely tree metrics. By leverage a tree structure, we proposed an effective representation for probability measures whose supports are in tree metric space, e.g., flows from a root to each support instead of traditional pair-wise distances of supports for probability measures to scale up GW. Especially, the proposed *FlowTGW* is not only very fast, but its performances also compare favorably with other variants of GW. Moreover, the *FlowTGW* can be applied for large-scale applications (e.g., a million probability measures) which are usually prohibited for entropic GW. The questions about sampling efficiently tree metrics from support data points for the tree variants of GW, or using them for more involved parametric inference are left for future work.



## Acknowledgement

We would like to thank Marco Cuturi for helpful discussion. TL acknowledges the support of JSPS KAKENHI Grant number 17K12745.

## References

- Ahuja, R. K., Magnanti, T. L., and Orlin, J. B. Network flows. 1988.
- Alaya, M. Z., Berar, M., Gasso, G., and Rakotomamonjy, A. Screening Sinkhorn algorithm for regularized optimal transport. In *Advances in Neural Information Processing Systems*, pp. 12169–12179. 2019.
- Altschuler, J., Weed, J., and Rigollet, P. Near-linear time approximation algorithms for optimal transport via Sinkhorn iteration. In *Advances in neural information processing systems*, pp. 1964–1974, 2017.
- Altschuler, J., Bach, F., Rudi, A., and Niles-Weed, J. Massively scalable Sinkhorn distances via the Nyström method. In *Advances in Neural Information Processing Systems*, pp. 4429–4439, 2019.
- Alvarez-Melis, D. and Jaakkola, T. Gromov-Wasserstein alignment of word embedding spaces. In *Proceedings of the Conference on Empirical Methods in Natural Language Processing (EMNLP)*, pp. 1881–1890, 2018.
- Arjovsky, M., Chintala, S., and Bottou, L. Wasserstein generative adversarial networks. In *International conference on machine learning*, pp. 214–223, 2017.
- Arthur, D. and Vassilvitskii, S. k-means++: The advantages of careful seeding. In *Proceedings of the eighteenth annual ACM-SIAM symposium on Discrete algorithms*, pp. 1027–1035, 2007.
- Bartal, Y. Probabilistic approximation of metric spaces and its algorithmic applications. In *Proceedings of 37th Conference on Foundations of Computer Science*, pp. 184–193, 1996.
- Bartal, Y. On approximating arbitrary metrics by tree metrics. In *ACM Symposium on Theory of Computing (STOC)*, volume 98, pp. 161–168, 1998.
- Bhushan Damodaran, B., Kellenberger, B., Flamary, R., Tuia, D., and Courty, N. Deepjdot: Deep joint distribution optimal transport for unsupervised domain adaptation. In *Proceedings of the European Conference on Computer Vision (ECCV)*, pp. 447–463, 2018.
- Bonneel, N., Peyré, G., and Cuturi, M. Wasserstein barycentric coordinates: histogram regression using optimal transport. *ACM Trans. Graph.*, 35(4):71–1, 2016.
- Bunne, C., Alvarez-Melis, D., Krause, A., and Jegelka, S. Learning generative models across incomparable spaces. In *International Conference on Machine Learning*, 2019.
- Charikar, M., Chekuri, C., Goel, A., Guha, S., and Plotkin, S. Approximating a finite metric by a small number of tree metrics. In *Proceedings 39th Annual Symposium on Foundations of Computer Science (FOCS)*, pp. 379–388, 1998.
- Courty, N., Flamary, R., Tuia, D., and Rakotomamonjy, A. Optimal transport for domain adaptation. *Pattern analysis and machine intelligence (PAMI)*, 39(9):1853–1865, 2016.
- Courty, N., Flamary, R., Habrard, A., and Rakotomamonjy, A. Joint distribution optimal transportation for domain adaptation. In *Advances in Neural Information Processing Systems*, pp. 3730–3739, 2017.
- Cuturi, M. Sinkhorn distances: Lightspeed computation of optimal transport. In *Advances in Neural Information Processing Systems*, pp. 2292–2300, 2013.
- Cuturi, M. and Doucet, A. Fast computation of Wasserstein barycenters. In *International conference on machine learning*, pp. 685–693, 2014.
- Dvurechensky, P., Gasnikov, A., and Kroshnin, A. Computational optimal transport: Complexity by accelerated gradient descent is better than by Sinkhorns algorithm. In *International conference on machine learning*, pp. 1367–1376, 2018.
- Fakcharoenphol, J., Rao, S., and Talwar, K. A tight bound on approximating arbitrary metrics by tree metrics. *Journal of Computer and System Sciences*, 69(3):485–497, 2004.
- Feder, T. and Greene, D. Optimal algorithms for approximate clustering. In *Proceedings of the twentieth annual ACM symposium on Theory of computing*, pp. 434–444. ACM, 1988.
- Genevay, A., Cuturi, M., Peyré, G., and Bach, F. Stochastic optimization for large-scale optimal transport. In *Advances in neural information processing systems*, pp. 3440–3448, 2016.
- Genevay, A., Peyre, G., and Cuturi, M. Learning generative models with sinkhorn divergences. In *Proceedings of the Twenty-First International Conference on Artificial Intelligence and Statistics*, pp. 1608–1617, 2018.
- Gonzalez, T. F. Clustering to minimize the maximum intercluster distance. *Theoretical Computer Science*, 38: 293–306, 1985.

- Grave, E., Joulin, A., and Berthet, Q. Unsupervised alignment of embeddings with Wasserstein procrustes. In *International Conference on Artificial Intelligence and Statistics (AISTATS)*, pp. 1880–1890, 2019.
- Gulrajani, I., Ahmed, F., Arjovsky, M., Dumoulin, V., and Courville, A. C. Improved training of Wasserstein GANs. In *Advances in Neural Information Processing Systems*, pp. 5767–5777, 2017.
- Indyk, P. Algorithmic applications of low-distortion geometric embeddings. In *Proceedings 42nd IEEE Symposium on Foundations of Computer Science (FOCS)*, pp. 10–33, 2001.
- Kolouri, S., Pope, P. E., Martin, C. E., and Rohde, G. K. Sliced Wasserstein auto-encoders. In *International Conference on Learning Representations*, 2019.
- Kusner, M., Sun, Y., Kolkin, N., and Weinberger, K. From word embeddings to document distances. In *International conference on machine learning*, pp. 957–966, 2015.
- Lavenant, H., Claiici, S., Chien, E., and Solomon, J. Dynamical optimal transport on discrete surfaces. In *SIGGRAPH Asia 2018 Technical Papers*, pp. 250. ACM, 2018.
- Le, T. and Cuturi, M. Unsupervised Riemannian metric learning for histograms using Aitchison transformations. In *International Conference on Machine Learning*, pp. 2002–2011, 2015.
- Le, T., Yamada, M., Fukumizu, K., and Cuturi, M. Tree-sliced variants of Wasserstein distances. In *Advances in neural information processing systems*, pp. 12283–12294, 2019.
- Lin, T., Ho, N., and Jordan, M. On efficient optimal transport: An analysis of greedy and accelerated mirror descent algorithms. In *Proceedings of the 36th International Conference on Machine Learning*, pp. 3982–3991, 2019.
- Liutkus, A., Simsekli, U., Majewski, S., Durmus, A., and Stöter, F.-R. Sliced-Wasserstein flows: Nonparametric generative modeling via optimal transport and diffusions. In *Proceedings of the 36th International Conference on Machine Learning*, pp. 4104–4113, 2019.
- Luise, G., Salzo, S., Pontil, M., and Ciliberto, C. Sinkhorn barycenters with free support via Frank-Wolfe algorithm. In *Advances in Neural Information Processing Systems*, pp. 9318–9329, 2019.
- Manning, C. D., Raghavan, P., and Schütze, H. *Introduction to information retrieval*. Cambridge university press, 2008.
- Mémoli, F. Gromov-Wasserstein distances and the metric approach to object matching. *Foundations of Computational Mathematics*, 11(4):417487, 2011.
- Mena, G. and Niles-Weed, J. Statistical bounds for entropic optimal transport: sample complexity and the central limit theorem. In *Advances in Neural Information Processing Systems*, pp. 4543–4553, 2019.
- Mikolov, T., Sutskever, I., Chen, K., Corrado, G. S., and Dean, J. Distributed representations of words and phrases and their compositionality. In *Advances in neural information processing systems*, pp. 3111–3119, 2013.
- Muzellec, B. and Cuturi, M. Generalizing point embeddings using the Wasserstein space of elliptical distributions. In *Advances in Neural Information Processing Systems*, pp. 10237–10248, 2018.
- Nadjahi, K., Durmus, A., Simsekli, U., and Badeau, R. Asymptotic guarantees for learning generative models with the sliced-Wasserstein distance. In *Advances in Neural Information Processing Systems*, pp. 250–260, 2019.
- Paty, F.-P. and Cuturi, M. Subspace robust Wasserstein distances. In *Proceedings of the 36th International Conference on Machine Learning*, pp. 5072–5081, 2019.
- Perrot, M., Courty, N., Flamary, R., and Habrard, A. Mapping estimation for discrete optimal transport. In *Advances in Neural Information Processing Systems*, pp. 4197–4205, 2016.
- Peyré, G. and Cuturi, M. Computational optimal transport. *Foundations and Trends® in Machine Learning*, 11(5-6): 355–607, 2019.
- Peyré, G., Cuturi, M., and Solomon, J. Gromov-Wasserstein averaging of kernel and distance matrices. In *Proceedings of the International Conference on Machine Learning*, 2016.
- Peyré, G., Cuturi, M., and Solomon, J. Gromov-Wasserstein averaging of kernel and distance matrices. In *International Conference on Machine Learning*, pp. 2664–2672, 2016.
- Rabin, J., Peyré, G., Delon, J., and Bernot, M. Wasserstein barycenter and its application to texture mixing. In *International Conference on Scale Space and Variational Methods in Computer Vision*, pp. 435–446, 2011.
- Redko, I., Courty, N., Flamary, R., and Tuia, D. Optimal transport for multi-source domain adaptation under target shift. In *International Conference on Artificial Intelligence and Statistics*, pp. 849–858, 2019.

- Rupp, M., Tkatchenko, A., Müller, K.-R., and Von Lilienfeld, O. A. Fast and accurate modeling of molecular atomization energies with machine learning. *Physical review letters*, 108(5):058301, 2012.
- Salton, G. and Buckley, C. Term-weighting approaches in automatic text retrieval. *Information processing & management*, 24(5):513–523, 1988.
- Santambrogio, F. *Optimal transport for applied mathematicians*. Birkäuser, 2015.
- Schmitzer, B. Stabilized sparse scaling algorithms for entropy regularized transport problems. *SIAM Journal on Scientific Computing*, 41(3):A1443–A1481, 2019.
- Semple, C. and Steel, M. Phylogenetics. *Oxford Lecture Series in Mathematics and its Applications*, 2003.
- Solomon, J. and Vaxman, A. Optimal transport-based polar interpolation of directional fields. *ACM Transactions on Graphics (TOG)*, 38(4):1–13, 2019.
- Solomon, J., De Goes, F., Peyré, G., Cuturi, M., Butscher, A., Nguyen, A., Du, T., and Guibas, L. Convolutional Wasserstein distances: Efficient optimal transportation on geometric domains. *ACM Transactions on Graphics (TOG)*, 34(4):66, 2015.
- Solomon, J., Peyré, G., Kim, V. G., and Sra, S. Entropic metric alignment for correspondence problems. *ACM Transactions on Graphics (TOG)*, 35(4):72, 2016.
- Togninalli, M., Ghisu, E., Llinares-López, F., Rieck, B., and Borgwardt, K. Wasserstein Weisfeiler-Lehman graph kernels. In *Advances in Neural Information Processing Systems*, pp. 6436–6446. 2019.
- Vayer, T., Flamary, R., Tavenard, R., Chapel, L., and Courty, N. Sliced Gromov-Wasserstein. *Advances in Neural Information Processing Systems*, 2019.
- Villani, C. *Topics in Optimal Transportation*. American Mathematical Society, 2003.
- Wu, J., Huang, Z., Acharya, D., Li, W., Thoma, J., Paudel, D. P., and Gool, L. V. Sliced Wasserstein generative models. In *Proceedings of the IEEE conference on computer vision and pattern recognition*, pp. 3713–3722, 2019.
- Xu, H., Luo, D., and Carin, L. Scalable Gromov-Wasserstein learning for graph partitioning and matching. In *Advances in neural information processing systems*, 2019a.
- Xu, H., Luo, D., Zha, H., and Carin, L. Gromov-Wasserstein learning for graph matching and node embedding. In *International conference on machine learning*, 2019b.

## Supplement to “Fast Tree Variants of Gromov-Wasserstein”

We organize this supplementary material as follow:

- In Section A, we provide proofs for technical results: Theorem 1 and Theorem 2 in the main text.
- In Section B, we show more illustrations for flow-based tree GW (*FlowTGW*) mentioned in the main text.
- In Section C, we describe further details for *FlowTGW* and depth-based tree GW (*DepthTGW*).
- In Section D, we illustrate
  - further experimental results in *qm7*, TWITTER, and RECIPE datasets considered in the main text;
  - experiments on larger document datasets (e.g., AMAZON and CLASSIC datasets) for document classification with non-registered word embeddings;
  - time consumption for the clustering-based tree metric sampling;
  - and results with different parameters for tree metric sampling.
- In Section E, we give some brief reviews for
  - the farthest-point clustering;
  - clustering-based tree metric sampling;
  - tree metric;
  - $F_\beta$  measure for clustering evaluation;
  - and more information for datasets.
- In Section F, we provide some further discussions.
- In Section G, we investigate empirical relations among variants of GW (e.g., *FlowTGW*, *DepthTGW*, sliced GW, entropic GW and a variant of entropic GW).

**Notations.** We use same notations as in the main text.

### A. Proofs

In this section, we provide the proofs for the pseudo-distances of *FlowTGW* and *DepthTGW* discrepancies, i.e., Theorem 1 and Theorem 2 in the main text.

#### A.1. Proof of Theorem 1 in the main text

From the definition of *FlowTGW*  $\mathcal{GW}_{T_f}$ , it is symmetric, namely,  $\mathcal{GW}_{T_f}(\mu, \nu) = \mathcal{GW}_{T_f}(\nu, \mu)$ . In addition, when  $\mathcal{GW}_{T_f}(\mu, \nu) = 0$ , there exist two optimal roots  $r_x^*$  and  $r_z^*$  such that  $k = k'$ ,  $\{a_i \mid i \in [k]\} \equiv \{b_j \mid j \in [k']\}$ , and  $\{d_{T_X}(r_x^*, x_i) \mid i \in [k]\} \equiv \{d_{T_Z}(r_z^*, z_j) \mid j \in [k']\}$ . Finally, we show that  $\mathcal{GW}_{T_f}$  also satisfies triangle inequality as in Proposition 1.

**Proposition 1.** *Given three probability measures  $\mu, \nu, \gamma$  in three different metric spaces  $(\mathcal{T}_X, d_{T_X})$ ,  $(\mathcal{T}_Y, d_{T_Y})$ , and  $(\mathcal{T}_Z, d_{T_Z})$ . Then, we have:*

$$\mathcal{GW}_{T_f}(\mu, \gamma) \leq \mathcal{GW}_{T_f}(\mu, \nu) + \mathcal{GW}_{T_f}(\nu, \gamma).$$

*Proof.* It is sufficient to demonstrate that

$$\widehat{\mathcal{GW}}_{T_f}(\mu, \gamma; r_x, r_y) \leq \widehat{\mathcal{GW}}_{T_f}(\mu, \nu; r_x, r_z) + \widehat{\mathcal{GW}}_{T_f}(\nu, \gamma; r_y, r_z), \quad (8)$$

for any roots  $r_x, r_y, r_z$  of  $\mathcal{T}_X, \mathcal{T}_Y, \mathcal{T}_Z$  respectively. Our proof for the above inequality is a direct application of the gluing lemma in (Villani, 2003). In particular, for any roots  $r_x, r_y, r_z$  of  $\mathcal{T}_X, \mathcal{T}_Y, \mathcal{T}_Z$ , we denote  $\widehat{T}^1 \in \Pi(\mu, \nu)$  and  $\widehat{T}^2 \in \Pi(\nu, \gamma)$  as optimal transport plans for  $\widehat{\mathcal{GW}}_{T_f}(\mu, \nu; r_x, r_z)$  and  $\widehat{\mathcal{GW}}_{T_f}(\nu, \gamma; r_y, r_z)$  respectively. Based on the gluing lemma, there



exists  $T$  with marginal of the first and the third factors as  $\widehat{T}^1$  and marginal of the second and the third factors as  $\widehat{T}^2$ . We denote the marginal of its first and second factors as  $\bar{T}$ , which is a transport plan between  $\mu$  and  $\gamma$ . Therefore, from the definition of aligned-root *FlowTGW* discrepancy, we have

$$\begin{aligned}
 \widehat{\mathcal{GW}}_{T_f}^2(\mu, \gamma; r_x, r_y) &\leq \sum_{i,j} |d_{T_X}(r_x, x_i) - d_{T_Y}(r_y, y_j)|^2 \bar{T}_{ij} \\
 &= \sum_{i,j,k} |d_{T_X}(r_x, x_i) - d_{T_Y}(r_y, y_j)|^2 T_{ijk} \\
 &= \sum_{i,j,k} |d_{T_X}(r_x, x_i) - d_{T_Z}(r_z, z_k)|^2 T_{ijk} + \sum_{i,j,k} |d_{T_X}(r_y, y_j) - d_{T_Z}(r_z, z_k)|^2 T_{ijk} \\
 &\quad - 2 \sum_{i,j,k} (d_{T_X}(r_x, x_i) - d_{T_Z}(r_z, z_k))(d_{T_Y}(r_y, y_j) - d_{T_Z}(r_z, z_k)) T_{ijk} \\
 &\leq \widehat{\mathcal{GW}}_{T_f}^2(\mu, \nu; r_x, r_z) + \widehat{\mathcal{GW}}_{T_f}^2(\nu, \gamma; r_y, r_z) \\
 &\quad + 2\widehat{\mathcal{GW}}_{T_f}(\mu, \nu; r_x, r_z)\widehat{\mathcal{GW}}_{T_f}(\nu, \gamma; r_y, r_z) \\
 &= (\widehat{\mathcal{GW}}_{T_f}(\mu, \nu; r_x, r_z) + \widehat{\mathcal{GW}}_{T_f}(\nu, \gamma; r_y, r_z))^2,
 \end{aligned} \tag{9}$$

where we used Hölder's inequality for the third term for the second inequality. As a consequence, we obtain the conclusion of the inequality in Equation (8).  $\square$

## A.2. Proof of Theorem 2 in the main text

In fact, from the definition of *DepthTGW*  $\mathcal{GW}_{T_d}$ , it is clear that  $\mathcal{GW}_{T_d}(\mu, \nu) = \mathcal{GW}_{T_d}(\nu, \mu)$  and  $\mathcal{GW}_{T_d}(\mu, \mu) = 0$ . Furthermore,  $\mathcal{GW}_{T_d}$  also satisfies triangle inequality as in Proposition 2.

**Proposition 2.** *Given three probability measures  $\mu, \nu, \gamma$  in three different metric spaces  $(\mathcal{T}_X, d_{T_X})$ ,  $(\mathcal{T}_Y, d_{T_Y})$ , and  $(\mathcal{T}_Z, d_{T_Z})$ . Then, we have:*

$$\mathcal{GW}_{T_d}(\mu, \gamma) \leq \mathcal{GW}_{T_d}(\mu, \nu) + \mathcal{GW}_{T_d}(\nu, \gamma).$$

*Proof.* Similar to the proof of Proposition 1, it is sufficient to demonstrate that

$$\widehat{\mathcal{GW}}_{T_d}(\mu, \gamma; r_x, r_y) \leq \widehat{\mathcal{GW}}_{T_d}(\mu, \nu; r_x, r_z) + \widehat{\mathcal{GW}}_{T_d}(\nu, \gamma; r_y, r_z), \tag{10}$$

for any roots  $r_x, r_y, r_z$  of  $\mathcal{T}_X, \mathcal{T}_Y, \mathcal{T}_Z$  respectively. According to the definition of aligned-root *DepthTGW*, the above inequality is equivalent to

$$\begin{aligned}
 \sum_h \sum_{(x,y) \in \mathcal{M}_{h-1}^{1,2}} T_h^*(x,y) \widehat{\mathcal{GW}}_{T_f}(\mu_{\mathcal{T}_x^2}, \gamma_{\mathcal{T}_y^2}; x,y) &\leq \sum_h \sum_{(x,z) \in \mathcal{M}_{h-1}^{1,3}} \bar{T}_h^*(x,z) \widehat{\mathcal{GW}}_{T_f}(\mu_{\mathcal{T}_x^2}, \nu_{\mathcal{T}_z^2}; x,z) \\
 &\quad + \sum_h \sum_{(y,z) \in \mathcal{M}_{h-1}^{2,3}} \tilde{T}_h^*(y,z) \widehat{\mathcal{GW}}_{T_f}(\mu_{\mathcal{T}_y^2}, \nu_{\mathcal{T}_z^2}; y,z),
 \end{aligned} \tag{11}$$

where  $\mathcal{M}_h^{1,2}, \mathcal{M}_h^{1,3}, \mathcal{M}_h^{2,3}$  are respectively sets of optimal aligned pairs at the depth level  $h$  from trees  $\mathcal{T}_X$  and  $\mathcal{T}_Y$ , from trees  $\mathcal{T}_X$  and  $\mathcal{T}_Z$ , and from trees  $\mathcal{T}_Y$  and  $\mathcal{T}_Z$ ;  $T_h^*(x,y), \bar{T}_h^*(x,z), \tilde{T}_h^*(y,z)$  are respectively optimal matching masses for the pairs  $(x,y) \in \mathcal{M}_{h-1}^{1,2}, (x,z) \in \mathcal{M}_{h-1}^{1,3}, (y,z) \in \mathcal{M}_{h-1}^{2,3}$ . In order to demonstrate the above inequality, we only need to verify that

$$\begin{aligned}
 \sum_{(x,y) \in \mathcal{M}_h^{1,2}} T_h^*(x,y) \widehat{\mathcal{GW}}_{T_f}(\mu_{\mathcal{T}_x^2}, \gamma_{\mathcal{T}_y^2}; x,y) &\leq \sum_{(x,z) \in \mathcal{M}_h^{1,3}} \bar{T}_h^*(x,z) \widehat{\mathcal{GW}}_{T_f}(\mu_{\mathcal{T}_x^2}, \nu_{\mathcal{T}_z^2}; x,z) \\
 &+ \sum_{(y,z) \in \mathcal{M}_h^{2,3}} \tilde{T}_h^*(y,z) \widehat{\mathcal{GW}}_{T_f}(\mu_{\mathcal{T}_y^2}, \nu_{\mathcal{T}_z^2}; y,z), \tag{12}
 \end{aligned}$$

for any depth level  $h \geq 1$ . We respectively denote  $\mathcal{T}_X^h = \{\bar{x}_1^{(h)}, \dots, \bar{x}_{k_{1,h}}^{(h)}\}$ ,  $\mathcal{T}_Y^h = \{\bar{y}_1^{(h)}, \dots, \bar{y}_{k_{2,h}}^{(h)}\}$ ,  $\mathcal{T}_Z^h = \{\bar{z}_1^{(h)}, \dots, \bar{z}_{k_{3,h}}^{(h)}\}$  the set of nodes in depth level  $h$  of the trees  $\mathcal{T}_X, \mathcal{T}_Y, \mathcal{T}_Z$ . The inequality in Equation (12) can be rewritten as

$$\begin{aligned}
 &\sum_{i=1}^{k_{1,h-1}} \sum_{j=1}^{k_{2,h-1}} \sum_{x \in \mathcal{S}(\bar{x}_i^{(h-1)}), y \in \mathcal{S}(\bar{y}_j^{(h-1)})} T_h^*(x,y) \widehat{\mathcal{GW}}_{T_f}(\mu_{\mathcal{T}_x^2}, \gamma_{\mathcal{T}_y^2}; x,y) \\
 &\leq \sum_{i=1}^{k_{1,h-1}} \sum_{j=1}^{k_{3,h-1}} \sum_{x \in \mathcal{S}(\bar{x}_i^{(h-1)}), z \in \mathcal{S}(\bar{z}_j^{(h-1)})} \bar{T}_h^*(x,z) \widehat{\mathcal{GW}}_{T_f}(\mu_{\mathcal{T}_x^2}, \nu_{\mathcal{T}_z^2}; x,z) \\
 &\quad + \sum_{i=1}^{k_{2,h-1}} \sum_{j=1}^{k_{3,h-1}} \sum_{y \in \mathcal{S}(\bar{y}_i^{(h-1)}), z \in \mathcal{S}(\bar{z}_j^{(h-1)})} \tilde{T}_h^*(y,z) \widehat{\mathcal{GW}}_{T_f}(\gamma_{\mathcal{T}_y^2}, \nu_{\mathcal{T}_z^2}; y,z). \tag{13}
 \end{aligned}$$

In order to obtain the conclusion of inequality in Equation (13), we only need to prove that

$$\begin{aligned}
 &\sum_{x \in \mathcal{S}(\bar{x}_i^{(h-1)}), y \in \mathcal{S}(\bar{y}_j^{(h-1)})} T_h^*(x,y) \widehat{\mathcal{GW}}_{T_f}(\mu_{\mathcal{T}_x^2}, \gamma_{\mathcal{T}_y^2}; x,y) \\
 &\leq \sum_{x \in \mathcal{S}(\bar{x}_i^{(h-1)}), z \in \mathcal{S}(\bar{z}_l^{(h-1)})} \bar{T}_h^*(x,z) \widehat{\mathcal{GW}}_{T_f}(\mu_{\mathcal{T}_x^2}, \nu_{\mathcal{T}_z^2}; x,z) \\
 &\quad + \sum_{y \in \mathcal{S}(\bar{y}_j^{(h-1)}), z \in \mathcal{S}(\bar{z}_l^{(h-1)})} \tilde{T}_h^*(y,z) \widehat{\mathcal{GW}}_{T_f}(\gamma_{\mathcal{T}_y^2}, \nu_{\mathcal{T}_z^2}; y,z),
 \end{aligned}$$

for any  $i \in \{1, \dots, k_{1,h-1}\}$ ,  $j \in \{1, \dots, k_{2,h-1}\}$ , and  $l \in \{1, \dots, k_{3,h-1}\}$ . We can make use of the gluing lemma (Villani, 2003) to prove that inequality. In fact, there exists  $T$  with marginal of its first and third factors as  $\bar{T}_h^*(x,z)$  and marginal of its second and third factors as  $\tilde{T}_h^*(y,z)$ . We denote the marginal of its first and second factors as  $\hat{T}$ , which is the transport plan for probability measures with supports at  $x \in \mathcal{S}(\bar{x}_i^{(h-1)})$  and  $y \in \mathcal{S}(\bar{y}_j^{(h-1)})$ . Now, we have the following inequalities

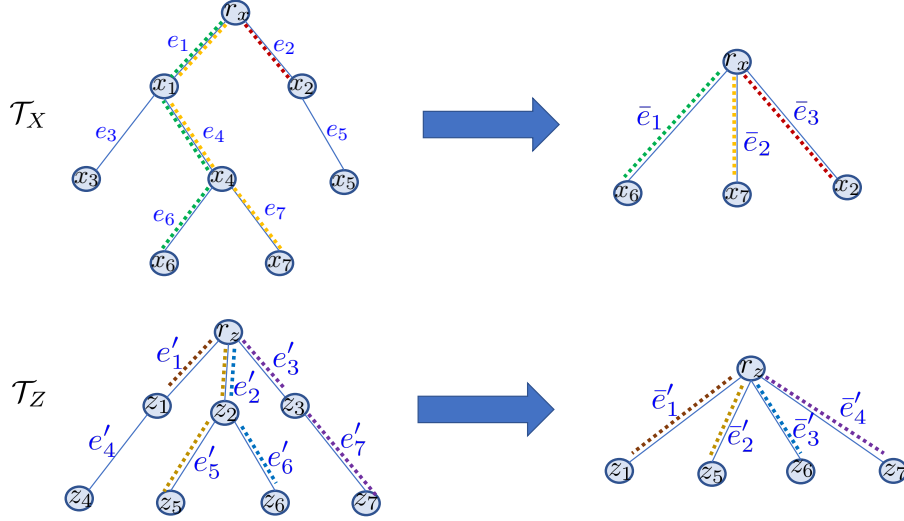


Figure 8. An illustration for the aligned-root  $\text{FlowTGW } \widehat{\mathcal{GW}}_{T_f}$  between  $\mu = a_1\delta_{x_6} + a_2\delta_{x_7} + a_3\delta_{x_2}$  on  $\mathcal{T}_X$  and  $\nu = b_1\delta_{z_1} + b_2\delta_{z_5} + b_3\delta_{z_6} + b_4\delta_{z_7}$  on  $\mathcal{T}_Z$ . In  $\widehat{\mathcal{GW}}_{T_f}$ , we consider the flows from the root to each support of a measure as illustrated in the corresponding right figures where the length of each edge in the right figures is equal to the length of the path from the root to that node on the corresponding tree  $\mathcal{T}$  in the left figures respectively.

$$\begin{aligned}
 & \sum_{x \in \mathcal{S}(\bar{x}_i^{(h-1)}), y \in \mathcal{S}(\bar{y}_j^{(h-1)})} T_h^*(x, y) \widehat{\mathcal{GW}}_{T_f}(\mu_{\mathcal{T}_x^2}, \gamma_{\mathcal{T}_y^2}; x, y) \\
 &= \sum_{x \in \mathcal{S}(\bar{x}_i^{(h-1)}), y \in \mathcal{S}(\bar{y}_j^{(h-1)}), z \in \mathcal{S}(\bar{z}_l^{(h-1)})} T_{xyz} \widehat{\mathcal{GW}}_{T_f}(\mu_{\mathcal{T}_x^2}, \gamma_{\mathcal{T}_y^2}; x, y) \\
 &\leq \sum_{x \in \mathcal{S}(\bar{x}_i^{(h-1)}), y \in \mathcal{S}(\bar{y}_j^{(h-1)}), z \in \mathcal{S}(\bar{z}_l^{(h-1)})} T_{xyz} \widehat{\mathcal{GW}}_{T_f}(\mu_{\mathcal{T}_x^2}, \nu_{\mathcal{T}_z^2}; x, z) \\
 &\quad + \sum_{x \in \mathcal{S}(\bar{x}_i^{(h-1)}), y \in \mathcal{S}(\bar{y}_j^{(h-1)}), z \in \mathcal{S}(\bar{z}_l^{(h-1)})} T_{xyz} \widehat{\mathcal{GW}}_{T_f}(\gamma_{\mathcal{T}_y^2}, \nu_{\mathcal{T}_z^2}; y, z) \\
 &= \sum_{x \in \mathcal{S}(\bar{x}_i^{(h-1)}), z \in \mathcal{S}(\bar{z}_l^{(h-1)})} \bar{T}_h^*(x, z) \widehat{\mathcal{GW}}_{T_f}(\mu_{\mathcal{T}_x^2}, \nu_{\mathcal{T}_z^2}; x, z) \\
 &\quad + \sum_{y \in \mathcal{S}(\bar{y}_j^{(h-1)}), z \in \mathcal{S}(\bar{z}_l^{(h-1)})} \bar{T}_h^*(y, z) \widehat{\mathcal{GW}}_{T_f}(\gamma_{\mathcal{T}_y^2}, \nu_{\mathcal{T}_z^2}; y, z).
 \end{aligned}$$

As a consequence, we obtain the conclusion of the proposition.  $\square$

## B. Further illustrations of $\text{FlowTGW}$

In this section, we provide further illustrations for  $\text{FlowTGW}$  mentioned in the main text. We illustrate the aligned-root  $\text{FlowTGW } \widehat{\mathcal{GW}}_{T_f}$  in Figure 8, and supports in  $\Omega_\nu$  in the Case 2 in the efficient computation approach for  $\text{FlowTGW } \mathcal{GW}_{T_f}$  in Figure 9.

## C. Further details for $\text{FlowTGW}$ and $\text{DepthTGW}$

In this section, we first derive a computation for a univariate optimal transport for empirical measures. Then, we give some further details about  $\text{FlowTGW}$  and  $\text{DepthTGW}$  proposed in the main text.

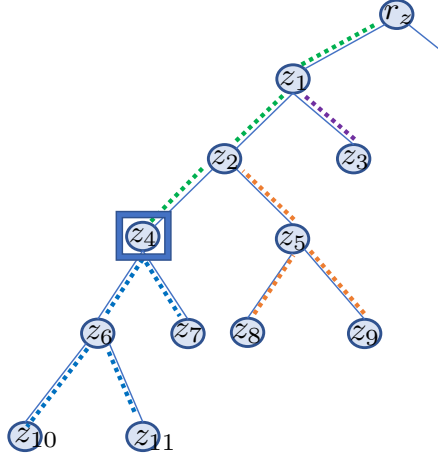


Figure 9. An illustration for supports in  $\Omega_\nu$  in the Case 2 in the efficient computation approach for  $\mathcal{GW}_{T_f}$ . Assume that  $\Omega_\nu = \{z_1, z_2, z_3, z_7, z_8, z_9, z_{10}, z_{11}\}$  and the new root  $\bar{r}_z = z_4$  (emphasized by the square border). We have supports  $z_7, z_{10}, z_{11}$  for Case 2a (blue dots), supports  $z_1, z_2$  for Case 2b (green dots), and supports  $z_3, z_8, z_9$  for Case 2c (purple and orange dots) where the corresponding closest common ancestors  $\zeta_3 = z_1$ ,  $\zeta_8 = z_2$ , and  $\zeta_9 = z_2$  respectively. Note that,  $\zeta_8 = \zeta_9$  (orange dots), therefore the order of supports  $z_8, z_9$  is preserved when one changes into the new root.

### C.1. Univariate optimal transport (OT) for empirical measures

Recall that the univariate OT, i.e., univariate Wasserstein, is equal to the integral of the absolute difference between the generalized quantile functions of two univariate probability distributions (Santambrogio, 2015) (§2). Therefore, one only needs to sort their supports for the computation with linearithmic complexity.

---

#### Algorithm 1 Univariate optimal transport for empirical measures

---

**Input:** Input empirical measures with sorted supports  $\mu = \sum_{i \in [n]} a_i \delta_{x_i}$ , and  $\nu = \sum_{j \in [m]} b_j \delta_{z_j}$  (i.e.,  $x_1 \leq x_2 \leq \dots \leq x_n$ , and  $z_1 \leq z_2 \leq \dots \leq z_m$ ), and a ground distance  $\ell$  (e.g.,  $\ell(x, z) = \ell_1(x, z) = |x - z|$ ).

**Output:** OT distance  $d$  and optimal transport plan  $T$ .

- 1: Initialize  $d \leftarrow 0$ ,  $T \leftarrow 0_{n \times m}$ ,  $i \leftarrow 1$ ,  $j \leftarrow 1$ .
  - 2: **while**  $i \leq n$  and  $j \leq m$  **do**
  - 3:   **if**  $a_i \leq b_j$  **then**
  - 4:      $T_{ij} \leftarrow a_i$ .
  - 5:      $d \leftarrow d + a_i \ell(x_i, z_j)$ .
  - 6:     Update  $b_j \leftarrow b_j - a_i$ ,  $i \leftarrow i + 1$ .
  - 7:     **if**  $b_j == 0$  **then**
  - 8:        $j \leftarrow j + 1$ .
  - 9:     **end if**
  - 10:  **else**
  - 11:     $T_{ij} \leftarrow b_j$ .
  - 12:     $d \leftarrow d + b_j \ell(x_i, z_j)$ .
  - 13:    Update  $a_i \leftarrow a_i - b_j$ ,  $j \leftarrow j + 1$ .
  - 14:    **if**  $a_i == 0$  **then**
  - 15:       $i \leftarrow i + 1$ .
  - 16:    **end if**
  - 17:  **end if**
  - 18: **end while**
- 

In particular, given two empirical measures  $\mu = \sum_{i \in [n]} \bar{a}_i \delta_{\bar{x}_i}$  and  $\nu = \sum_{j \in [m]} \bar{b}_j \delta_{\bar{z}_j}$  whose supports are in one-dimensional space, i.e.,  $\bar{x}_i, \bar{z}_j \in \mathbb{R}, \forall i \in [n], j \in [m]$ . Firstly, we sort supports of  $\mu, \nu$  in an increasing order, denoted as  $\mu = \sum_{i \in [n]} a_i \delta_{x_i}$



and  $\nu = \sum_{j \in [m]} b_j \delta_{z_j}$  (i.e.,  $x_1 \leq x_2 \leq \dots \leq x_n$ , and  $z_1 \leq z_2 \leq \dots \leq z_m$ ). Without loss of generality, assume that  $n \geq m$ , the complexity of this sorting is  $O(n \log n)$ . We summarize the algorithm for the univariate OT between  $\mu$  and  $\nu$  (whose supports are already sorted) in Algorithm 1.

The complexity of Algorithm 1 is  $O(n)$ . Therefore, the complexity of the univariate OT for empirical measures is  $O(n \log n)$ , or its main complexity is to sort supports of empirical measures.

## C.2. FlowTGW

There are two types of applications: *without* or *with* priori knowledge about tree metrics for supports in probability measures.

### C.2.1. APPLICATIONS *without* PRIORI KNOWLEDGE ABOUT TREE METRICS FOR SUPPORTS IN PROBABILITY MEASURES

In general applications, one usually does not have priori knowledge about tree metrics for supports in probability measures. However, one can sample tree metrics for the space of supports of probability measures, e.g., using clustering-based tree metric sampling (Le et al., 2019) (§4), for *FlowTGW*.

One can compute *FlowTGW* between  $\mu = \sum_{i \in [n]} a_i \delta_{x_i}$  and  $\nu = \sum_{j \in [m]} b_j \delta_{z_j}$  as follow:

- Step 1: Sample aligned-root tree metrics  $\mathcal{T}_X$  and  $\mathcal{T}_Z$  for supports  $x_i |_{i \in [n]}$ , and  $z_j |_{j \in [m]}$  of probability measures  $\mu$  and  $\nu$  respectively, e.g., by choosing means of support data distributions as roots when using the clustering-based tree metric sampling (Le et al., 2019) (§4) (See Section E.2 for a review about clustering-based tree metric sampling).
- Step 2: Based on the sampled aligned-root tree metrics, *FlowTGW* (Equation (2) in the main text) is equivalent to aligned-root *FlowTGW* (Equation (4) in the main text). Consequently, *FlowTGW* between  $\mu$  and  $\nu$  is equivalent to the univariate OT distance between  $\tilde{\mu} := \sum_{i \in [n]} a_i \delta_{d_{\mathcal{T}_X}(r_x, x_i)}$  and  $\tilde{\nu} := \sum_{j \in [m]} b_j \delta_{d_{\mathcal{T}_Z}(r_z, z_j)}$  where  $r_x, r_z$  are roots of  $\mathcal{T}_X, \mathcal{T}_Z$  respectively.
- Step 3: Sort supports of  $\tilde{\mu}$  and  $\tilde{\nu}$ , and then apply Algorithm 1 to compute the univariate OT between  $\tilde{\mu}$  and  $\tilde{\nu}$ .

We next show a complexity analysis for *FlowTGW*:

- The complexity of Step 1 is  $O(\bar{N} H_{\mathcal{T}} \log \kappa)$  where  $H_{\mathcal{T}}$  is a predefined deepest level of tree  $\mathcal{T}$  and  $\kappa$  is the number of clusters in the farthest-point clustering used in the clustering-based tree metric sampling (Le et al., 2019);  $\bar{N}$  is the input number of supports<sup>4</sup>. Let  $N$  be the number of nodes in the sampled tree  $\mathcal{T}$ , we have  $N \leq (\kappa^{H_{\mathcal{T}}} - 1) / (\kappa - 1)$ .
- The complexity of Step 2 is  $O(n H_{\mathcal{T}})$  for computing supports of  $\tilde{\mu}, \tilde{\nu}$ .
- The complexity of Step 3 is  $O(n \log n)$  as in Section C.1.

In general, one usually chooses small values for  $H_{\mathcal{T}}$  and  $\kappa$  (e.g.,  $(H_{\mathcal{T}} = 6, \kappa = 4)$  are suggested parameters for the clustering-based tree metric sampling (Le et al., 2019)); and has  $n \leq N$  (each support is corresponding to a node in a tree). Therefore, the overall complexity of *FlowTGW* is  $O(\bar{N} H_{\mathcal{T}} \log \kappa + n H_{\mathcal{T}} + n \log n)$ , or approximately  $O(N \log N)$ .

### C.2.2. APPLICATIONS *with* PRIORI KNOWLEDGE ABOUT TREE METRICS FOR SUPPORTS IN PROBABILITY MEASURES

In some specific applications where one has a priori knowledge about tree metric for supports in each probability measure. One can compute *FlowTGW* as in Equation (2) in the main text, where one can exhaustedly search the optimal aligned roots, or apply the efficient computation in Section 3.2 in the main text to reduce this complexity.

Assume that one have priori knowledge about tree metrics<sup>5</sup>  $\mathcal{T}_X, \mathcal{T}_Z$  for supports of probability measure  $\mu, \nu$  respectively. In general, one needs to search the optimal aligned roots  $r_x, r_z$  for tree  $\mathcal{T}_X, \mathcal{T}_Z$ . The complexity of exhausted search is  $O(N^2)$

<sup>4</sup>One can use supports of the input probability measures, or a (sub)set of supports from several input probability measures, e.g., in case, supports are in non-registered, but same-dimensional spaces, to sample tree metrics having the same tree structure. Therefore, we have  $\bar{N} \approx tn$ , where  $t$  is the number of probability measures whose supports are used to sample tree metrics.

<sup>5</sup>Assume that for each tree metric, each node has at most  $\kappa$  child nodes, and the deepest level is  $H_{\mathcal{T}}$ .

where  $N$  is the number of nodes in trees. Additionally, the complexity of aligned-root *FlowTGW* is  $O(\bar{N}H_{\mathcal{T}} \log \kappa + nH_{\mathcal{T}} + n \log n)$ , or approximately  $O(N \log N)$  (See Section C.2.1). Therefore, the overall complexity of *FlowTGW* with exhausted search for optimal aligned-roots is  $O(\bar{N}H_{\mathcal{T}} \log \kappa + N^2nH_{\mathcal{T}} + N^2n \log n + N^2)$ <sup>6</sup>, or approximately  $O(N^3 \log N)$ .

As described in Section 3.2 in the main text, those computational steps, e.g., tree metrics between a root to each support, and sorting for those tree metrics between a root to each support or its efficient computation, can be done separately for each tree before one applies Algorithm 1 for those sorted tree metrics between a root and each support, then compares those  $N^2$  values to find the optimal pair of roots, one can reduce the complexity of *FlowTGW*

- into  $O(\bar{N}H_{\mathcal{T}} \log \kappa + NnH_{\mathcal{T}} + n \log n + N^2)$ , or  $O(N^2)$  for Case 1 in the main text, since one needs to compute tree metrics from a root to each support with complexity  $O(nH_{\mathcal{T}})$  for  $N$  times due to changing a root in a tree; sort tree metrics between a root to each support for only 1 time; and compare aligned-root *FlowTGW* results for  $N^2$  cases of pairs of roots.
- or nearly into  $O(\bar{N}H_{\mathcal{T}} \log \kappa + NnH_{\mathcal{T}} + n \log n + Nn + N^2)$ , or nearly  $O(N^2)$  for Case 2 in the main text, since one needs to compute tree metrics from a root to each support with complexity  $O(nH_{\mathcal{T}})$  for  $N$  times due to changing a root in a tree; sort tree metrics between a root to each support for only 1 time; merge some ordered arrays with complexity nearly  $O(n)$  for  $N$  times due to changing a root in a tree; and compare aligned-root *FlowTGW* results for  $N^2$  cases of pairs of roots.

When the degenerated case happens, one needs to merge  $n$  ordered arrays, where each array only has 1 node. Therefore, the complexity is  $O(n \log n)$ , or one simply needs to resort for those  $n$  tree metrics from a root to each support when changing a root of a tree. Hence, the overall complexity for the degenerated case is  $O(\bar{N}H_{\mathcal{T}} \log \kappa + NnH_{\mathcal{T}} + Nn \log n + N^2)$ , or approximately  $O(N^2 \log N)$ .

Thus, for *FlowTGW*, one can reduce its complexity  $O(N^3 \log N)$  for a naive implementation into nearly  $O(N^2)$  (or into  $O(N^2 \log N)$  for the degenerate case) with the proposed efficient computation in Section 3.2 in the main text.

Note that when one can not screen out any aligned-root *FlowTGW*s, the computation of *FlowTGW* requires at least  $N^2$  comparisons among aligned-root *FlowTGW* (choosing the optimal pair of roots from the values of  $N^2$  aligned-root *FlowTGW*). Therefore, for this case,  $O(N^2)$  is also the optimal complexity for *FlowTGW*.

### C.3. *DepthTGW*

Similar to *FlowTGW* in Section C.2, there are two types of applications: *without* or *with* priori knowledge about tree metrics for supports in probability measures. For general applications where one usually does not have priori knowledge about tree metrics for probability measures, one can apply clustering-based tree metric sampling (Le et al., 2019) to sample tree metrics for supports of probability measures. For some specific applications where one knows tree metric for each probability measure, one needs to search the optimal aligned roots, e.g., by exhausted search.

#### C.3.1. APPLICATIONS *without* PRIORI KNOWLEDGE ABOUT TREE METRICS FOR SUPPORTS IN PROBABILITY MEASURES

For those general applications without priori knowledge about tree metrics for supports in probability measures, one can use clustering-based tree metric approach to sample tree metrics for supports of the probability measures.

One can compute *DepthTGW* between  $\mu = \sum_{i \in [n]} a_i \delta_{x_i}$  and  $\nu = \sum_{j \in [m]} b_j \delta_{z_j}$  as follow:

- Step 1: Sample aligned-root tree metrics  $\mathcal{T}_X$  and  $\mathcal{T}_Z$  for supports  $x_i \mid_{i \in [n]}$  and  $z_j \mid_{j \in [m]}$  in probability measures  $\mu$  and  $\nu$  respectively (similar to Step 1 for *FlowTGW*).
- Step 2: Based on the sampled aligned-root tree metrics, *DepthTGW* (Equation (7) in the main text) is equivalent to aligned-root *DepthTGW* (Equation (6) in the main text). For each probability measure, we construct 2-depth-level tree for all nodes from the tree root to each support of the probability measure as in Algorithm 2<sup>7</sup>.

<sup>6</sup>Naively computing  $N^2$  aligned-roots *FlowTGW*, and comparing those  $N^2$  values to obtain the optimal.

<sup>7</sup>Constructing 2-depth-level tree for all nodes from the tree root to each support of probability measures as in Algorithm 2 can be considered as a preprocessing step since those 2-depth-level trees are needed during the hierarchical alignment along each deep level in trees for a computation of *DepthTGW*.

**Algorithm 2** Construct 2-depth-level tree

---

**Input:** Input empirical measure  $\mu = \sum_{i \in [n]} a_i \delta_{x_i}$ , tree metric  $\mathcal{T}_X$ .

**Output:** Set of 2-depth-level trees for  $\mu$ .

- 1: Construct a set of paths  $S_{\bar{p}}$  for supports  $x_i \mid_{i \in [n]}$  where each element is a path from a root to each support.
  - 2: From the set of paths  $S_{\bar{p}}$ , construct a set of nodes where each node belongs to at least one path of the set of paths  $S_{\bar{p}}$ .
  - 3: For each node in  $S_{\bar{p}}$ , construct a 2-depth-level tree for that node in tree  $\mathcal{T}$  for  $\mu$ , as in Section 4 in the main text.
  - 4: Gather all those 2-depth-level trees to form the set of 2-depth-level trees for  $\mu$ .
- 

- Step 3: Compute the aligned-root *DepthTGW* (Equation (6) in the main text). It starts from a comparison between 2-depth-level tree constructed from each root of  $\mathcal{T}_X$ , and  $\mathcal{T}_Z$  for  $\mu$  and  $\nu$  respectively, with optimal matching mass 1.
  - If it is *not* a simple case<sup>8</sup>, then we compute the discrepancy between 2-depth-level tree as aligned-root *FlowTGW* by simply sorting supports and using Algorithm 1. Then, we push all the matching pairs between child nodes and their optimal matching mass into the queue.
  - If it is a simple case where both two nodes of the considered pair do not have child nodes, or sum of their child-node weights is equal to 0, then their discrepancy is equal to 0.
  - If it is a simple case where one of two considered nodes, but not both of them, does not have child nodes, or sum of its child-node weights is equal to 0, then their discrepancy is equal to sum of normalized-weighted lengths of paths from that node to supports of a corresponding measure which are in the subtree rooted at that node.

We stop the computation when the queue is empty. The aligned-root *DepthTGW* is equal to sum of all weighted discrepancies between 2-depth-level trees.

We summarize the computation for *DepthTGW* by sampling aligned-root tree metrics in Algorithm 3.

We next give a complexity analysis for *DepthTGW*:

- Recall that the complexity of sampling tree metric  $O(\bar{N}H_{\mathcal{T}} \log \kappa)$  where  $H_{\mathcal{T}}$  is a predefined deepest level of tree  $\mathcal{T}$  and  $\kappa$  is the number of clusters in the farthest-point clustering for the clustering-based tree metric sampling (Le et al., 2019);  $\bar{N}$  is the input number of supports.
- The complexity of constructing 2-depth-level trees is  $O(nH_{\mathcal{T}}\kappa)$  (we have  $n$  supports, each path from a root to a support has less than  $H_{\mathcal{T}}$  nodes, and each 2-depth-level tree has less than or equal  $(\kappa + 1)$  nodes).
- The complexity to compute the univariate OT between 2-depth-level trees is  $O(\kappa \log \kappa)$ .
- At deep level  $(h + 1)$ , the number of nodes is not more than  $\kappa^h$ . So, the number of pairs of nodes at deep level  $(h + 1)$  is not more than  $\kappa^{2h}$ . Let  $\Delta$  be the number of comparisons  $\Delta$  for 2-depth-level trees, we have  $\Delta \leq (\kappa^{2H_{\mathcal{T}}} - 1) / (\kappa^2 - 1)$ .

Therefore, one can implement the computation of *DepthTGW* with a complexity  $O(\bar{N}H_{\mathcal{T}} \log \kappa + nH_{\mathcal{T}}\kappa + \Delta\kappa \log \kappa)$ .

### C.3.2. APPLICATIONS *with* PRIORI KNOWLEDGE ABOUT TREE METRICS FOR SUPPORTS IN PROBABILITY MEASURES

For some specific applications where one has a priori knowledge about tree metric for supports in each probability measures, one can easily tailor Algorithm 3 with existing tree metrics to compute aligned-root *DepthTGW*. Thus, for the *DepthTGW*, one needs to search the optimal pair of roots for the given tree metrics<sup>9</sup>, where one uses the aligned-root *DepthTGW* for each pair of roots. Overall, the complexity of *DepthTGW* with exhausted search for the optimal pair of roots is approximately  $O(N^2nH_{\mathcal{T}}\kappa + N^2\Delta\kappa \log \kappa)$ .

<sup>8</sup>A simple case for a pair of considered nodes is defined as: at least one node of the considered pair does not have child nodes, or sum of its child-node weights is equal to 0.

<sup>9</sup>Assume that for each tree metric, each node has at most  $\kappa$  child nodes, the tree deep is  $H_{\mathcal{T}}$ , and the number of nodes in tree is about  $N$ .

**Algorithm 3** *DepthTGW* for probability measures by sampling aligned-root tree metrics

---

**Input:** Input probability measures  $\mu = \sum_{i \in [n]} a_i \delta_{x_i}$ , and  $\nu = \sum_{j \in [m]} b_j \delta_{z_j}$ .

**Output:** *DepthTGW* discrepancy  $d$ .

- 1: Sample aligned-root tree metrics  $\mathcal{T}_X, \mathcal{T}_Z$  for  $\mu, \nu$  respectively, e.g., by choosing a mean of support data as its root for the clustering-based tree metric sampling (Le et al., 2019).
  - 2: Construct  $S_{\mathcal{T}_X}, S_{\mathcal{T}_Z}$ : sets of 2-depth-level trees for  $\mu, \nu$  in tree  $\mathcal{T}_X, \mathcal{T}_Z$  respectively by using Algorithm 2.
  - 3: Initialization with a pair of roots  $(r_x, r_z)$  of tree  $\mathcal{T}_X, \mathcal{T}_Z$  respectively, and the optimal matching mass  $T^*(r_x, r_z) = 1$ , and  $d \leftarrow 0$ .
  - 4: Push  $\{(r_x, r_z), T^*(r_x, r_z)\}$  into a queue  $\mathcal{Q}$ .
  - 5: **while**  $\mathcal{Q}$  is not empty **do**
  - 6:   Pull  $(x, z), T^*(x, z)$  from queue  $\mathcal{Q}$ .
  - 7:   Get corresponding 2-depth-level trees:  $\mathcal{T}_x^2, \mathcal{T}_z^2$  for  $\mu, \nu$  from  $S_{\mathcal{T}_X}, S_{\mathcal{T}_Z}$  respectively.
  - 8:   % For two simple 2-depth-level trees, the discrepancy between  $\mu_{\mathcal{T}_x^2}, \nu_{\mathcal{T}_z^2}$  is equal to 0.
  - 9:   **if** One of two 2-depth-level trees  $\mathcal{T}_x^2, \mathcal{T}_z^2$  is simple, but not both of them **then**
  - 10:     **if**  $\mathcal{T}_x^2$  is simple **then**
  - 11:       Get all paths from  $x$  to each support of  $\mu$  in the subtree of  $\mathcal{T}_X$  rooted at  $x$ .
  - 12:       Normalize for weights of those supports of corresponding paths.
  - 13:       Compute  $\tilde{d}$  as a sum of weighted lengths for those paths.
  - 14:        $d \leftarrow d + T^*(x, z)\tilde{d}$ .
  - 15:     **else**
  - 16:       Get all paths from  $z$  to each support of  $\nu$  in the subtree of  $\mathcal{T}_Z$  rooted at  $z$ .
  - 17:       Normalize for weights of those supports of corresponding paths.
  - 18:       Compute  $\tilde{d}$  as a sum of weighted lengths for those paths.
  - 19:        $d \leftarrow d + T^*(x, z)\tilde{d}$ .
  - 20:     **end if**
  - 21:     **else if** Two 2-depth-level trees  $\mathcal{T}_x^2, \mathcal{T}_z^2$  are not simple **then**
  - 22:       Sort the distances from a root to each node in tree  $\mathcal{T}_x^2, \mathcal{T}_z^2$ .
  - 23:       Compute univariate OT  $\tilde{d}$  and the optimal transportation plan  $\tilde{T}^*$  for empirical measures with sorted supports  $\mu_{\mathcal{T}_x^2}, \nu_{\mathcal{T}_z^2}$  by using Algorithm 1.
  - 24:        $d \leftarrow d + T^*(x, z)\tilde{d}$ .
  - 25:       Compute weighted optimal transport plan  $\tilde{T}^* \leftarrow T^*(x, z)\tilde{T}^*$ .
  - 26:       For all child nodes  $u, v$  of  $\mathcal{T}_x^2, \mathcal{T}_z^2$  respectively, if their optimal matching mass  $\tilde{T}^*(u, v) > 0$ , push  $\{(u, v), \tilde{T}^*(u, v)\}$  into queue  $\mathcal{Q}$ .
  - 27:     **end if**
  - 28: **end while**
- 

## D. Further experimental results

### D.1. Further experimental results on qm7, TWITTER and RECIPE datasets

We give zoom-in results of averaged accuracy and time consumption for  $k$ -NN in TWITTER and RECIPE datasets (for Figure 4 in the main text) in Figure 10 and Figure 11 respectively.

We further illustrate the trade-off between performances and time consumption for those variants of GW when their parameters are changed, e.g., entropic regularization in entropic GW and its variant, and the number of slices in sliced GW, *FlowTGW*, and *DepthTGW*, for qm7 and RECIPE datasets in Figure 12 and Figure 13 respectively (similar to Figure 5 in the main text for TWITTER dataset).

### D.2. More experiments on larger document datasets: AMAZON and CLASSIC for document classification with non-registered word embeddings

We further evaluate our proposed tree variants of GW against other baselines on larger document datasets: AMAZON and CLASSIC for document classification with non-registered word embeddings. For these datasets, we used the same preprocessing procedure, and experimental setup as for TWITTER and RECIPE datasets described in Section 6.1 in the



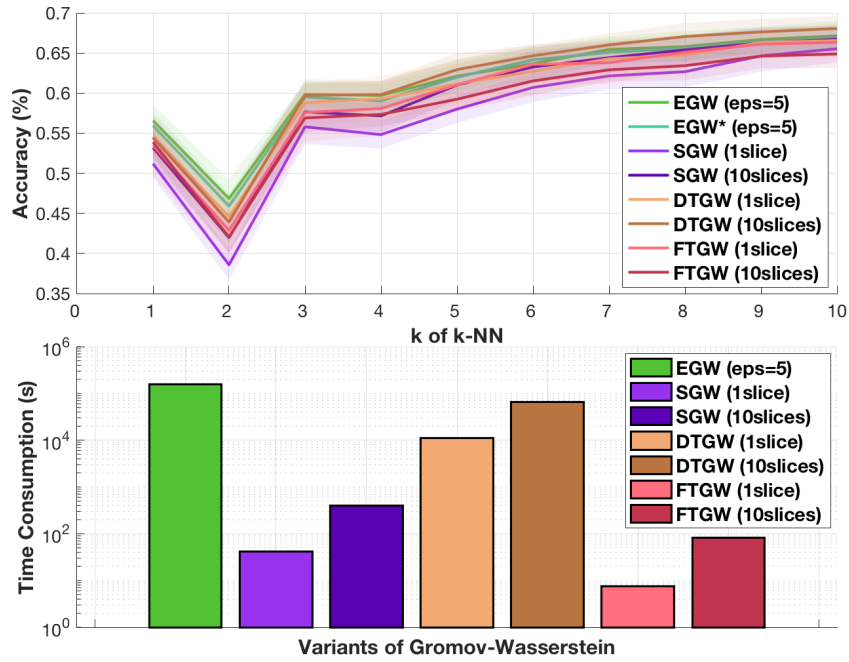


Figure 10. Zoom-in results of averaged accuracy and time consumption for  $k$ -NN in TWITTER dataset in Figure 4 in the main text.

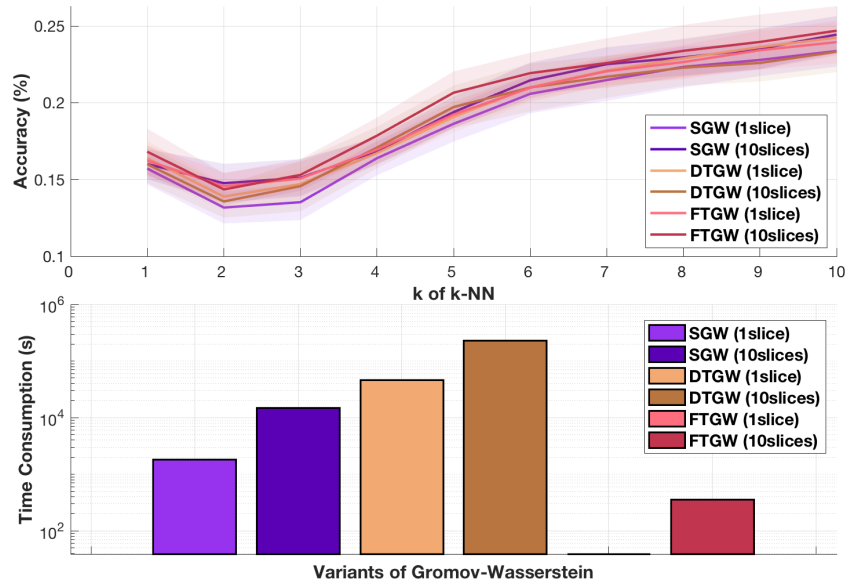


Figure 11. Zoom-in results of averaged accuracy and time consumption for  $k$ -NN in RECIPE dataset in Figure 4 in the main text.

### Fast Tree Variants of Gromov-Wasserstein

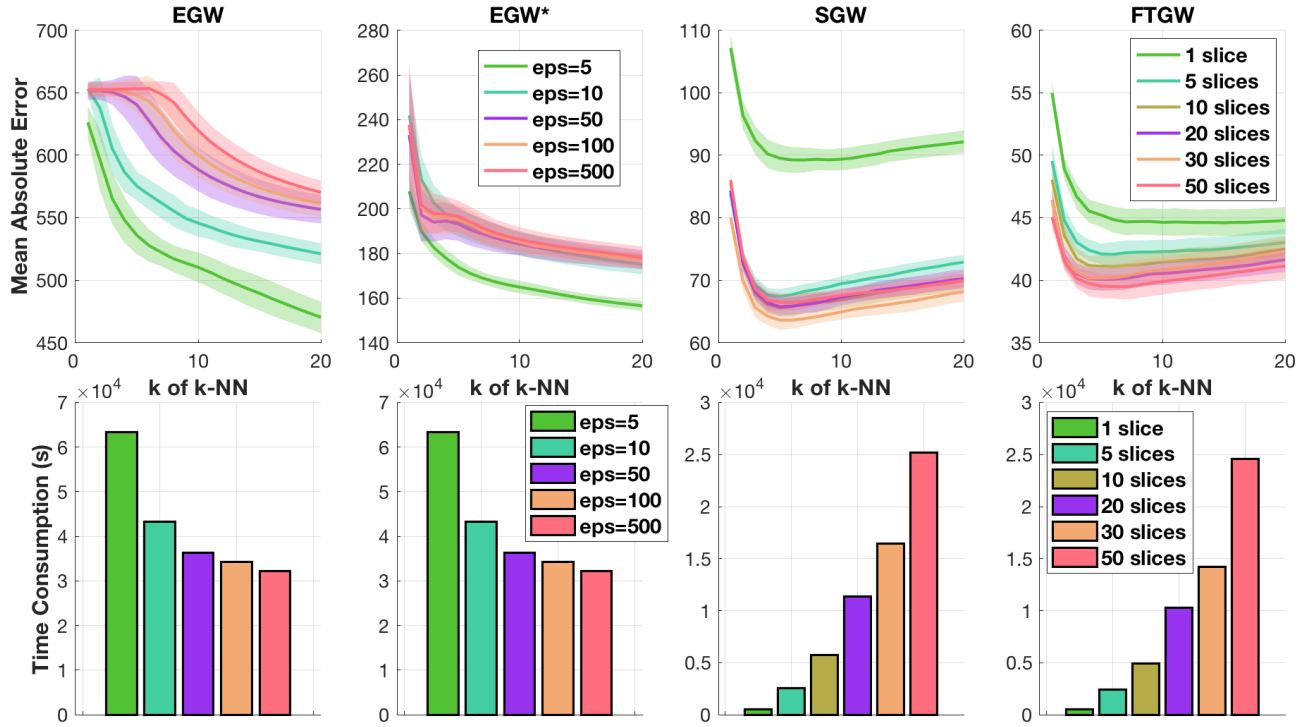


Figure 12. Results of MAE and time consumption for variants of GW with different parameters (e.g. entropic regularization in EGW/EGW\*, and number of slices in SGW/FTGW) in  $k$ -NN regression in  $qm7$  dataset. For clustering-based tree metric approach, we used its suggested parameters ( $\kappa = 4, H_T = 6$ ).

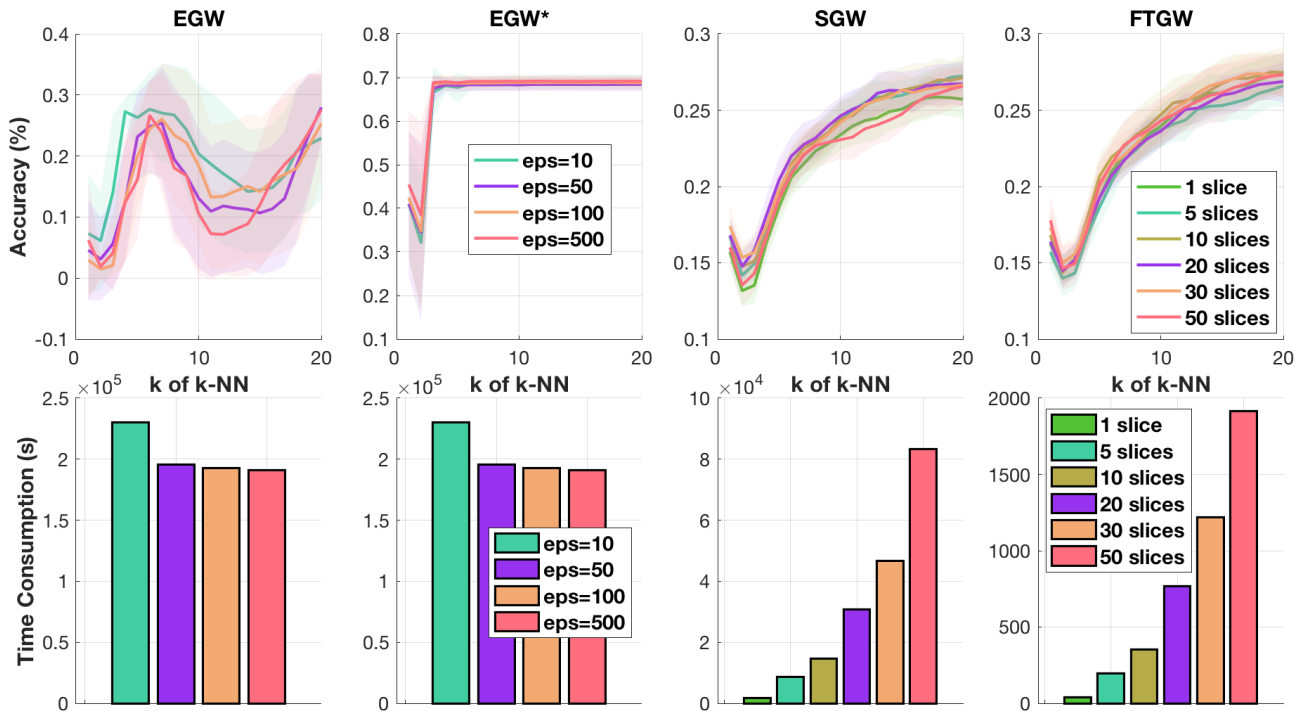


Figure 13. Results of averaged accuracy and time consumption for variants of GW with different parameters, e.g., entropic regularization in EGW/EGW\*, and the number of slices in SGW/FTGW in  $k$ -NN in RECIPE dataset. For clustering-based tree metric approach, we used its suggested parameters ( $\kappa = 4, H_T = 6$ ).

main text.

After preprocessing, there are 8000 documents in 4 classes where each document length is not more than 4592 in AMAZON dataset, and 7093 documents in 4 classes where each document length is not more than 348 in CLASSIC dataset.

We illustrate results of averaged accuracy and time consumption for  $k$ -NN in AMAZON and CLASSIC datasets in Figure 14 (similar to Figure 4 in the main text for  $qm7$ , TWITTER, and RECIPE datasets). We also observe similar results as in TWITTER and RECIPE datasets discussed in the main text. *FlowTGW* is several orders faster than other variants of GW. However, *DepthTGW* is quite slow due to solving a large number of subproblems. The performances of tree variants of GW (*FlowTGW* and *DepthTGW*) compare favorably with other variants of GW in these datasets. Similar to experiments in  $qm7$  and RECIPE datasets, the entropic term in entropic GW computation also harm its performances in AMAZON and CLASSIC datasets. Performances of entropic GW and its variant are improved when entropic regularization (eps) is smaller, but their computational time is considerably increased.

Recall that sliced GW requires to use *extra artificial zeros padding* and *uniform weights*<sup>10</sup> for probability measures with different number of supports (i.e., documents with different lengths), while note that other variants of GW work with an original number of supports (i.e., unique words in documents), and general weights (i.e., frequencies of unique words) for supports in probability measures. The limits of using uniform weights and extra artificial zeros padding of slice GW may harm its computation in datasets whose documents are long. For an example, in AMAZON dataset whose document length can reach 4592, *FlowTGW* is two orders faster than sliced GW. In details, as in Figure 14 for AMAZON dataset, the computation of *FlowTGW* (10 slices) is about *15 minutes*, while more than *45 hours* (roughly about 2 days) for sliced GW (10 slices), and more than *69 hours* (roughly about 3 days) for entropic GW (even with entropic regularization  $\text{eps}=50$ ).

Furthermore, we illustrate the trade-off between performances and time consumption for those variants of GW when their parameters are changed, e.g., entropic regularization in entropic GW and its variant, and the number of slices in sliced GW, *FlowTGW*, and *DepthTGW*, for AMAZON and CLASSIC datasets in Figure 15 and Figure 16 respectively (similar to Figure 5 in the main text for TWITTER dataset). Note that for sliced GW in AMAZON dataset, we only evaluate it until 10 slices due to its slowness with a larger number of slices.

### D.3. Time consumption for the clustering-based tree metric sampling

Time consumption for tree metric sampling by the clustering-based tree metric method (Le et al., 2019) is negligible in computation for both *FlowTGW* and *DepthTGW*. Indeed, we illustrate time consumption for tree metric sampling with different parameters, e.g., the predefined deepest level  $H_{\mathcal{T}}$ , the number of clusters  $\kappa$ , for the clustering-based tree metric sampling (Le et al., 2019) in  $qm7$ , TWITTER, RECIPE, AMAZON, and CLASSIC datasets in Figure 17. For examples, for each tree metric sampling with the suggested parameters ( $H_{\mathcal{T}} = 6, \kappa = 4$ ), it only took about 0.4 seconds for  $qm7$  dataset, 1.5 seconds for TWITTER dataset, 11.0 seconds for RECIPE dataset, 20.5 seconds for AMAZON dataset, and 17.5 seconds for CLASSIC dataset. Furthermore, we give a brief review for the clustering-based tree metric sampling in Section E.2.

### D.4. Experiment results with different parameters for tree metric sampling

We illustrate results of mean absolute error (MAE) and time consumption for *FlowTGW* with different parameters, e.g., the predefined deepest level  $H_{\mathcal{T}}$ , the number of clusters  $\kappa$ , in the clustering-based tree metric sampling (similar to Figure 6 in the main text for *FlowTGW* (10 slices) in TWITTER dataset):

- in  $qm7$  dataset for 1 slice and 10 slices in Figure 18 and Figure 19 respectively.
- in TWITTER dataset for 1 slice and 10 slices in Figure 20 and Figure 21 respectively.
- in RECIPE dataset for 1 slice and 10 slices in Figure 22 and Figure 23 respectively.
- in AMAZON dataset for 1 slice and 10 slices in Figure 24 and Figure 25 respectively.
- in CLASSIC dataset for 1 slice and 10 slices in Figure 26 and Figure 27 respectively.

<sup>10</sup>Due to a requirement of uniform weights, sliced GW considers each word in a document as a Dirac function and pads several artificial Dirac functions at zero when documents have different length. (Other variants of GW only need to consider unique words and their corresponding frequencies to represent a document as an empirical measure.)

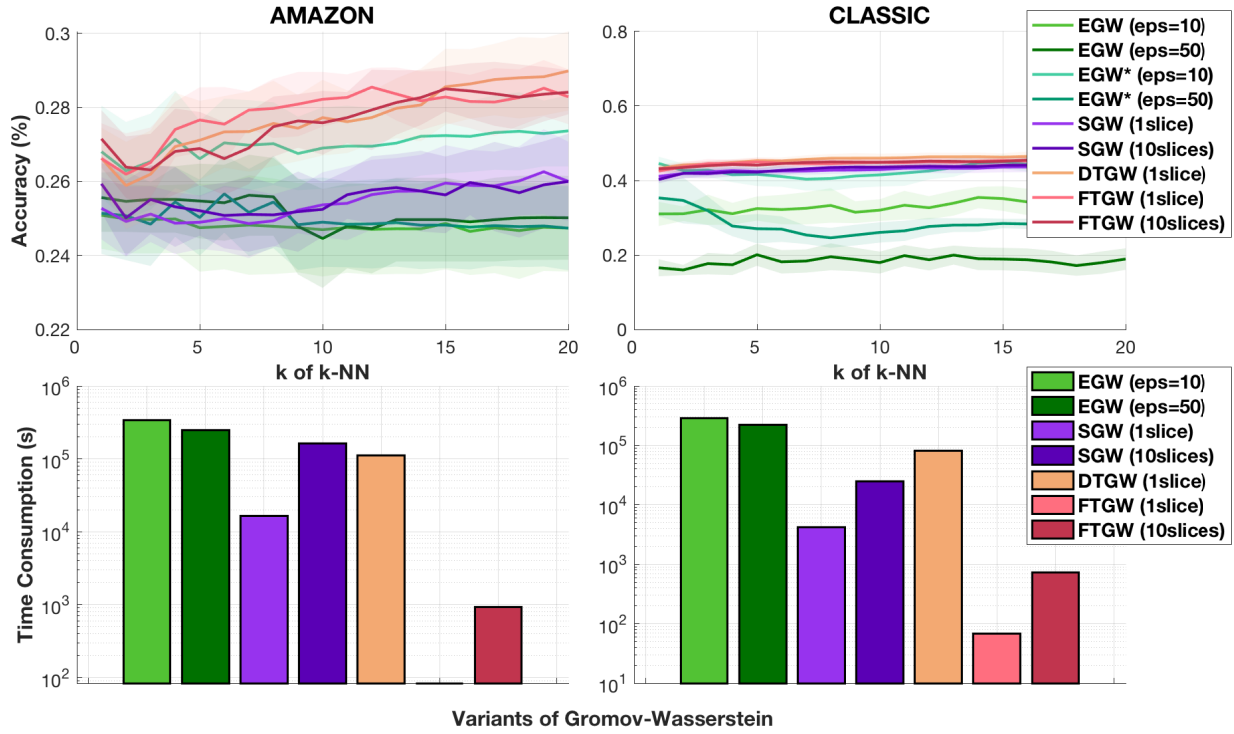


Figure 14. Results of averaged accuracy and time consumption for  $k$ -NN in AMAZON and CLASSIC datasets. For EGW/EGW\*, it is too slow for  $\text{eps}=5$  where  $\text{eps}$  is the value of entropic regularization, we used  $\text{eps}=10$  as the smallest entropic regularization for evaluation. For DTGW, we used only 1 slice due to its slowness. For clustering-based tree metric sampling, we used its suggested parameters ( $\kappa = 4$ ,  $H_T = 6$ ).

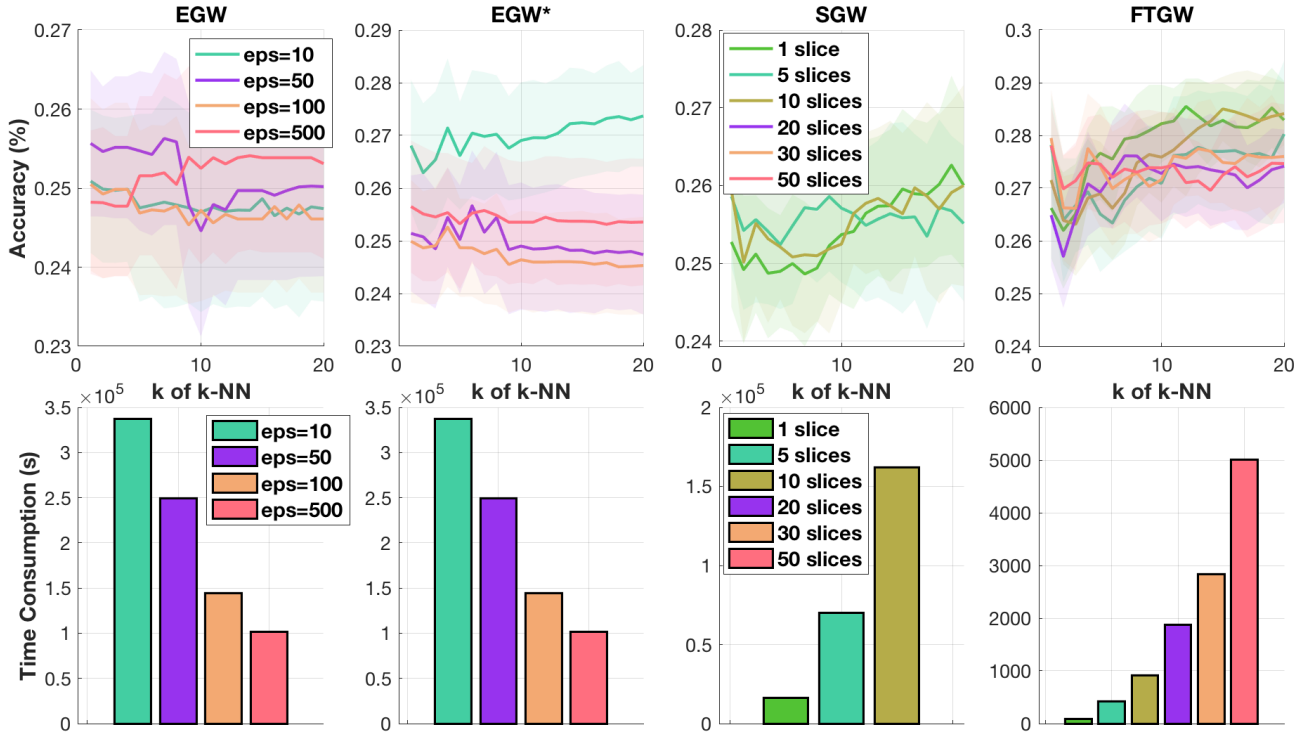


Figure 15. Results of averaged accuracy and time consumption for variants of GW with different parameters, e.g., entropic regularization in EGW/EGW\*, and the number of slices in SGW/FTGW in  $k$ -NN in AMAZON dataset. For clustering-based tree metric approach, we used its suggested parameters ( $\kappa = 4$ ,  $H_T = 6$ ). Note that for sliced GW in AMAZON dataset, we only evaluate it until 10 slices due to its slowness with a larger number of slices.

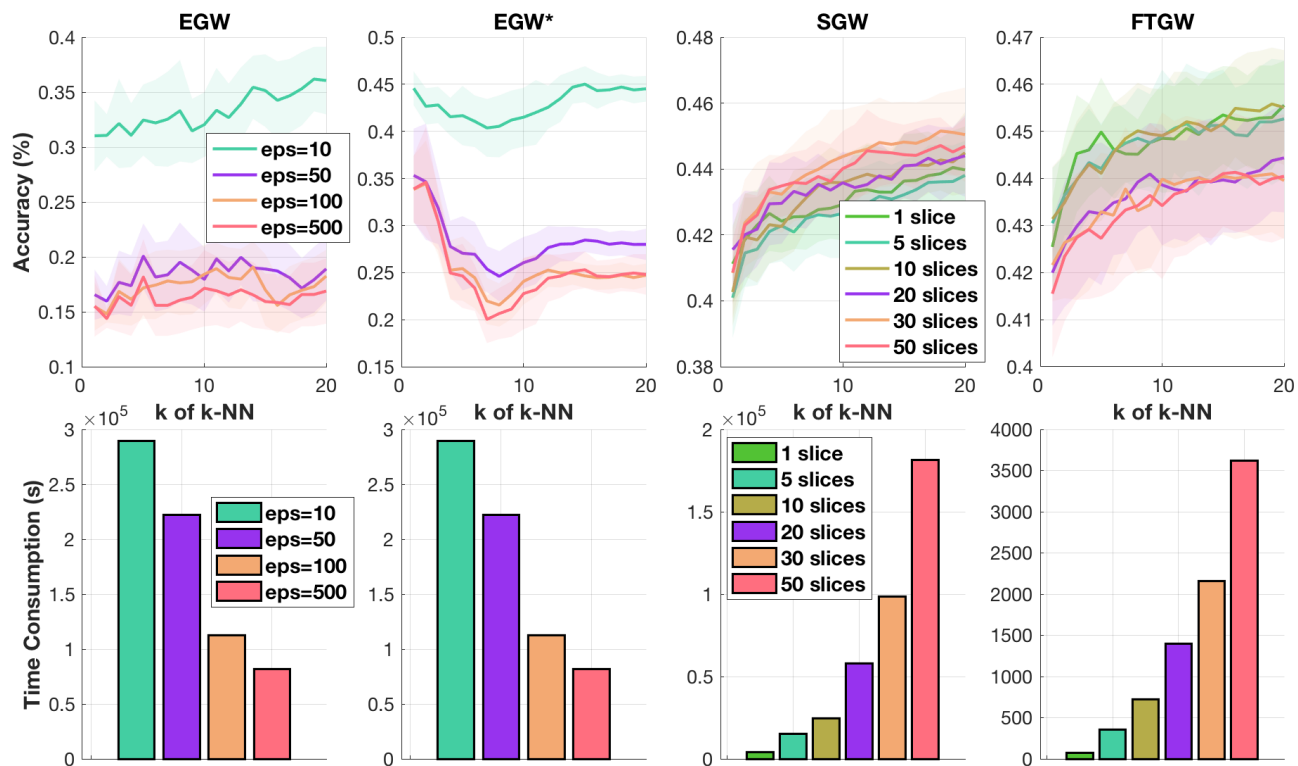


Figure 16. Results of averaged accuracy and time consumption for variants of GW with different parameters, e.g., entropic regularization in EGW/EGW\*, and the number of slices in SGW/FTGW in  $k$ -NN in CLASSIC dataset. For clustering-based tree metric approach, we used its suggested parameters ( $\kappa = 4$ ,  $H_{\mathcal{T}} = 6$ ).

## E. Some brief reviews

We give brief reviews for the farthest-point clustering (Gonzalez, 1985) (a more detail summarization and discussion can be seen in (Le et al., 2019)), the clustering-based tree metric sampling (Le et al., 2019), tree metric in (Semple & Steel, 2003), and  $F_{\beta}$  measure for clustering evaluation (Manning et al., 2008) where  $\beta$  is chosen as in (Le & Cuturi, 2015).

### E.1. The farthest-point clustering

The farthest-point clustering (Gonzalez, 1985) is a simple fast greedy approach for a  $\kappa$ -center problem. The  $\kappa$ -center problem is defined as finding a partition of  $n$  points into  $\kappa$  clusters to minimize the maximum radius of clusters. The complexity of a direct implementation, e.g., Algorithm 4, is  $O(n\kappa)$ . Moreover, by using the algorithm in (Feder & Greene, 1988)<sup>11</sup>, the complexity for the farthest-point clustering can be reduced into  $O(n \log \kappa)$ .

### E.2. Clustering-based tree metric sampling

The clustering-based tree metric sampling (Le et al., 2019) is a practical fast approach to sample tree metric from input data points. Its main idea is to use a (fast) clustering method, e.g., the farthest-point clustering, to cluster input data points hierarchically to build a tree structure, as summarized in Algorithm 5<sup>12</sup>. As discussed in (Le et al., 2019), one can use any clustering method for the clustering-based tree metric sampling. The farthest-point clustering is suggested due to its fast computation (see Section E.1). The complexity of the clustering-based tree metric sampling for  $n$  input data points where one uses the same number of clusters  $\kappa$  for the farthest-point clustering and  $H_{\mathcal{T}}$  for the predefined deepest level of tree  $\mathcal{T}$ , is  $O(nH_{\mathcal{T}} \log \kappa)$ . Therefore, the clustering-based tree metric sampling is very fast for applications.

<sup>11</sup>Code is available at <https://github.com/vmorariu/figtree/blob/master/matlab/figtreeKCenterClustering.m>

<sup>12</sup>Code is available at [https://github.com/lttam/TreeWasserstein/blob/master/BuildTreeMetric\\_HighDim\\_V2.m](https://github.com/lttam/TreeWasserstein/blob/master/BuildTreeMetric_HighDim_V2.m)

## Fast Tree Variants of Gromov-Wasserstein

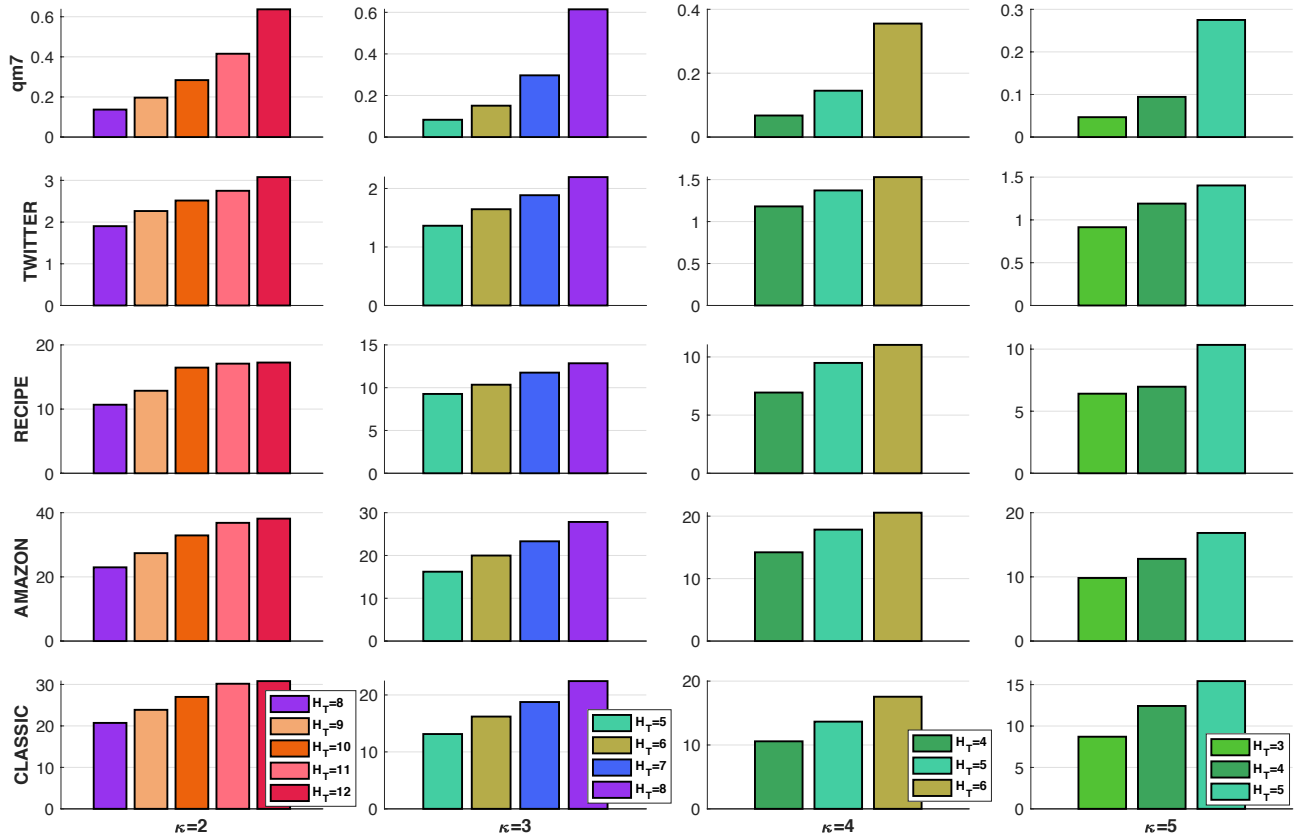


Figure 17. Time consumption (seconds) for a tree metric sampling in *FlowTGW* and *DepthTGW* by the clustering-based tree metric method (Le et al., 2019) with different parameters (e.g. the predefined deepest level  $H_T$ , the number of clusters  $\kappa$ ) in *qm7*, *TWITTER*, *RECIPE*, *AMAZON*, and *CLASSIC* datasets.

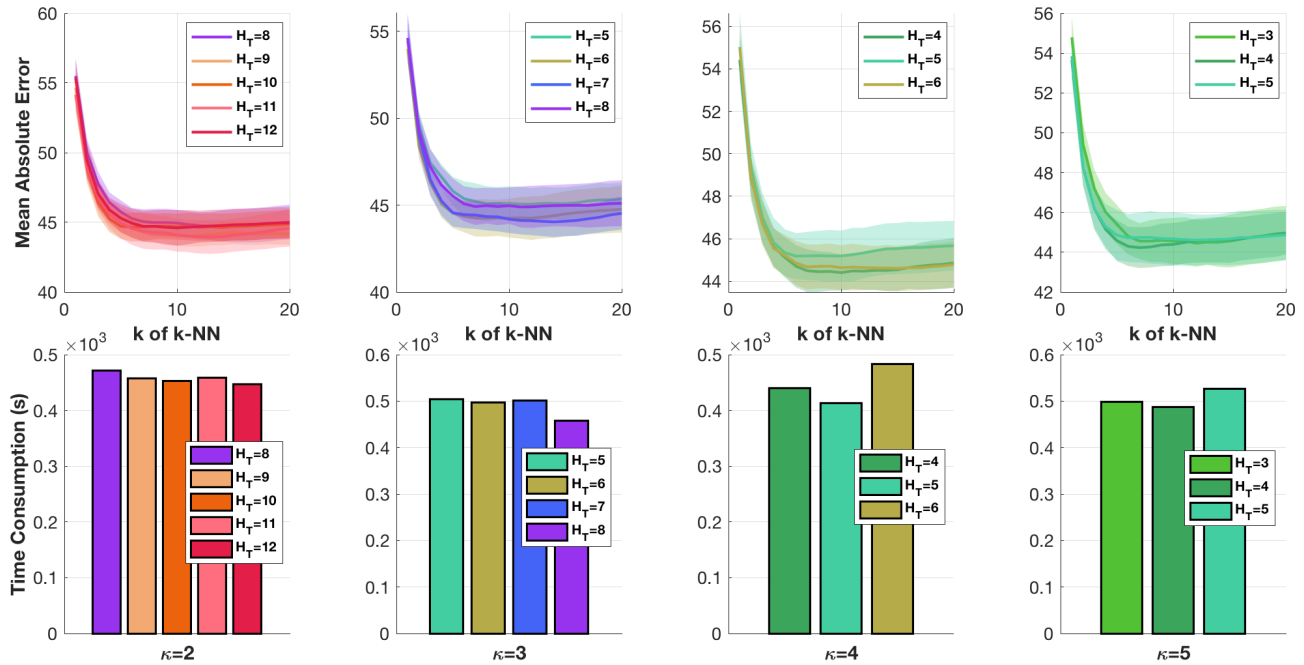


Figure 18. Results of mean absolute error and time consumption for *FlowTGW* (1 slice) with different parameters (e.g. the predefined deepest level  $H_T$ , the number of clusters  $\kappa$ ) in the clustering-based tree metric sampling in *qm7* dataset.



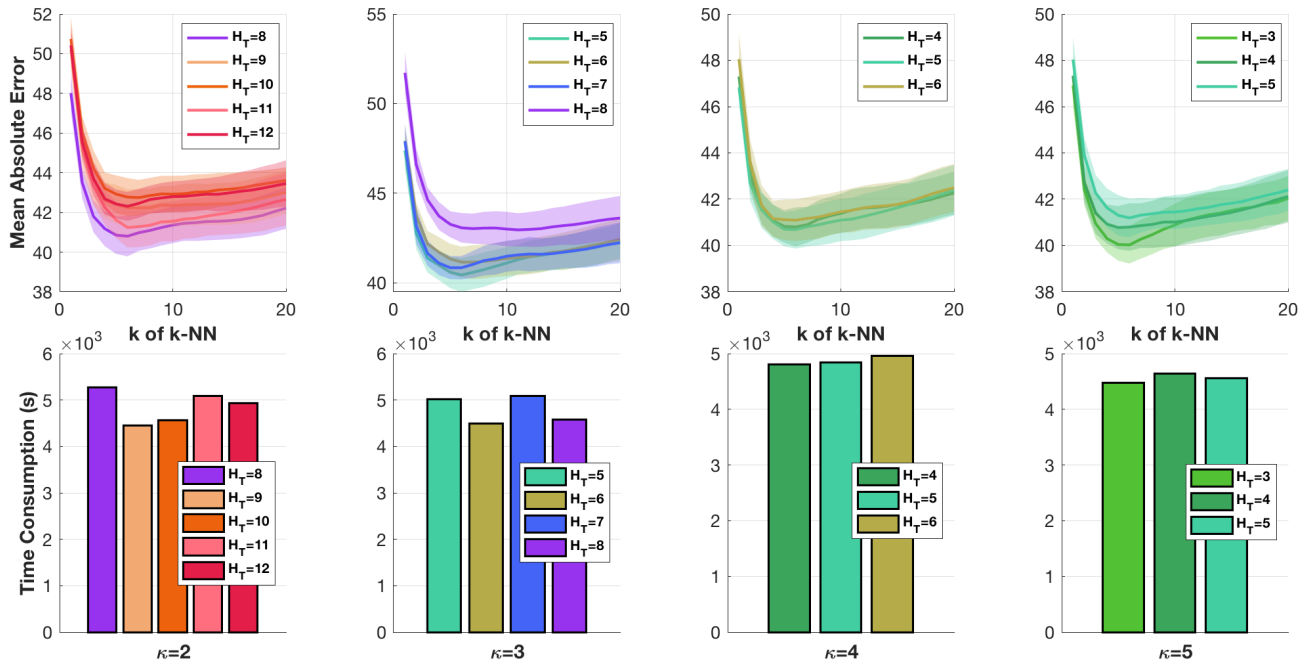


Figure 19. Results of mean absolute error and time consumption for *FlowTGW* (10 slices) with different parameters (e.g. the predefined deepest level  $H_T$ , the number of clusters  $\kappa$ ) in the clustering-based tree metric sampling in *qm7* dataset.

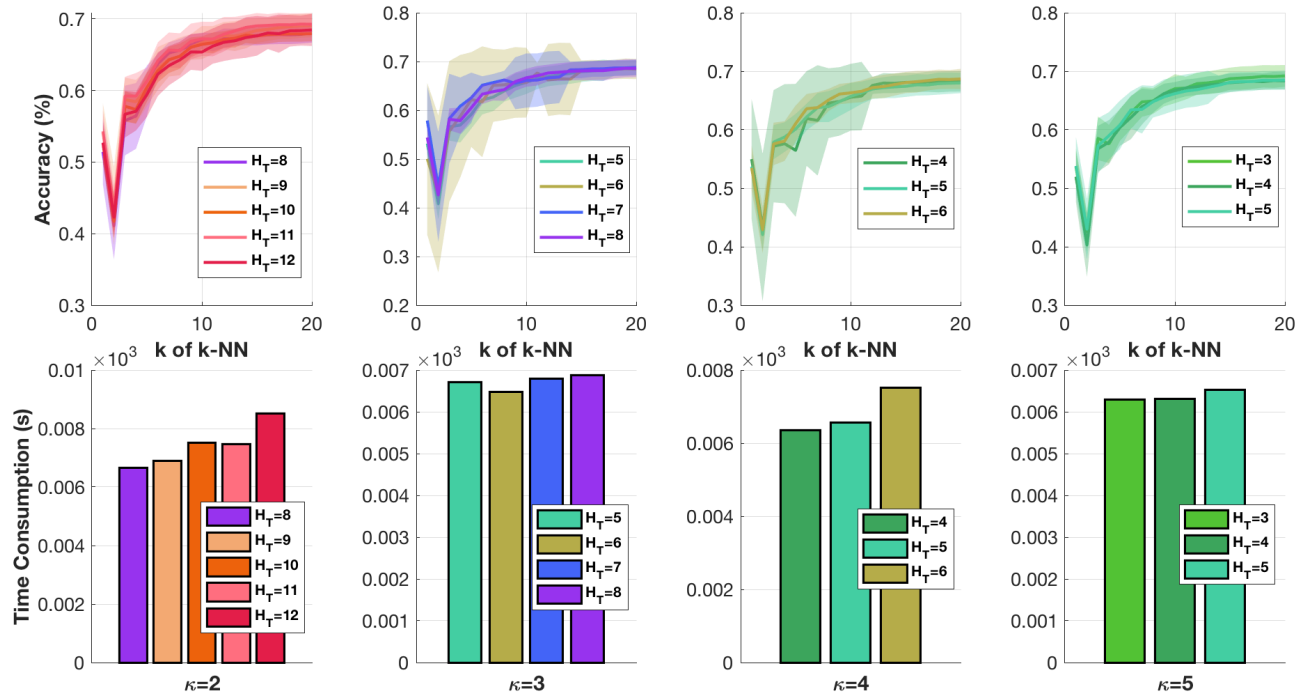


Figure 20. Results of averaged accuracy and time consumption for *FlowTGW* (1 slice) with different parameters (e.g. the predefined deepest level  $H_T$ , the number of clusters  $\kappa$ ) in the clustering-based tree metric sampling in *TWITTER* dataset.

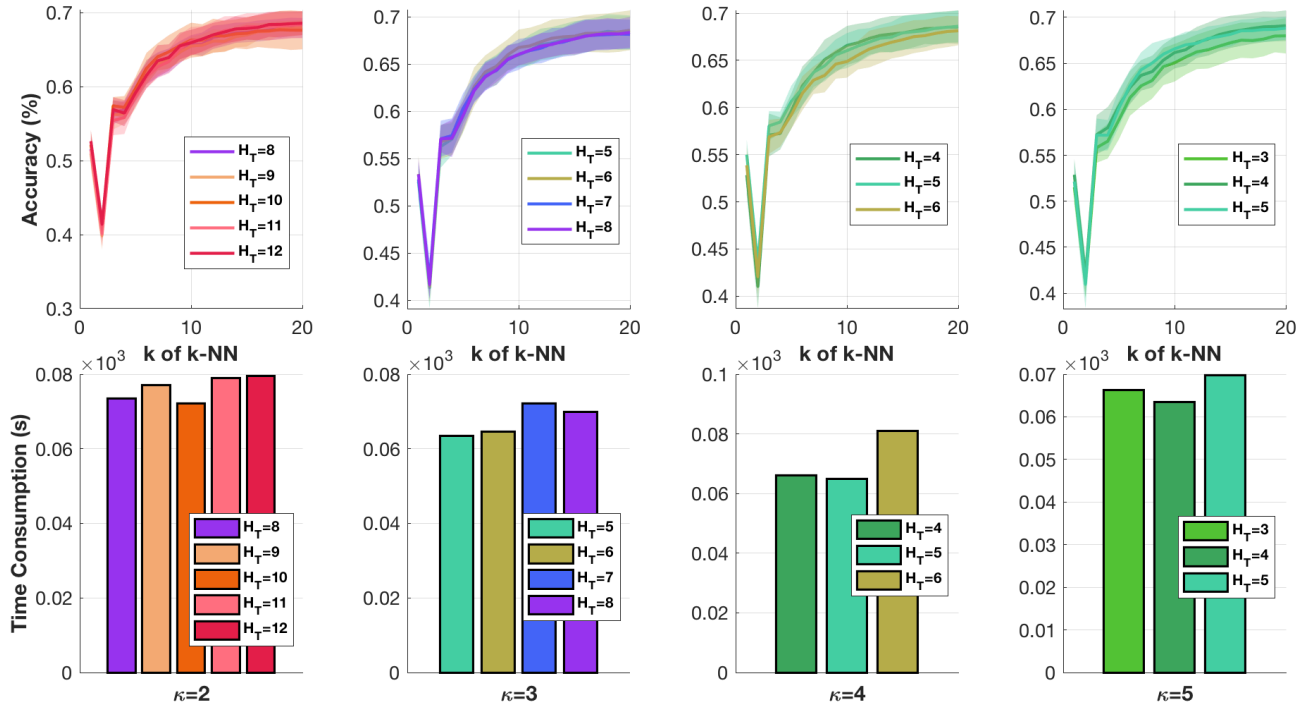


Figure 21. Results of averaged accuracy and time consumption for *FlowTGW* (10 slices) with different parameters (e.g. the predefined deepest level  $H_T$ , the number of clusters  $\kappa$ ) in the clustering-based tree metric sampling in TWITTER dataset.

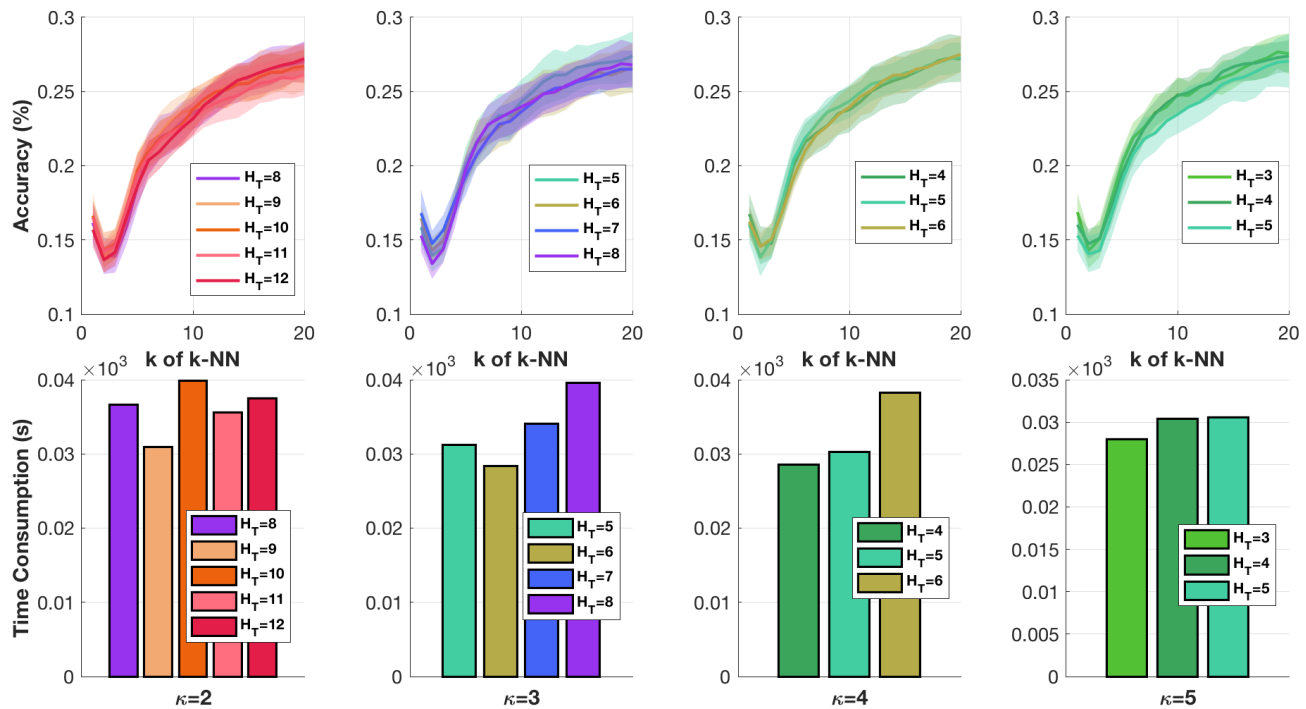


Figure 22. Results of averaged accuracy and time consumption for *FlowTGW* (1 slice) with different parameters (e.g. the predefined deepest level  $H_T$ , the number of clusters  $\kappa$ ) in the clustering-based tree metric sampling in RECIPE dataset.

### Fast Tree Variants of Gromov-Wasserstein

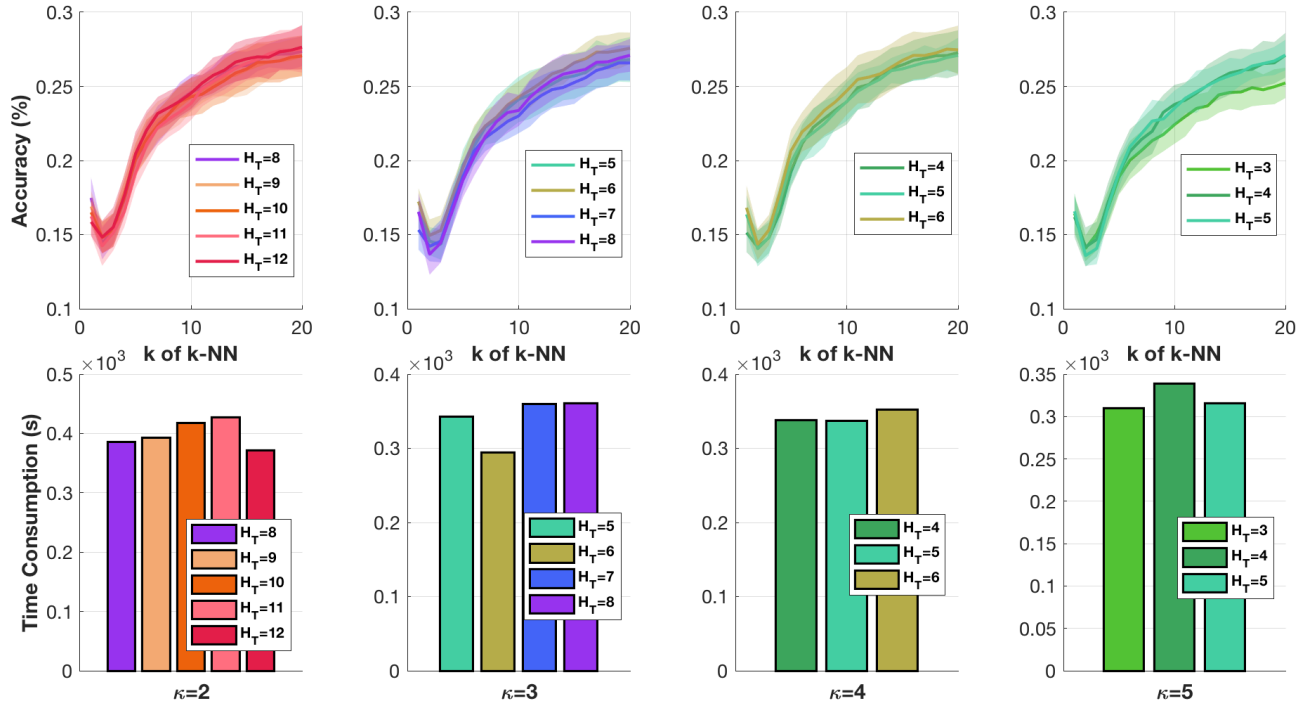


Figure 23. Results of averaged accuracy and time consumption for *FlowTGW* (10 slices) with different parameters (e.g. the predefined deepest level  $H_T$ , the number of clusters  $\kappa$ ) in the clustering-based tree metric sampling in RECIPE dataset.

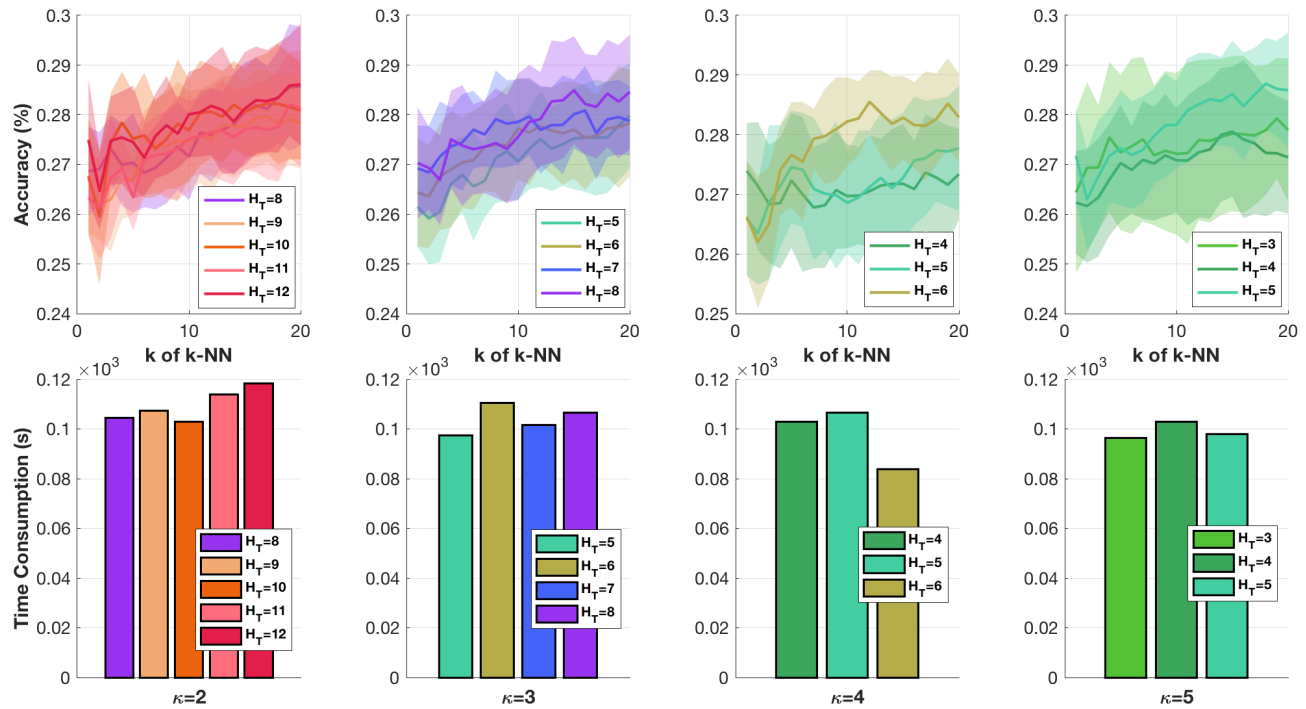


Figure 24. Results of averaged accuracy and time consumption for *FlowTGW* (1 slice) with different parameters (e.g. the predefined deepest level  $H_T$ , the number of clusters  $\kappa$ ) in the clustering-based tree metric sampling in AMAZON dataset.

### Fast Tree Variants of Gromov-Wasserstein

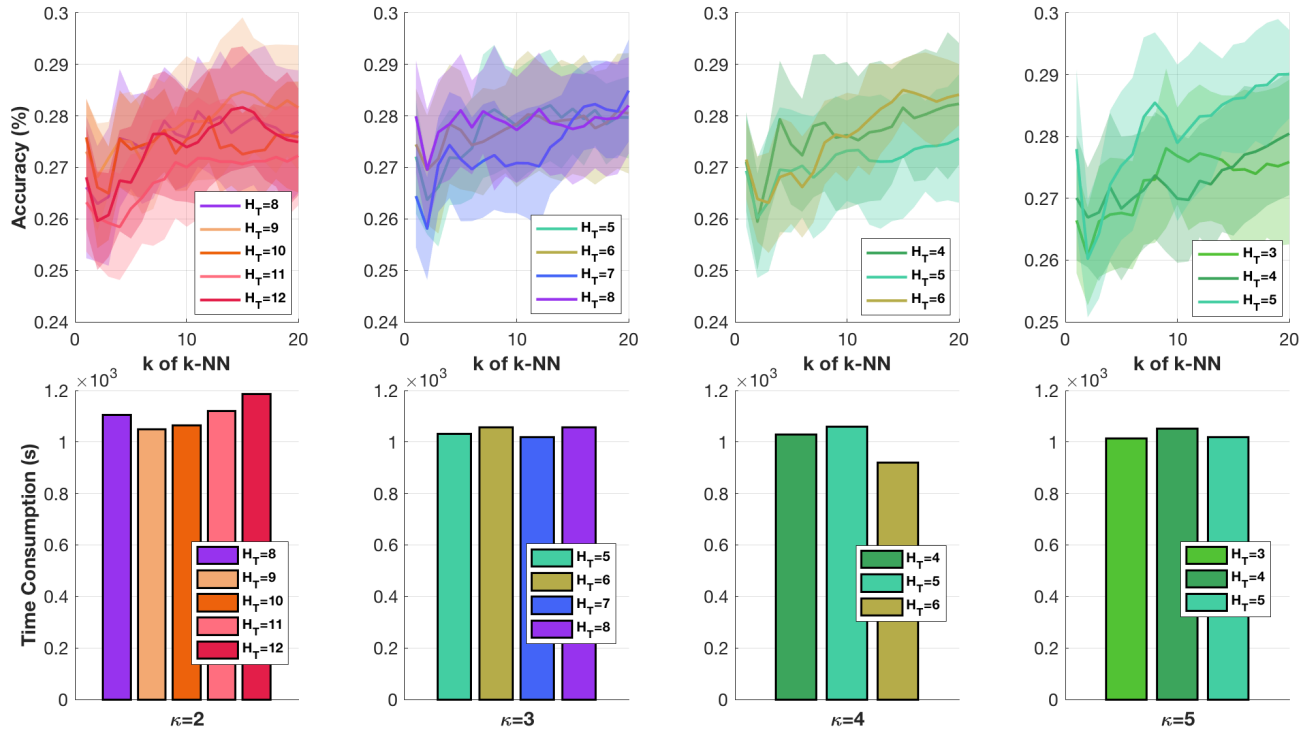


Figure 25. Results of averaged accuracy and time consumption for *FlowTGW* (10 slices) with different parameters (e.g. the predefined deepest level  $H_T$ , the number of clusters  $\kappa$ ) in the clustering-based tree metric sampling in AMAZON dataset.

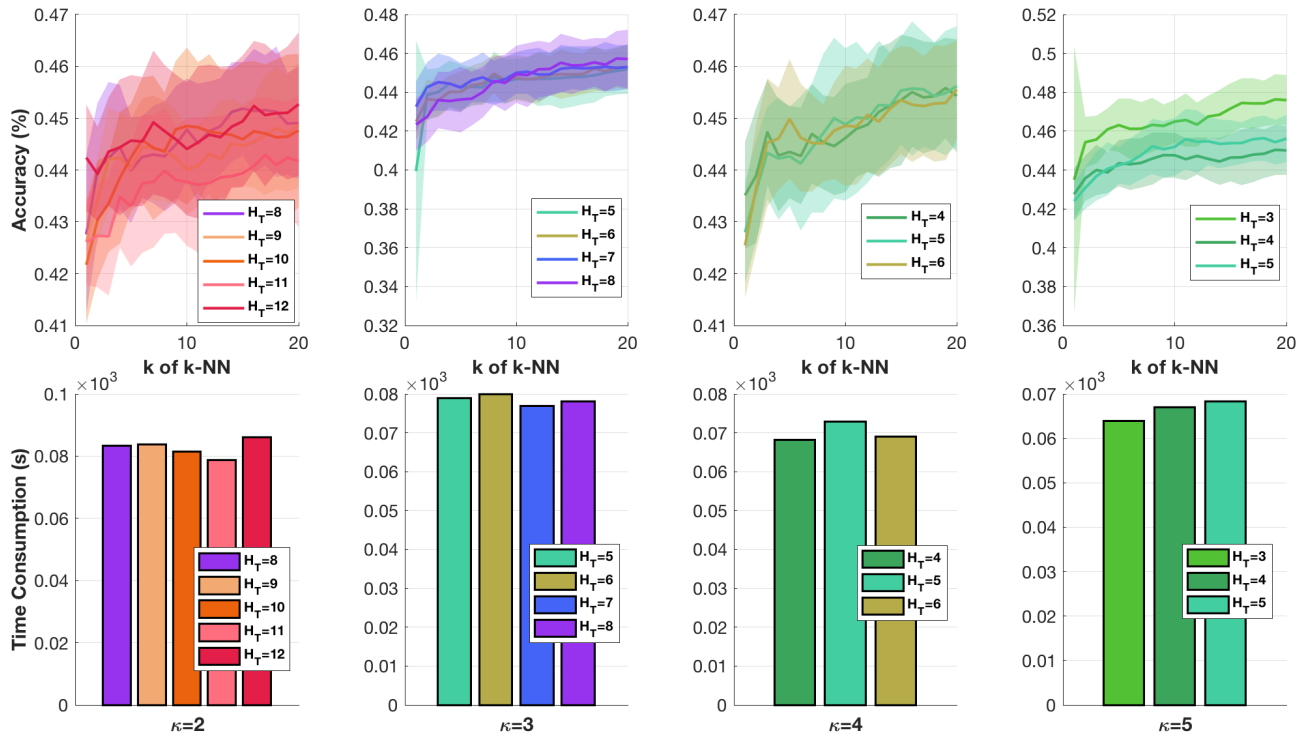


Figure 26. Results of averaged accuracy and time consumption for *FlowTGW* (1 slice) with different parameters (e.g. the predefined deepest level  $H_T$ , the number of clusters  $\kappa$ ) in the clustering-based tree metric sampling in CLASSIC dataset.



**A cluster sensitivity problem.** As discussed in (Le et al., 2019), for data points near a border of adjacent, but different clusters, they are close to each other but in different clusters. The fact that whether those data points are clustered in the same cluster or not, depends on an initialization of the farthest-point clustering. Therefore, by leveraging various clustering results, obtained with different initializations for the farthest-point clustering, e.g. as in our proposed tree-sliced variants of GW, one can reduce an affect of the cluster sensitivity problem.

---

**Algorithm 5** Clustering-based tree metric (with the farthest-point clustering)

---

**Input:**  $X$  is a set of  $m$  input data points,  $\tilde{x}_p$  is a parent node for those input data points in  $X$ ,  $h$  is a current depth level,  $H_{\mathcal{T}}$  is the predefined deepest level of tree  $\mathcal{T}$ ,  $\kappa$  is the predefined number of clusters for the farthest-point clustering.

**Output:** tree metric  $\mathcal{T}$

```

1: if  $m > 0$  then
2:   if  $h > 0$  then
3:     Node  $\tilde{x}_c \leftarrow$  a center of  $X$ , e.g., the mean data point of  $X$ .
4:     Length of edge  $(\tilde{x}_p, \tilde{x}_c) \leftarrow$  distance  $(\tilde{x}_p, \tilde{x}_c)$ .
5:   else
6:     Node  $\tilde{x}_c \leftarrow \tilde{x}_p$ .
7:   end if
8:   if  $m > 1$  and  $h < H_{\mathcal{T}}$  then
9:     Run the farthest-point clustering for  $X$  into  $\kappa$  clusters  $X_i \mid_{i \in [\kappa]}$ .
10:    for each cluster  $X_i \mid_{i \in [\kappa]}$  do
11:      Recursive the clustering-based tree metric for input data points in set  $X_i$ , a parent node  $\tilde{x}_c$ , a current depth level  $(h + 1)$  with the predefined deepest level  $H_{\mathcal{T}}$  for tree  $\mathcal{T}$ , and the predefined number of clusters  $\kappa$  for the farthest-point clustering).
12:    end for
13:  end if
14: end if

```

---

### E.3. Tree metric

We recall the definition of tree metric in (Semple & Steel, 2003) (§7, p.145–182).

**Definition 6.** A metric  $d : \Omega \times \Omega \rightarrow \mathbb{R}_+$  is a tree metric on a finite set  $\Omega$  if there exists a tree  $\mathcal{T}$  with non-negative edge lengths such that all elements of  $\Omega$  are nodes in  $\mathcal{T}$ , and for  $x, z \in \Omega$ ,  $d(x, z)$  equals to the length of the (unique) path in  $\mathcal{T}$  between  $x$  and  $z$ .

### E.4. $F_{\beta}$ measure for clustering evaluation

We summarize the  $F_{\beta}$  measure for clustering evaluation as in (Manning et al., 2008) where  $\beta$  is chosen as in (Le & Cuturi, 2015). The main idea is that a pair of data points is assigned to the same cluster if and only if they are in the same class and otherwise. We have some following quantities:

- TP: the number of a true positive decisions which assign a pair of data points in the same class to the same cluster.
- TN: the number of a true negative decisions which assign a pair of data points in the different classes to the different clusters.
- FP: the number of a false positive decisions which assign a pair of data points of different classes to the same cluster.
- FN: the number of a false negative decisions which assign a pair of data points of the same class to different clusters.

Consequently, we have the precision

$$\mathbf{P} = \frac{\text{TP}}{\text{TP} + \text{FP}}, \quad (14)$$

and recall

$$\mathbf{R} = \frac{\text{TP}}{\text{TP} + \text{FN}}. \quad (15)$$



Note that we usually have many more pairs of data points in different classes than in the same class in clustering. Therefore, we need to penalize false negative error more strongly than false positive error.  $\mathbf{F}_\beta$  measure can take into account of this idea by using a scalar  $\beta > 1$ , defined as follow:

$$\mathbf{F}_\beta = \frac{(\beta^2 + 1) \mathbf{P} \mathbf{R}}{\beta^2 \mathbf{P} + \mathbf{R}}. \quad (16)$$

Following (Le & Cuturi, 2015), we plug Equation (14), and Equation (15) into Equation (16), and observe that  $\mathbf{F}_\beta$  penalizes false negative error  $\beta^2$  times more than false positive error. Then, we can set

$$\beta = \sqrt{\frac{|\mathcal{D}|}{|\mathcal{S}|}}, \quad (17)$$

where  $|\cdot|$  denotes a cardinality of a set let;  $\mathcal{D}$ ,  $\mathcal{S}$  are sets of pairs of data points in different and same classes respectively.

### E.5. More information about datasets

**Quantum chemistry.** One can download *qm7* dataset from: <http://quantum-machine.org/datasets/>. We emphasize that for simplicity, we only use the Cartesian coordinate of each atom ( $\mathbb{R}^3$ ) in the molecules. We do *not* use the atomic nuclear charge for each molecule for the atomization energy prediction task as used in experiments of (Rupp et al., 2012; Peyré et al., 2016).

**Document classification with non-registered word embeddings.** One can download document datasets, e.g., TWITTER, RECIPE, AMAZON, and CLASSIC datasets from: <https://github.com/mkusner/wmd>.

## F. Some further discussions

**Network flow.** In combinatorial optimization, network flow is a class of computational problems in which the input is a graph with capacities on its edges (Ahuja et al., 1988). The minimum-cost flow problem is one of popular classes of network flow problems. Especially, optimal transport (OT) for probability measures whose supports are in the same space, can be regarded as one of instances of the minimum-cost flow problems, and one can use the network simplex algorithm to solve it. However, for GW, the supports of input probability measures are in different spaces. Therefore, one may not use algorithms for minimum-cost flow problems, e.g., network simplex, to optimize the alignment in tree GW problem (Equation (1) in the main text) where supports of input probability measures are in different tree metric spaces.

Recall that our proposed flow-based representation for a probability measure in a tree metric space is based on *flows* from a root to each support in the probability measure, and a mass for each flow is equal to a weight on the corresponding support in the probability measure. Thus, one should distinguish between the flow-based representation for probability measures in tree metric spaces for our proposed tree variants of GW and algorithms for minimum-cost flow problems. Note that the flows of our flow-based representation shares the same spirit with the flows modeled in the proof for the closed-form computation of tree-Wasserstein distance (Le et al., 2019) (§3).

**Tree metric sampling.** Our goal is not to approximate the GW distance between probability measures whose supports are in the Euclidean space (i.e., the ground metric is Euclidean metric), but rather to sample tree metrics for each space of supports, and then use those random sampled tree metrics as ground metrics for supports of input probability measures in GW, similar to tree-sliced-Wasserstein (Le et al., 2019).

Like the case of one-dimensional projections for sliced Wasserstein, or sliced GW, which do not give good properties from a distortion point of view, but remain useful for sliced Wasserstein or sliced GW in applications, we believe that tree metrics with a large distortion can be useful, similar to the case of tree-sliced-Wasserstein in practical applications.

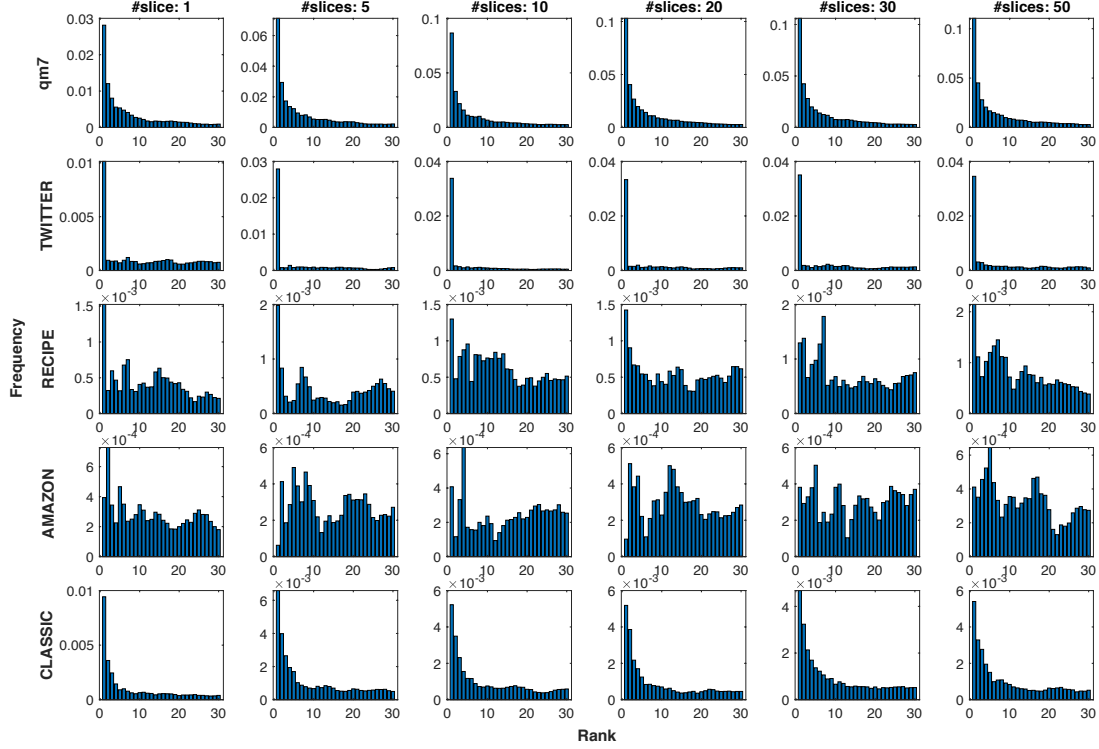


Figure 28. Empirical relation:  $\text{GW}_\alpha := \text{FTGW}$  and  $\text{GW}_\beta := \text{DTGW}$ . We used DTGW with 1 slice for *qm7*, 10 slices for TWITTER, 5 slices for RECIPE, 1 slice for AMAZON, and 1 slice for RECIPE as in Figure 4 in the main text for DTGW ( $Y$  slices) for *qm7*, TWITTER, and RECIPE datasets; and Figure 14 for DTGW for AMAZON and CLASSIC datasets.

**A correction of the binomial expansion trick in (Vayer et al., 2019).** There is a typo in the binomial expansion trick in (Vayer et al., 2019). We correct it as follows:

$$\begin{aligned}
 \sum_{i,j} ((x_i - x_j)^2 - (y_{\sigma_i} - y_{\sigma_j})^2)^2 &= 2n \left( \sum_i x_i^4 \right) - 8 \left( \sum_i x_i^3 \right) \left( \sum_i x_i \right) + 6 \left( \sum_i x_i^2 \right)^2 \\
 &\quad + 2n \left( \sum_i y_i^4 \right) - 8 \left( \sum_i y_i^3 \right) \left( \sum_i y_i \right) + 6 \left( \sum_i y_i^2 \right)^2 \\
 &\quad - 4 \left( \sum_i x_i^2 \right) \left( \sum_i y_i^2 \right) - 4n \left( \sum_i x_i^2 y_{\sigma_i}^2 \right) \\
 &\quad + 8 \left( \sum_i x_i \right) \left( \sum_i x_i y_{\sigma_i}^2 \right) + 8 \left( \sum_i y_i \right) \left( \sum_i x_i^2 y_{\sigma_i} \right) \\
 &\quad - 8 \left( \sum_i x_i y_{\sigma_i} \right)^2. \tag{18}
 \end{aligned}$$

The  $\sigma$  in Equation (18) is a permutation. Note that the binomial expansion trick can be applied for GW when one uses the squared  $\ell_2$  loss and input probability measures have the same number of supports with uniform weights as considered in sliced GW (Vayer et al., 2019).

## G. Empirical relation for variants of Gromov-Wasserstein

We emphasize that the proposed *FlowTGW* and *DepthTGW* are two novel tree variants of GW, and we do not try to mimic/approximate either the entropic GW and its variants or sliced GW.

In this section, we investigate an empirical relation between a pair of variants of GW, e.g., let denote those considered variants of GW as  $GW_\alpha$  and  $GW_\beta$ . We carried out following experiments<sup>13</sup>:

For a query point  $q$ , we denote  $q_{NN}$  as the nearest neighbor of  $q$  with respect to  $GW_\alpha$ . Then, we investigate the frequency of rank order of  $q_{NN}$  among nearest neighbor of  $q$  with respect to  $GW_\beta$ . For those experiments, we randomly split 90%/10% for training and test. Reported results are averaged over 1000 runs.

We recall some following notations: FTGW for *FlowTGW*, DTGW for *DepthTGW*, SGW for sliced GW, EGW for entropic GW and EGW\* for the variant of entropic GW. We also recall that supports for probability measures are in low-dimensional spaces (dim=3) in *qm7* dataset; and in high-dimensional spaces (dim=300) in TWITTER, RECIPE, AMAZON and CLASSIC datasets. The number of supports for probability measures are small in *qm7* (#supports  $\leq 23$ ), and TWITTER (#supports  $\leq 29$ ) datasets; and are large in RECIPE (#supports  $\leq 628$ ), AMAZON (#supports  $\leq 4592$ ), and CLASSIC (#supports  $\leq 348$ ) datasets.

### G.1. Empirical relation between FTGW and DTGW

We set  $GW_\alpha := FTGW$  and  $GW_\beta := DTGW$ . Figure 28 illustrates an empirical relation between FTGW and DTGW in *qm7*, TWITTER, and RECIPE datasets. We used DTGW with 1 slice for *qm7*, 10 slices for TWITTER, 5 slices for RECIPE, 1 slice for AMAZON, and 1 slice for RECIPE as in Figure 4 in the main text for DTGW ( $Y$  slices) for *qm7*, TWITTER, and RECIPE datasets; and Figure 14 for DTGW for AMAZON and CLASSIC datasets.

The empirical results show that FTGW agrees with some aspects of DTGW, especially when the number of support for probability measures is small (information about relative deep levels of supports is small), and the degree of agreement may increase when supports for probability measures are low-dimensional space (tree structure becomes simpler) as in *qm7*. From Figure 28, we also observe that the degree of agreement decreases when the number of supports in datasets increases.

Recall that DTGW is a generalized version of FTGW which takes into account deep levels of supports in tree structures of tree metric spaces. When the number of supports for probability measures is large, the information about relative deep levels of supports is increased. Therefore, DTGW operates differently to FTGW, e.g., in RECIPE and AMAZON datasets. In addition, tree structure for high-dimensional spaces of supports (e.g., in TWITTER and CLASSIC datasets) is usually more complex than that of low-dimensional space of supports (e.g., in *qm7* dataset). Thus, DTGW behaves more similar to FTGW in *qm7* dataset than in TWITTER and CLASSIC datasets.

### G.2. Empirical relation between FTGW and SGW

We first set  $GW_\alpha := SGW$  and  $GW_\beta := FTGW$ . For sliced GW in AMAZON dataset, we only evaluate it until 10 slices due to its slowness with a larger number of slices. We illustrate an empirical relation between FTGW and DTGW in *qm7*, TWITTER, and RECIPE datasets where we used 10 slices for FTGW in Figure 29, and 50 slices for FTGW in Figure 30.

Secondly, we set  $GW_\alpha := FTGW$  and  $GW_\beta := SGW$ . We illustrate another empirical relation between FTGW and DTGW in *qm7*, TWITTER, and RECIPE datasets where we used 10 slices for SGW in Figure 31, and 50 slices for SGW in Figure 32.

The empirical results show that SGW and FTGW may agree with each other some aspects when supports are in low-dimensional spaces, e.g., in *qm7* dataset, but they become more different when supports are in high-dimensional spaces, e.g., in document datasets: TWITTER, RECIPE, AMAZON, and CLASSIC datasets. Note that a one-dimensional space is a special case of tree metric (a tree metric is a chain). For supports in low-dimensional spaces, both projecting those supports in one-dimensional spaces and using tree metric sampling seem to be able to capture the structure of a distribution of supports at a certain level. However, for supports in high-dimensional spaces, projecting the supports in one-dimensional space limits its capacity to capture the structure of a distribution of supports (Liutkus et al., 2019) while sampling tree metric can remedy this problem (Le et al., 2019).

<sup>13</sup>The experimental setup is similar to that of (Le et al., 2019) for investigating an empirical relation between tree-sliced-Wasserstein and optimal transport with Euclidean ground metric.

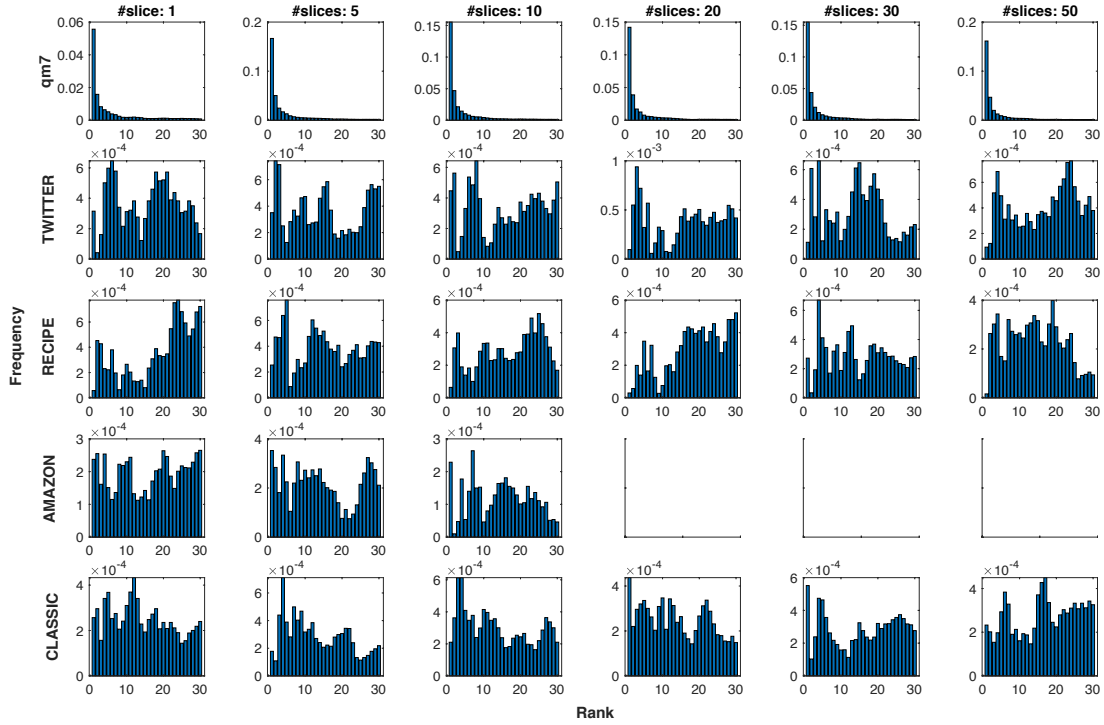


Figure 29. Empirical relation:  $GW_\alpha := SGW$  and  $GW_\beta := FTGW$  (10 slices). For sliced GW in AMAZON dataset, we only evaluate it until 10 slices due to its slowness with a larger number of slices.

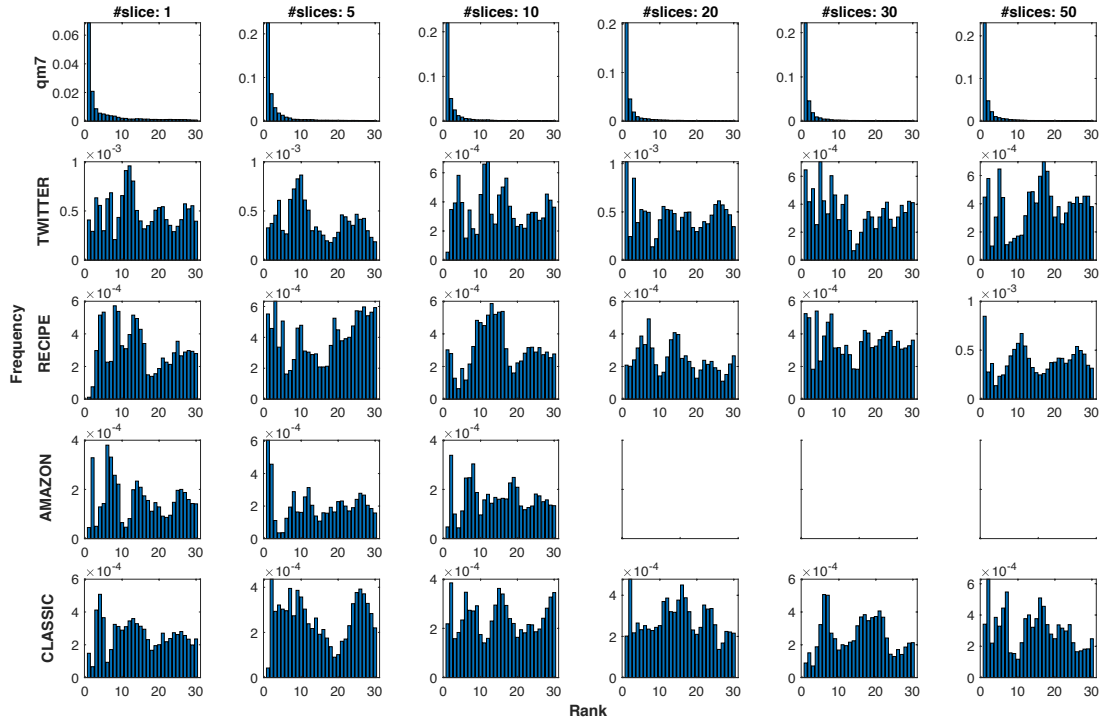


Figure 30. Empirical relation:  $GW_\alpha := SGW$  and  $GW_\beta := FTGW$  (50 slices). For sliced GW in AMAZON dataset, we only evaluate it until 10 slices due to its slowness with a larger number of slices.

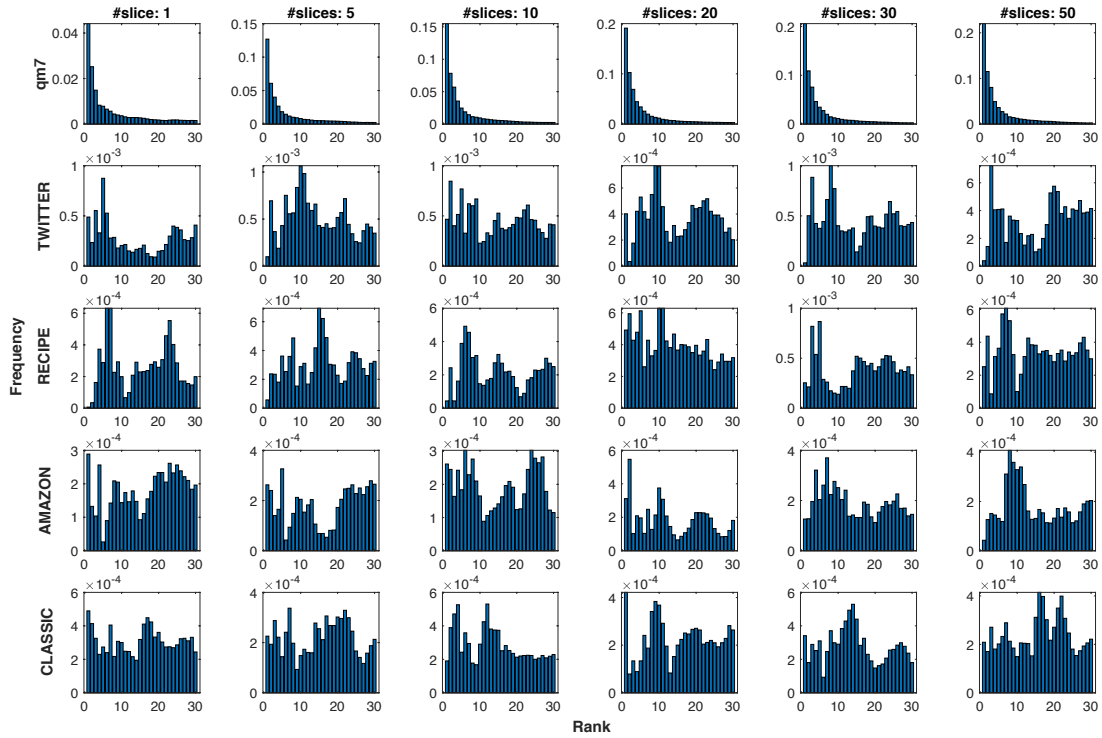


Figure 31. Empirical relation:  $GW_\alpha := FTGW$  and  $GW_\beta := SGW$  (10 slices).

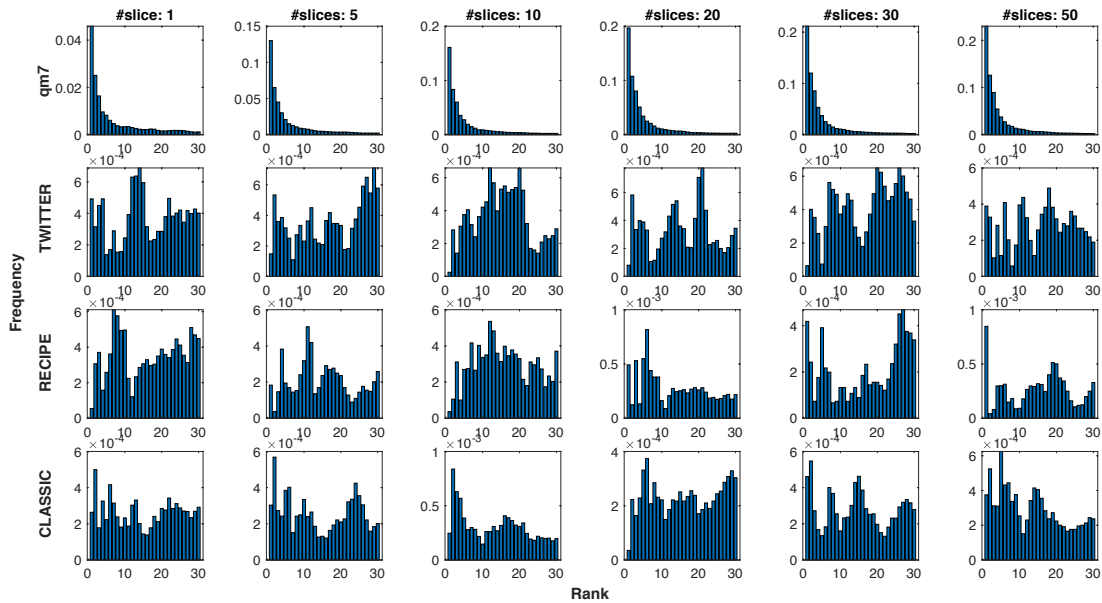


Figure 32. Empirical relation:  $GW_\alpha := FTGW$  and  $GW_\beta := SGW$  (50 slices). Note that for sliced GW in AMAZON dataset, we only evaluate it until 10 slices due to its slowness with a larger number of slices. Therefore, there is no result for sliced GW with 50 slices in AMAZON dataset.

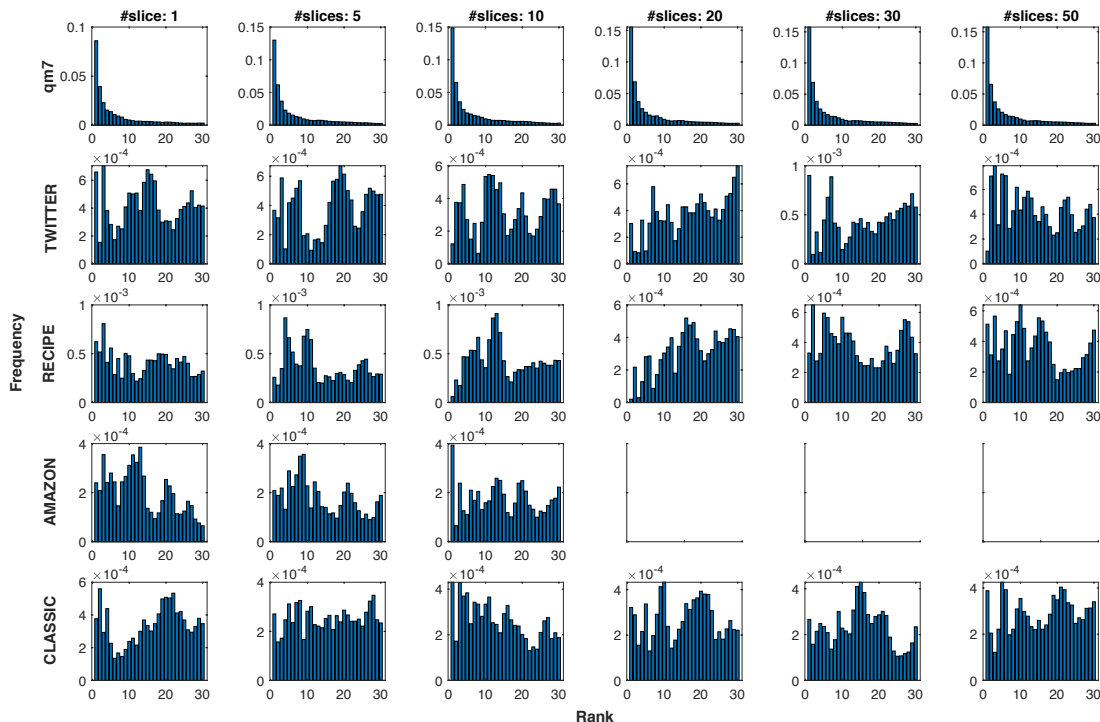


Figure 33. Empirical relation:  $\text{GW}_\alpha := \text{SGW}$  and  $\text{GW}_\beta := \text{DTGW}$ . We used DTGW with 1 slice for *qm7*, 10 slices for TWITTER, 5 slices for RECIPE, 1 slice for AMAZON, and 1 slice for RECIPE as in Figure 4 in the main text for DTGW ( $Y$  slices) for *qm7*, TWITTER, and RECIPE datasets; and Figure 14 for DTGW for AMAZON and CLASSIC datasets. For sliced GW in AMAZON dataset, we only evaluate it until 10 slices due to its slowness with a larger number of slices.

### G.3. Some other empirical relations

#### G.3.1. EMPIRICAL RELATION BETWEEN SGW AND DTGW

We set  $\text{GW}_\alpha := \text{SGW}$  and  $\text{GW}_\beta := \text{DTGW}$ . Figure 33 illustrates an empirical relation between SGW and DTGW in *qm7*, TWITTER, RECIPE, AMAZON, and CLASSIC datasets. We used DTGW with 1 slice for *qm7*, 10 slices for TWITTER, 5 slices for RECIPE, 1 slice for AMAZON, and 1 slice for RECIPE as in Figure 4 in the main text for DTGW ( $Y$  slices) for *qm7*, TWITTER, and RECIPE datasets; and Figure 14 for DTGW for AMAZON and CLASSIC datasets. For sliced GW in AMAZON dataset, we only evaluate it until 10 slices due to its slowness with a larger number of slices.

The empirical results show that SGW agrees with some aspects of DTGW when supports for probability measures are in a low-dimensional space (tree structure becomes simpler), as in *qm7* dataset. When supports for probability measure are in a low-dimensional space (e.g., in *qm7* dataset), both SGW and DTGW agree with some aspect of FTGW (see more discussions in Section G.1, and Section G.2), or SGW and DTGW agrees with each other some aspects. However, when supports for probability measure are in high-dimensional spaces (e.g., in document datasets: TWITTER, RECIPE, AMAZON, and CLASSIC datasets), they become different (similar to the empirical relation between SGW and FTGW as discussed in Section G.2).

#### G.3.2. EMPIRICAL RELATION BETWEEN FTGW/SGW AND EGW/EGW\*

For those experiments, the entropic regularization for EGW/EGW\* is set 5 for *qm7* and TWITTER datasets, and 10 for RECIPE, AMAZON, and CLASSIC datasets as Figure 4 in the main text for EGW/EGW\* ( $\text{eps}=X$ ) for *qm7*, TWITTER, and RECIPE datasets; and Figure 14 for EGW/EGW\* for AMAZON and CLASSIC datasets. For sliced GW in AMAZON dataset, we only evaluate it until 10 slices due to its slowness with a larger number of slices.

**Empirical relation between FTGW/SGW and EGW.** We first set  $\text{GW}_\alpha := \text{FTGW}$  and  $\text{GW}_\beta := \text{EGW}$ . We illustrate an empirical relation between FTGW and EGW in *qm7*, TWITTER, RECIPE, AMAZON, and CLASSIC datasets in Figure 34.



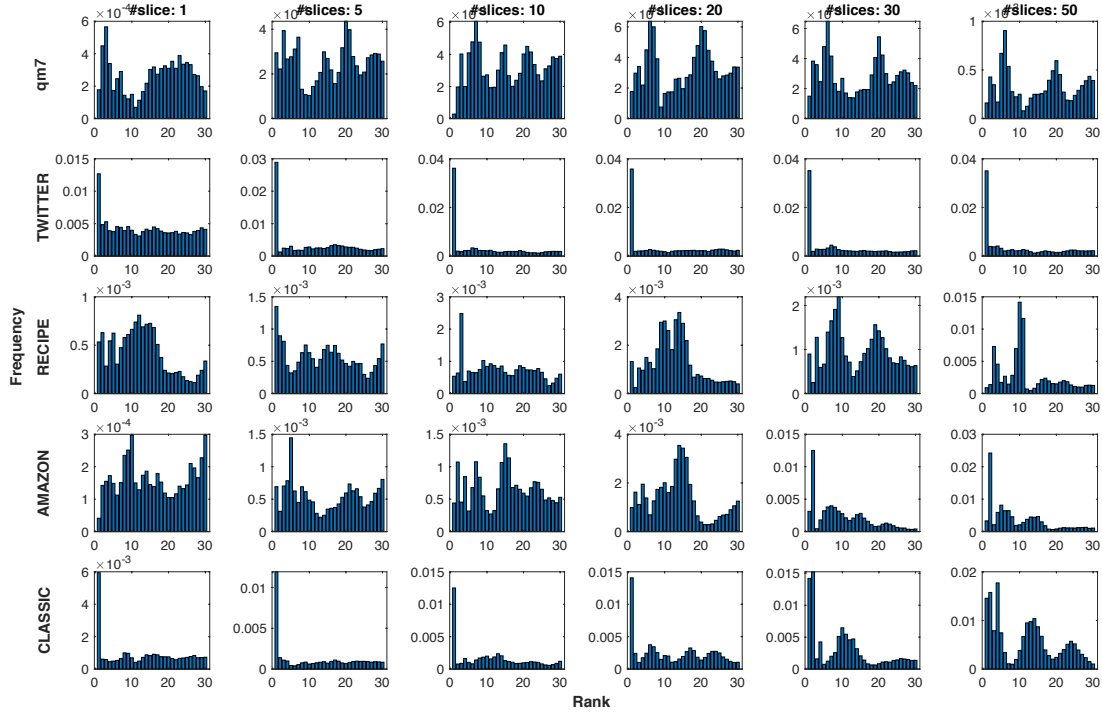


Figure 34. Empirical relation:  $\text{GW}_\alpha := \text{FTGW}$  and  $\text{GW}_\beta := \text{EGW}$ . The entropic regularization for EGW is set 5 for *qm7* and TWITTER datasets, and 10 for RECIPE, AMAZON, and CLASSIC datasets as Figure 4 in the main text for EGW ( $\text{eps}=\text{X}$ ) for *qm7*, TWITTER, and RECIPE datasets; and Figure 14 for EGW for AMAZON and CLASSIC datasets.

Secondly, we set  $\text{GW}_\alpha := \text{SGW}$  and  $\text{GW}_\beta := \text{EGW}$ . We illustrate an empirical relation between SGW and EGW in *qm7*, TWITTER, RECIPE, AMAZON, and CLASSIC datasets in Figure 35.

**Empirical relation between FTGW/SGW and EGW\*.** We first set  $\text{GW}_\alpha := \text{FTGW}$  and  $\text{GW}_\beta := \text{EGW}^*$ . We illustrate an empirical relation between FTGW and EGW\* in *qm7*, TWITTER, RECIPE, AMAZON, and CLASSIC datasets in Figure 36.

Secondly, we set  $\text{GW}_\alpha := \text{SGW}$  and  $\text{GW}_\beta := \text{EGW}^*$ . We illustrate an empirical relation between SGW and EGW\* in *qm7*, TWITTER, RECIPE, AMAZON, and CLASSIC datasets in Figure 37.

**Discussions.** It seems that there is no much empirical relation between FTGW/SGW and EGW/EGW\* on *qm7*, TWITTER, RECIPE, AMAZON, and CLASSIC datasets.

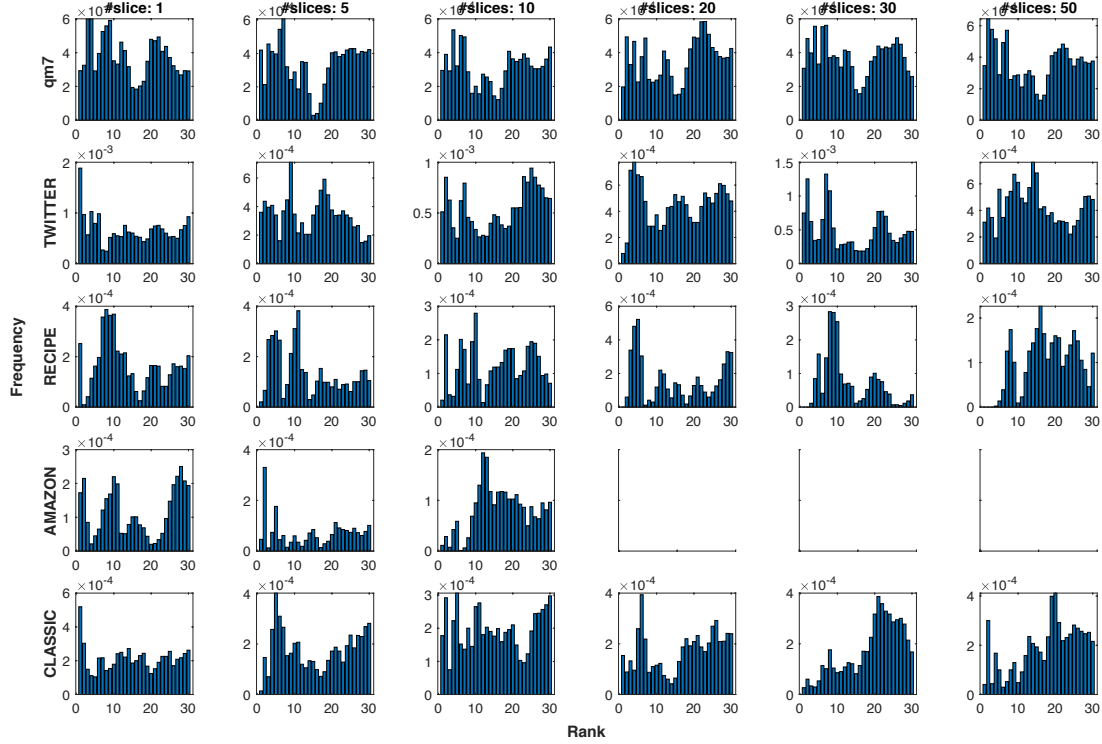


Figure 35. Empirical relation:  $GW_\alpha := SGW$  and  $GW_\beta := EGW$ . The entropic regularization for EGW is set 5 for *qm7* and TWITTER datasets, and 10 for RECIPE, AMAZON, and CLASSIC datasets as Figure 4 in the main text for EGW ( $\epsilon=X$ ) for *qm7*, TWITTER, and RECIPE datasets; and Figure 14 for EGW for AMAZON and CLASSIC datasets. For sliced GW in AMAZON dataset, we only evaluate it until 10 slices due to its slowness with a larger number of slices.

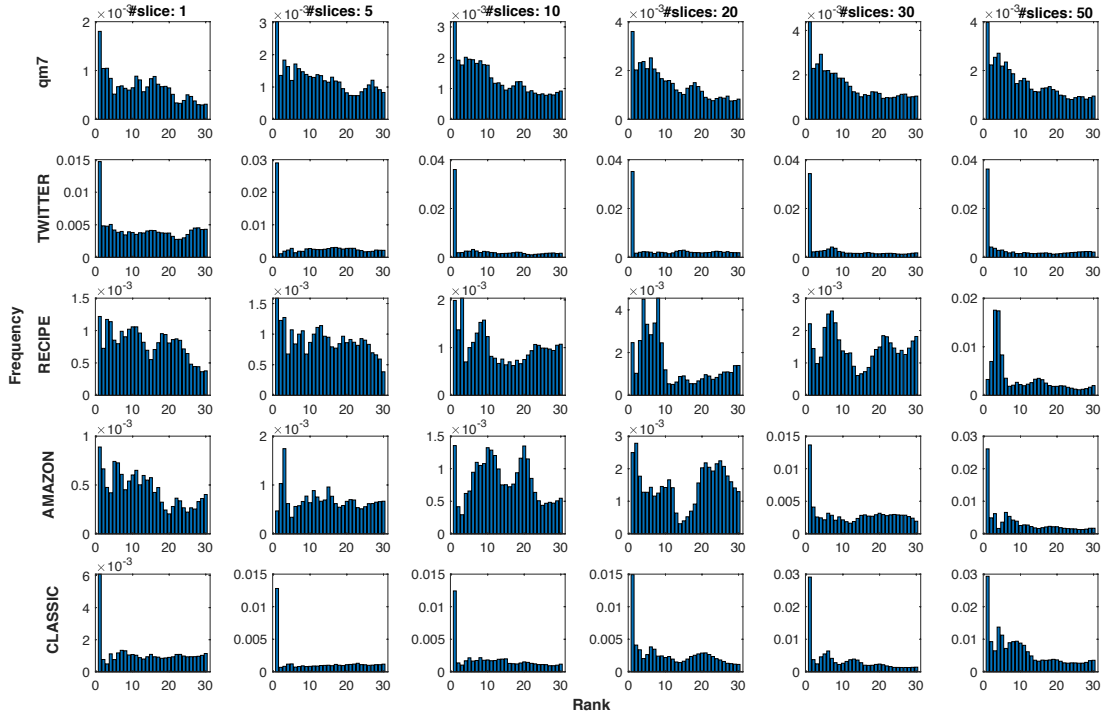


Figure 36. Empirical relation:  $GW_\alpha := FTGW$  and  $GW_\beta := EGW^*$ . The entropic regularization for EGW\* is set 5 for *qm7* and TWITTER datasets, and 10 for RECIPE, AMAZON, and CLASSIC datasets as Figure 4 in the main text for EGW\* ( $\epsilon=X$ ) for *qm7*, TWITTER, and RECIPE datasets; and Figure 14 for EGW\* for AMAZON and CLASSIC datasets.

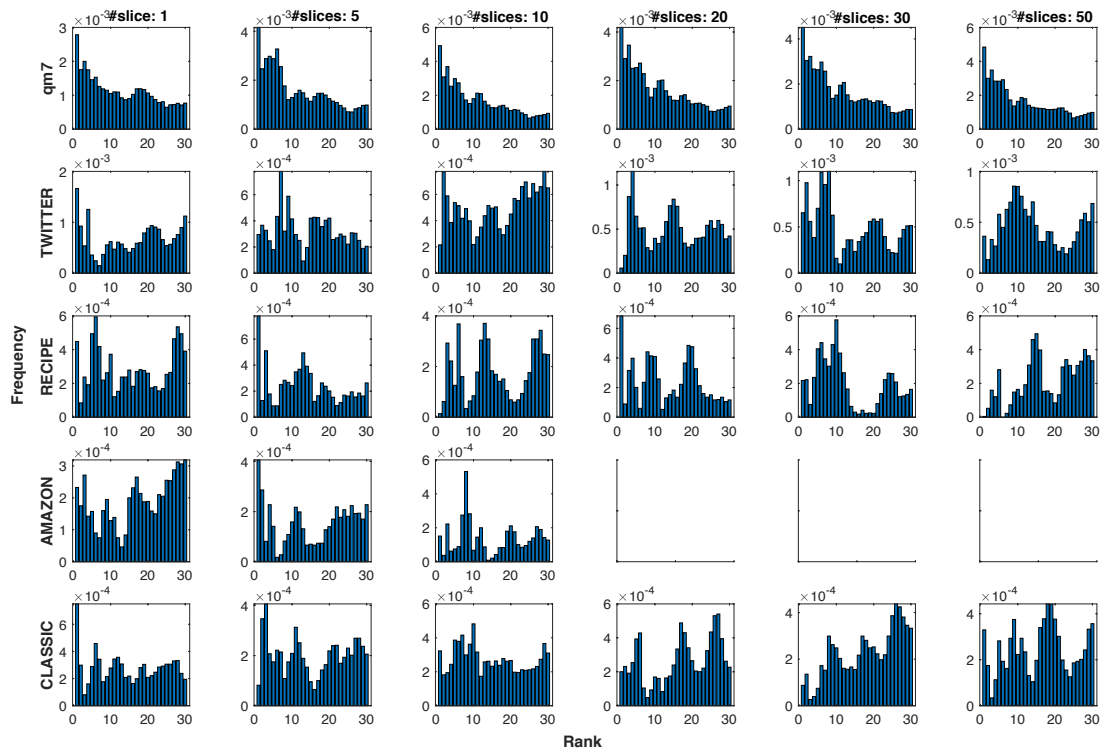


Figure 37. Empirical relation:  $GW_\alpha := SGW$  and  $GW_\beta := EGW^*$ . The entropic regularization for  $EGW^*$  is set 5 for *qm7* and *TWITTER* datasets, and 10 for *RECIPE*, *AMAZON*, and *CLASSIC* datasets as Figure 4 in the main text for  $EGW^*$  ( $\epsilon = X$ ) for *qm7*, *TWITTER*, and *RECIPE* datasets; and Figure 14 for  $EGW^*$  for *AMAZON* and *CLASSIC* datasets. For sliced  $GW$  in *AMAZON* dataset, we only evaluate it until 10 slices due to its slowness with a larger number of slices.